Felipe Santos de Castro

Experimental study of the dynamic behavior of a log boom employed at hydropower plants

São Paulo

2021

Felipe Santos de Castro

Experimental study of the dynamic behavior of a log boom employed at hydropower plants

Original version

MSc. Dissertation presented to Escola Politécnica of the University of São Paulo as a requirement to obtain the degree of Master of Science

Field of Study:
Naval Architecture and Ocean Engineering

Supervisor:
Prof. Dr. Gustavo Roque da Silva Assi
Co-supervisor:
Dr. João Lucas Dozzi Dantas

São Paulo
2021

Este exemplar foi revisado e corrigido em relação à versão original, sob responsabilidade única do autor e com a anuência de seu orientador.

São Paulo, _____ de _____ de _____

Assinatura do autor: _____

Assinatura do orientador: _____

Catalogação-na-publicação

Castro, Felipe Santos de

Experimental study of the dynamic behavior of a log boom employed at hydropower plants / F. S. Castro -- versão corr. -- São Paulo, 2021.

104 p.

Dissertação (Mestrado) - Escola Politécnica da Universidade de São Paulo. Departamento de Engenharia Naval e Oceânica.

1.Experimental Hydrodnyamics 2.Log Boom 3.Debris Containment I.Universidade de São Paulo. Escola Politécnica. Departamento de Engenharia Naval e Oceânica II.t.

Acknowledgements

First of all, I thank my family, my parents, Antenor and Maristela, for making me believe from the beginning that the search for knowledge must be continuous. I am also grateful to my siblings, Fernando and Fabiana, for all their love and companionship.

I am very grateful to my maternal grandmother Maria Joaquina. She welcomed me into her home in 2016, on my move to São Paulo. Thank you for all your love and dedication to our family.

To my girlfriend, Jackeline Araújo, for all the love and dedication. Thank you very much for the encouragement throughout this journey. You are one of the inspirational sources of my career. I love you so much!

To the friend, co-supervisor, and boss Dr. João Lucas Dozzi Dantas, for introducing me to this study's theme and allowing it to be developed with all the support of the IPT. Thank you for all the guidance, dedication, and patience you have had over these almost five years. Producing science at your side has been a rewarding experience.

To my supervisor Professor Gustavo Assi for all the conversations and support during graduate school time. I am thankful that he accepted me to work under his guidance, even with such a different theme. Thank you for your patience, serenity in teaching, and the trust placed in me. Professor Gustavo Assi's dedication is undoubtedly a positive differential within the University of São Paulo.

I am grateful to the friends and colleagues of IPT MSc. Eduardo Tadashi Katsuno and MSc. José Rodolfo Chreim, contemporary graduate fellows. Thank you for all the teachings, especially on the challenging theme of Fluid Mechanics. Thank you for the friendship, the conversations of the most varied themes, and the sharing of frustrations during tough times.

I thank the colleague of IPT Dr. André Mitsuo Kogishi, for all the support within the IPT, since my internship. I am very grateful for your teachings and for introducing me to Professor Gustavo Assi.

To all other IPT colleagues, in particular: Multiusuários' staff (Claudio, Fillipe, Gustavo, José Marcos, Lucas Grasseti, Lucas Miranda and Patrick) for the good times and all knowledge exchange; Ana Gilda, for all the support to the NAVAL team; David, Bruno, and Fidel, for all the technical support and sharing of good ideas.

To the Fundação de Apoio ao Instituto de Pesquisas Tecnológicas, FIPT, in addition to the Novos Talentos program for granting me a scholarship that made it possible to develop this study, in addition to participation at conferences.

This study was financed in part by the Coordenação de Aperfeiçoamento de Pessoal de Nível Superior – Brasil (CAPES) – Finance Code 001.

Abstract

The incidence of wooden debris in Santo Antônio hydropower plant (HPP) is a major issue to be addressed in order to avoid its own reduction efficiency. Log booms are floating structures assembled to form barriers upstream of the plant to protect its machinery, mainly against wood logs. Given their huge proportions and the turbulent environment where they operate, to understand its dynamics and movements is very important to achieve better performances in terms of design and operation. The use of experimental techniques to simulate the hydrodynamics response of log booms, with and without debris, can provide significant results to estimate their dynamic behavior. This study proposes to design and conduct hydrodynamic tests using scale log booms in two different perspectives: the log boom as a truncated line, to measure loads at its anchorage points and the motion of some modules of this line; and the log boom as a captive unity of this line, to characterize its dynamics, in a static approach, as a single bare body, in the presence of adjacent bodies, and subject to a flow with scale debris. The experiments with the truncated model helped to understand the behavior of scale log booms lines. The inclination with the flow, along with the variation of stream velocity and presence of debris, affected their load response, and their pitch and heave motion. These conclusions guided the hypothesis to design the experiments using a single captive model to measure drag, lift, and moment coefficients on the waterline plane, in a static two-dimensional approach. This second part considered variation of flow angle, flow velocity, and debris amount. The results caught the interference influence of adjacent log boom modules, the blockage effect generated by the test facility size, and the effects of debris in the log boom module resistance response.

Keywords: Experimental Hydrodynamics. Log Boom. Debris Containment

Resumo

A incidência de detritos de madeira na usina hidrelétrica de Santo Antônio é uma questão importante a ser tratada, a fim de evitar redução de sua própria eficiência. As barreiras de contenção de madeiras (*log booms*) são estruturas flutuantes, agrupadas com o intuito de formar obstáculos à montante da usina e proteger o maquinário, principalmente contra toras de madeira. Dados suas proporções enormes e o ambiente turbulento no qual operam, entender sua dinâmica e movimentos é fundamental para alcançar uma melhor performance de projeto e operação. O uso de técnicas experimentais a fim de simular a resposta hidrodinâmica de barreiras de contenção de madeiras, com e sem detritos, pode proporcionar resultados significantes para a estimativa do seu comportamento dinâmico. Este estudo se propõem a projetar e executar testes hidrodinâmicos utilizando barreiras de contenção de madeira em escala, em duas abordagens: a barreira de contenção de madeiras como uma linha truncada, a fim de medir carregamentos nos seus pontos de ancoragem e a movimentação de alguns dos modulos desta linha; e a barreira de contenção de madeiras como uma unidade cativa desta linha, para caracterizar sua dinâmica, em uma abordagem estática, como um corpo nu individual, na presença de corpos adjacentes, e sujeito ao escoamento com detritos de madeira em escala. Os experimentos com o modelo truncado ajudaram a entender o comportamento das linhas de barreiras de contenção de madeiras em escala. A inclinação em relação ao escomeanto, juntamente com a variação da velocidade do escoamento e a presença de detritos, afetou a resposta do carregamento, bem como seu afundamento e arfagem. Estas conclusões guiaram a formulação de hipóteses para projetar os experimentos utilizando um modelo cativo invidual de um módulo de barreira de contenção de madeiras, com o intuito de medir coeficientes de arrasto, sustentação e momento no plano de linha d'água, em uma abordagem estática bidimensional. Esta segunda parte considerou a variação do ângulo de escomento, velocidade do escoamento e quantidade de detritos. Os resultados capturaram o efeito de interferência de módulos vizinhos, o efeito de blocagem gerado pelas dimensões do modelo em relação as dimensões do local de teste, e os efeitos do detritos na resposta de resistência de um módulo de barreira de contenção de madeiras.

Palavras chave: Hidrodinâmica Experimental. *Log Boom*. Contenção de Detritos

List of Figures

List of Tables

List of abbreviations and acronyms

CAD	Computer Aided Design
NAVAL	Naval Architecture and Ocean Engineering Laboratory (in Portuguese: *Laboratório de Engenharia Naval e Oceânica*)
NDF	Fluids and Dynamics Research Group (in Portuguese: *Núcleo de Dinâmica e Fluidos*)
HPP	Hydropower Plant
IPT	Institute for Technological Research (in Portuguese: *Instituto de Pesquisas Tecnológicas do Estado de São Paulo*)
SAE	Santo Antônio Energia

List of symbols

a	Catenary coefficient [m]
A_b	Submerged projected area of the log boom model [m^2]
A_c	Cross-sectional area of water channel [m^2]
BR	Blockage ratio
C_D	Drag coefficient
C_L	Lift coefficient
C_M	Moment coefficient
C_T	Coefficient of total resistance of a line of log booms
d_L	Longitudinal distance between line model extremities [m]
d_T	Transversal distance between line model extremities [m]
D_s	Module hydrostatic draft [m]
D_{0-5}	Level of debris accumulation on 2^{nd} round of experiments
F_D	Drag force measured on captive module [N]
F_L	Lift force measured on captive module [N]
Fn	Froude number
F_R	Hydrodynamic resistance force [N]
F_x	Force measured on captive module in the x-direction [N]
F_y	Force measured on captive module in the y-direction [N]
g	Acceleration of gravity [m/s^2]
h	Catenary horizontal distance [m]
H	Module heave motion [m]
ℓ_L	Longitudinal debris length [m]
ℓ_V	Vertical debris length [m]

L_C	Log boom characteristic length [m]
L_M	Model characteristic length [m]
L_R	Real prototype characteristic length [m]
m	Catenary mass per unit length [kg/m]
M_z	Moment measured on captive module in the z-direction [Nm]
n	Number of modules in the line of log booms
R^2	Coefficient of determination
Re	Reynolds number
R_T	Total resistance of a line of log booms [N]
s	Catenary length [m]
T	Tension on extremity of catenary [N]
T_0	Catenary horizontal component of tension [N]
u_M	Model velocity [m/s]
u_R	River velocity [m/s]
Δu	Velocity increase [m/s]
v	Catenary vertical distance [m]
W_{0-5}	Level of debris accumulation on 3$^{\text{rd}}$ round of experiments
α	Module pitch angle [degrees]
β	Module yaw angle [degrees]
δ	Debris length factor
θ	Nominal angle of truncated line of log booms [degrees]
λ	Scale factor
ρ	Specific mass of water [kg/m^3]

Publications

Author's publications related to the present study.

In proceedings of conferences

CASTRO, F. S.; KATSUNO, E. T.; DANTAS, J. L. L. 2017 Instrumentation methodology for a log containment grid model in towing tank tests, In *ATTC2017 30th Towing Tank Conference*

CASTRO, F. S. et al. 2017 Structural Analysis for a Reduced Scale Model of a Hydropower Plant Debris Containment Grid, In *COBEM2017 24th ABCM International Congress of Mechanical Engineering*

CASTRO, F. S. et al. 2018 Structural Investigation of the Log Accumulation Effect in a Debris Containment Grid Through Towing Tank Experiments, In *OMAE2018 37th International Conference on Ocean, Offshore & Arctic Engineering*

CASTRO, F. S.; DANTAS, J. L. D. 2019 Motion analysis of scale truncated log boom structures tested in a towing tank, In *COBEM2019 25th ABCM International Congress of Mechanical Engineering*

Contents

1 Introduction

Hydropower is the most consolidated source of renewable energy. As the demand for energy supply enhances with progress, allied with sustainability, hydroelectricity plays a significant role in the world scenario. According to Girling et al. (2016), hydropower leads the renewable sources list for electricity generation, providing 71% of all renewable energy, and has grown 39% from 2005 to 2015, mostly at emergent markets. Brazil is an example of this development, corresponding to 8.6% of total global capacity, a result of plant installations in the Amazon rainforest region in the last years.

The Madeira River is a major tributary of the Amazon River. It is 3,315km long and is born in the Bolivian Andes Mountains. It contemplates two hydropower plants (HPP) over its course through the Brazilian territory: Jirau and Santo Antônio. Located near Porto Velho city, North of Brazil, Santo Antônio run-of-river HPP has 50 operational turbines with a total installed power capacity of 3.5GW, responsible for providing energy to 45 million consumers (Santo Antônio Energia, 2018). Climate and soil are advantageous to vast vegetation throughout the river extension, dragged to its course during flooding season. This natural phenomenon generates enormous amounts of wooden debris floating on the river that reaches the dam's machinery and affects its generation efficiency.

Debris in water flows is a widespread problem associated with energy exploitation or pollution difficulties. Control systems designed to manage debris presence and accumulation consider debris types, sizes, and ambiance in which they are located as project parameters. Debris booms are movable structures formed by a chain of buoys or pontoons anchored at their ends, usually installed on the water level. Since floating detritus tend to be deflected or retained, they present themselves as cost-effective solutions, generally applied on ice holding (ABDELNOUR, 2001; MORSE, 2001), litter containment (SLAT, 2014; BRAMBINI et al., 2017), oil spill (LO, 1996), or general river debris (WAHL, 1992).

From operational observations of Santo Antônio dam at high-flow seasons, measurements can achieve levels of 7,000 logs a day, with some reaching almost 3m in diameter. Flow rates create enormous log accumulation zones that flow through the river and somehow get the machinery. These massive and unavoidable jams interact with retainment structures installed at the dam, making them sink sometimes, in some cases almost irreversibly. Figure 1 shows some angles of the regions close to the dam, where it is possible to see substantial wood agglomerations with several sizes of debris.

Figure 1 – Log accumulation in different regions of the Santo Antônio dam

Source: Courtesy of IPT.

Study case

Santo Antônio's log booms are modular sets of buoys combined with grids connected adjacently to protect its equipment against fluvial debris and deflect them to the plant spillway. Those rows of log booms are installed upstream of the hydroelectric generation station and can reach up to 1,200m in length (Fig. 2). Each unit is composed of floats framed on a rigid steel cage attached to a grid, weighing approximately 5 tons. This modular structure is arranged continuously, creating a partially submerged line, as in Fig. 3. Its extremities are anchored to concrete pillars embedded into the riverbed. It has been conceived to operate at very severe conditions, influenced either by turbulence effects and the existence of numerous debris.

The log boom lines used by Santo Antônio HPP were designed as a system with several modules. Each prototype modular set comprises three floaters framed on a rigid

Figure 2 – Aerial view of Santo Antônio HPP. Arrows indicate some of the log booms lines

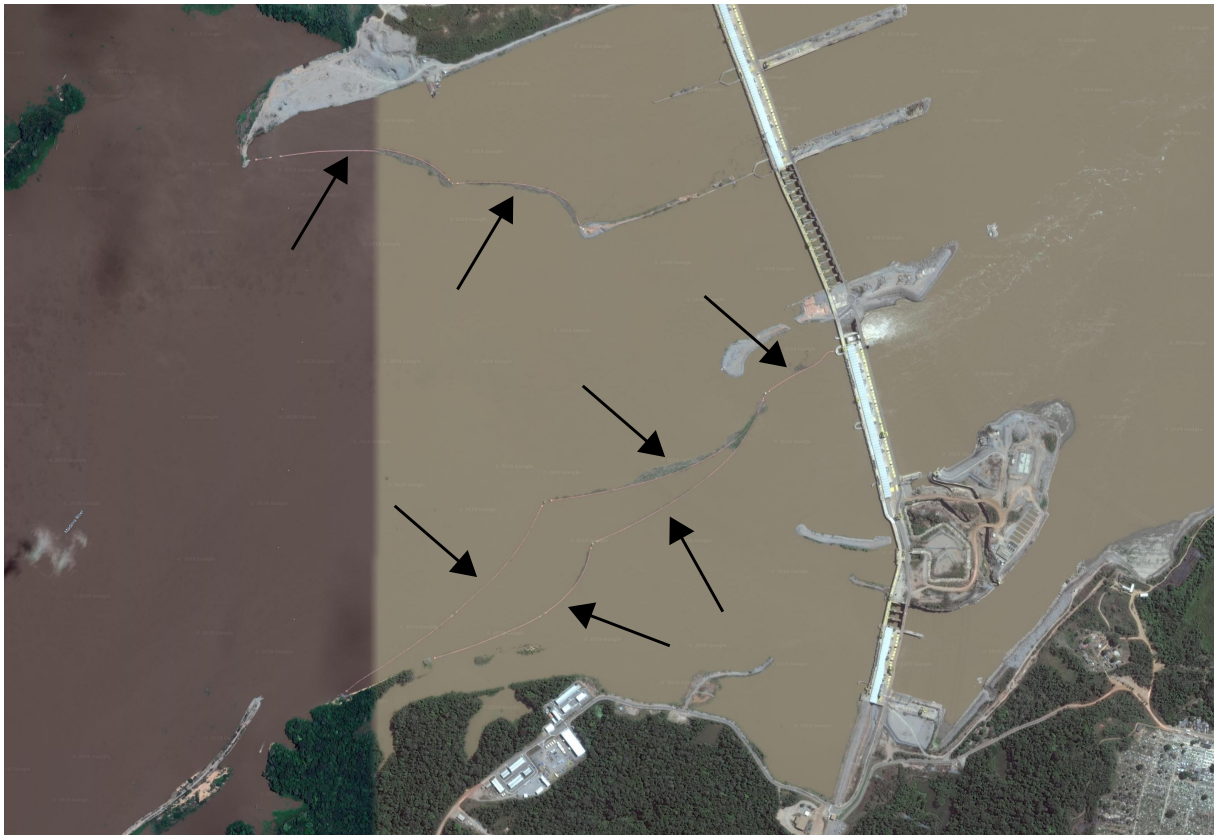

Source: Adapted from Google Maps (2018).

Figure 3 – Single log boom unity and line of log booms

Source: Adapted from Dantas (2017).

Figure 4 – Parametric view of the module indicating its components

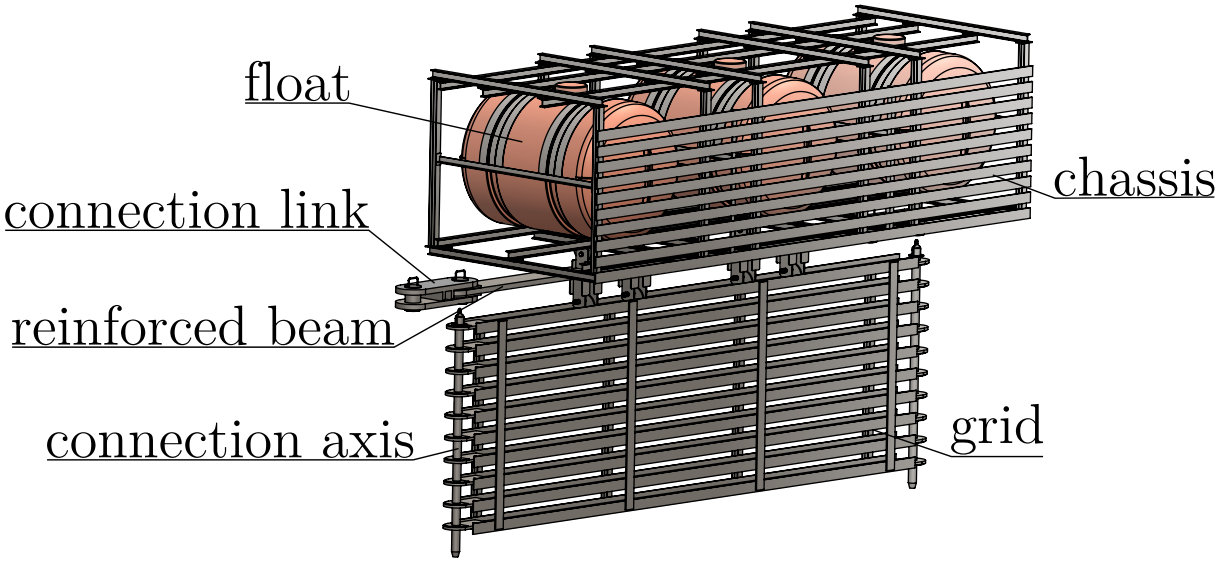

Source: Author.

structure, forming a sturdy chassis. This upper part connects to a longitudinal reinforced beam, which in turn is connected to a grid (Fig. 4). Figure 5 presents the main dimensions of a module. These unities are connected side by side through the steel connection link and shaft passing through the reinforced beam and grid, respectively, allowing them to rotate around it. Still, due to its geometry, the angle between adjacent log booms on the water surface cannot exceed 10°. Four rods link grid and reinforced beam, while four other rods link reinforced beam and chassis, all forming pin connections, in which rotational movement is allowed. Moreover, each module presents translational movement in the three main directions (Fig. 6), limited by their adjacent ones, once the lines submerge and bend related to the water surface during operation (CASTRO; DANTAS, 2019).

The log boom operation creates several hydrodynamic-structural engineering challenges: its interaction with the river stream and logs, the interference from the connection to other log booms, and the behavior of these structures thought as long lines. Therefore, identifying the main aspects that govern its dynamic movements and forces is part of the improvement process.

Given the accessibility, shape, and size, and extraordinary working conditions, a wholly controlled hydrodynamic study shows itself as a useful alternative to better comprehend the conditions imposed to log booms and their performance during operation. This work proposes to design and build log boom modules and lines on a reduced scale to allow for external flow measurements through towing tank and flume experiments, with and without the presence of debris. Results from tests with individual and a group of

Figure 5 – Real log boom main particulars

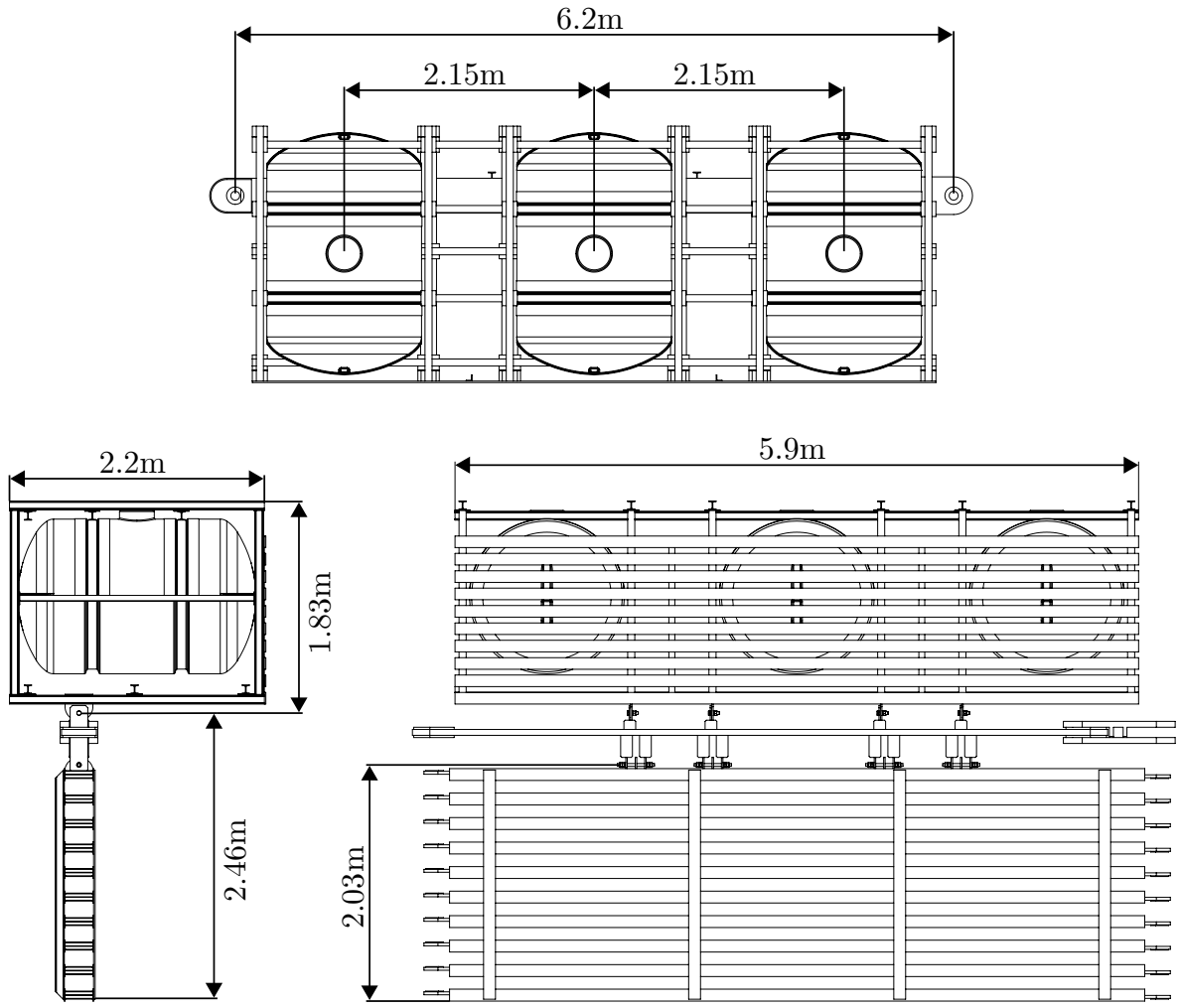

Source: Author.

Figure 6 – Log boom module detailing its rotational and translational motion axes

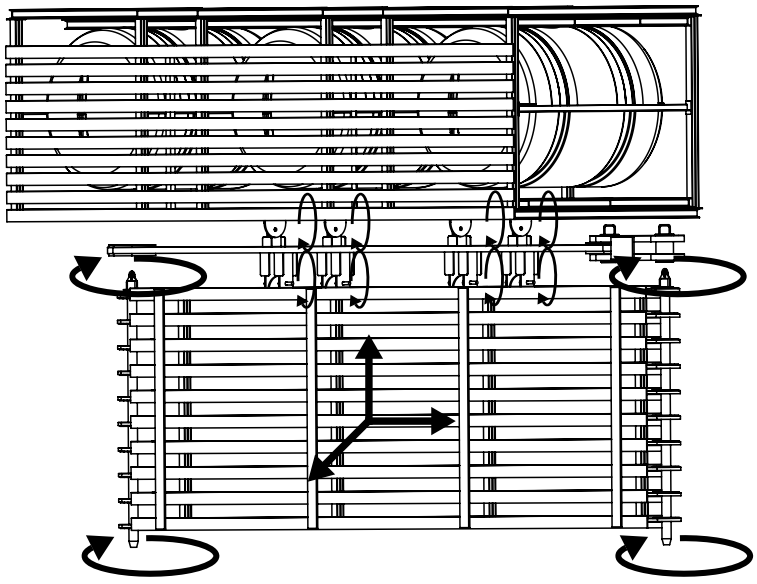

Source: Castro and Dantas (2019).

modules tests will support understanding the dynamic behavior of log booms systems.

All the experimental procedures are part of a technological research and development project developed in the Institute for Technological Research (IPT), requested and sponsored by Santo Antônio Energia (SAE)(PD-06683-0116/2019), through the Research and Development fund of the Brazilian Electricity Regulatory Agency (ANEEL). This project intends to assess the hydrodynamic and structural aspects of Santo Antonio's log booms and their integrity, and design an instrumentation and monitoring system to guarantee a safe operation for Santo Antônio HPP. Reduced-scale experiments in a towing basin are among the planned activities where the present study originated. Some tests are also conducted at the Fluids and Dynamics Research Group (NDF) open channel flume.

The determination of acting loads on the log boom lines is critical in terms of the project, allowing the proper understanding of the hydrodynamic and structural phenomena that influence their design. However, it is important to notice that there are no available solutions or tools to estimate forces on a line of log booms of this magnitude for a complex problem like this. The present study aims to develop a methodology to understand its functional behavior as a multibody system. Understanding the forces acting on each log boom unity might simplify the estimation of forces on a log boom line.

Research on the hydrodynamics of log booms contributes to the design process of fluvial and maritime hanging structures, which either or not have interactions with bodies in the stream. The adopted methodology has applications on systems for the fishing industry, ocean and river cleaning, mooring buoys, and management of aquatic ecosystems and species such as jellyfishes, duckweeds, and water hyacinths.

Objectives

The present study's objective is to develop an experimental methodology to study the dynamic behavior, through a static approach, of reduced-scale models of log booms modules used at Santo Antônio HPP.

Regarding the core objective, some specific tasks include:

- To design and set an experimental apparatus, for hydrodynamic tests in a towing tank and water channel, concerning the adopted instrumentation process, measurement devices, and test facilities.
- To perform tests on truncated lines of scale log booms, measuring force responses with a known volume of debris and their motion.
- To adapt and test a reduced portion of the model to study its individual behavior in the presence of adjacent log booms and with a known volume of debris.

2 Literature review

Due to the present study's unique characteristics, the literature review that now follows will support itself by two fundamental topics: devices and technologies to contain debris and their dynamics; and hydrodynamic assessment of complex geometries.

2.1 Dynamics and containment of debris

As pointed out by Perham (1987), for "the technical accuracy of the term floating debris, it should be noted that floating indicates not only floating on the water's surface but also suspended at some depth beneath it." Their presence on streams, either caused naturally or by human action, is a widespread problem. Its consequences impact areas such as hydraulics, dam engineering, and environmental engineering. Generally, the first two are associated with extracting energy from water streams. In this case, the accumulation of debris tends to be avoided regardless of their origin. Similarly, the effect of rubbish and liquid contaminants on living creatures and the environment is also undesirable.

Even though driftwood accumulation is a phenomenon governed by nature, its geometric properties and circumstances are correlated to river conditions and structures built along the river as bridges or piers (SCHMOCKER; HAGER, 2011; RUSYDA, 2015). Debris jams alter the velocity field on rivers and reduce flow area, which may induce bridge scour, i.e., removal of sediment from around bridge piers (PAGLIARA; CARNACINA, 2011). From an experimental approach, Rahimi et al. (2018) showed that wood debris accumulation upstream four different piers configurations affects local scour. Among other aspects, they found that debris shape, effective length, and distances from the free surface also collaborate with scouring depth. That influence seems to be an essential factor to consider structures to deal with log accumulation that are not embedded into the riverbed.

The entrainment of wood debris, especially on flood events, combined with their accumulation and blockage capacities urges the necessity for engineering studies and interventions (PITON; RECKING, 2016). Through on-site measurements and analysis of real events, models can be generated to predict the accumulation process that may lead to the design of structures to retain debris (CURRAN, 2010). Physical modeling on flume experiments of floating debris motion is also helpful, allowing visual interpretation and supporting the understanding of this problem (BRAUDRICK et al., 1997; DAVIDSON; MACKENZIE; EATON, 2015). Concomitantly, numerical modeling of log mobility is also an alternative to simulate the effects of wood clogging, for example, on river structures, such as bridges and debris control systems (STOCKSTILL; DALY; HOPKINS, 2009; RUIZ-VILLANUEVA et al., 2014).

Concerning the analysis of detritus entrainment and consequent countermeasures, state-of-the-art is concentrated on the debris themselves, i.e., understanding their motion on water, the accumulation process, and its outcomes, and applying physical measures to deal with this issue. Countermeasures to deal with debris accumulation depend on the dimensions of the site. Bradley, Richards and Bahner (2005) classified them between structural and non-structural solutions, which respectively consist of physically constructed structures and maintenance, like removing excess material.

To understand the effects of the interaction between flow debris and hydraulic structures to mitigate them is fundamental for engineering design. Schmocker and Weitbrecht (2013) have conducted tests on a flume regarding the modeling of wooden debris going to a model rack, a fixed grid used to protect intake regions, such as water conveyances or pumping stations. The purpose was to identify the influence of the accumulation process on backwater effect, i.e, difference between upstream and downstream water levels. Using different types of debris did not produce any effect. On the other hand, varying Froude number and volume of wooden debris contributed to the backwater rise phenomenon. Even on an immovable system as a rack, these seem to be considered variables while studying mechanisms to contain debris that could produce effects on the structure's hydrodynamic response.

Walczak, Walczak and Nieć (2020) also conducted tests on racks but to assess resistance values on them in the jam of ice debris. The experiment measured the resistance force, considering a change in ice volume reaching the upstream region of a trash rack, for the same flow velocity. The range of ice along the water surface on flow direction has been measured and related to the force response. Results showed a direct relation of force with the mass of debris and their accumulation length, but the small number of scenarios does not support that. It is important to note that ice debris are formed in cold regions and tend to form large blocks, which sometimes does not create a porous media as wood debris. However, to relate a visual variable, i.e., debris accumulation length, with the dynamic response seems to provide valuable insights to design structures to retain general debris.

Among the structural measures, debris boom systems are appropriate to mitigate floating detritus, either solid or liquid. They can be installed or removed more quickly compared to fixed solutions. Log booms have been historically applied to controlling floating debris on water dams. The first designs had tied up tree trunks as float devices, having walkways upon them (Fig. 7). Analyzing by another aspect, log booms can also be used as an alternative to transporting logs on rivers. Newman (1975) brings an interesting analytical prediction of the shape of a towed boom of logs designed to transport wood. Both ends have the same position, assuming a shape that resembles a water drop. Their shapes tell us the amount of transported logs and may help determine the power required to tow the boom along the river.

Figure 7 – Debris diversion boom and debris (top) and its cross section (bottom), Appalachian Power Company Station at Winfield Lock Dam, Kanawha, West Virginia

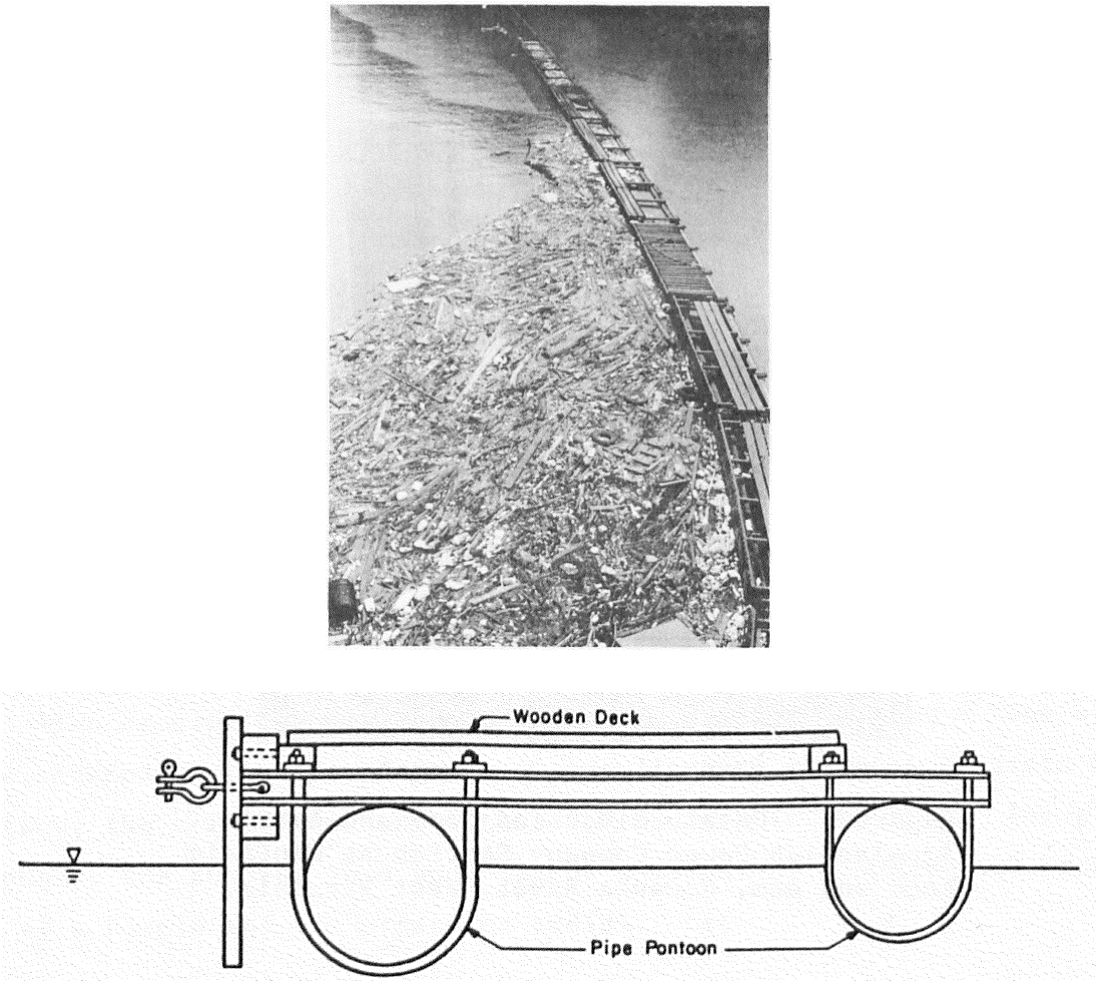

Source: Perham (1987).

From a practical perspective and assuming as an anchored hanging structure, Creager and Justin (1950 apud PERHAM, 1987) provides a method to estimate the tension load on log booms

$$T = \frac{wRdv^2}{g}(\sin\alpha), \tag{2.1}$$

which combines the distance the boom projects below the water surface, flow velocity, and sag in the boom, assuming it as an arc of a circle and pressures radial. R is the radius of curvature of the boom, α is the angle of the chord of the arc to the direction of flow, d stands for the draft of the boom, v is the velocity of water, g represents the acceleration of gravity, and w the specific weight of water. It is important to note that this formulation considers the line as a single body without heave motion, assumes just a single angle of flow direction, and neglects the debris accumulation effects.

In a similar approach, Foltyn and Tuthill (1996) have also contributed with insights

Figure 8 – Definition sketch for ice boom loading and geometry. A uniform loading is assumed across the channel width to produce a parabolic shape

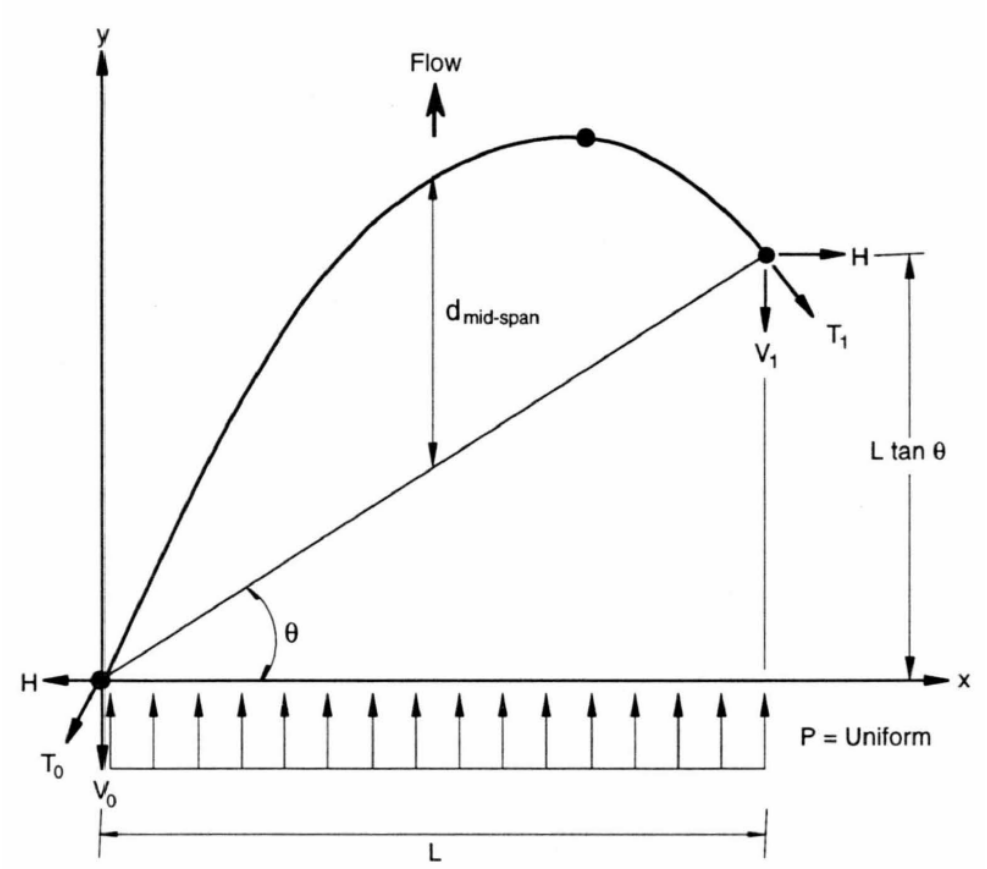

Source: Foltyn and Tuthill (1996).

on the structural composition of booms to retain ice in rivers, estimating geometries and loads involved as well as typical designs. They consist of timbers connected by a chain to a boom cable. From that assumption, they split the main sources of load on an ice boom, resulting in a total force per unit width. Their hypothesis assumes that the significant portion of the load comes from what they called "water shear on the underside of the ice accumulation," which from its formulation resembles the ice's buoyant force. Other minor components involve the wind drag on the ice cover and the downslope component of the ice accumulation's gravity force. With those components and assuming a uniform load and parabolic shape for the ice boom (Fig. 8), it is possible to calculate its tension T along the x-axis length

$$T = \frac{pL}{8s}\sqrt{1 + \left[\tan\theta + 4s\left(1 - \frac{2x}{L}\right)\right]^2}, \tag{2.2}$$

where p is the uniform load on the boom per unit width, L is the perpendicular chord length, and θ is the angle between the chord and the line perpendicular to the direction of force. The s is called the sag ratio and its relationship with the unstressed length S_0 may

be approximated by

$$S_0 = L\left(1 + \frac{8}{3}s^2 + \frac{1}{2}\tan^2\theta\right). \tag{2.3}$$

In general, the work of Foltyn and Tuthill (1996) is practical in terms of the first design, but it is made for a specific shape of boom and environment, in which debris tend not to have distinct shapes and densities once they are ice. Even with a load on each boom per unit width, the effects caused by its adjacent unities are not considered.

Debris booms must feature a reliable efficiency to retain debris. The capacity to hold or guide wooden debris was studied by Kennedy and Lazier (1965 apud PERHAM, 1987). They ran a series of laboratory tests to evaluate the wood-stopping ability of alternative design of booms, based on the percentage of logs lost with stream velocity. Models with a net extending below the water surface produced a lower wood loss. However, their field-scale efficiency can be compromised due to high velocities periods, resulting in significant losses over the top.

Comparably, Lo (1996) carried out experiments with floating booms under controlled current, wave, and wind conditions, to investigate their effectiveness in preventing oil slick and jellyfish movement. Although the results recommend a particular configuration for the booms, their field performance may differ due to limitations of the laboratory equipment and scaling problems.

It is seen that floating debris are managed in several ways, and different solutions can be applied to mitigate this issue. Aside from its use, the main design characteristics regarding these systems tend to be their holding strength and how effective they are in retaining debris. Studies are generally too specific regarding a single type of solution to deal with the problem. This may be associated with the fact that solutions at one site can not be directly replicated to other sites, explaining the literature gaps concerning this theme.

2.2 Experimental methods on the hydrodynamics of complex geometries

Important fluid mechanics problems consist of determining a body's main interactions immersed in a moving fluid. As an alternative, much of the physics of interacting conditions can be understood by conducting appropriate experiments (GAD-EL-HAK, 1989; SHAUGHNESSY Jr; KATZ; SCHAFFER, 2005). Despite canonical shapes (circular cylinders, spheres, or thin plates) have their surface forces, especially drag, well documented (see Blevins (1984)), measurements of loads due to external flow around single

and multi-bodies with complex geometries are restricted to their applicability and hence scarce at accessible literature.

Offshore hydrocarbons exploration systems have several mechanisms to maintain themselves fully operational. Manifolds (responsible for integrating multiple subsea offshore systems on the seabed) have their shape determined by their function, resulting on non-regular and rather complex geometries (Fig 9a). Fernandes and Mineiro (2007) compared numerical code results with towing tank measurements to assess the hydrodynamic properties of manifold models (essential data to predict their behavior during pendulous installation, for example). Apart from its Reynolds number limitations, added mass coefficients demonstrated similarity between numerical and experimental approaches, and drag coefficients presented a transition effect similar to that of known bluff bodies. Similarly, Fernandes et al. (2010) conducted an experimental study on flat plates to observe the flow-induced rotation on offshore manifolds. They determined non-dimensional coefficients and implemented them in a quasi-steady modeling to determine the natural frequency of rotation, comparing to experimental measurements. Results have shown reasonable agreement for some physical models, but a blockage effect — which generally induces some errors to hydrodynamic experiments — generated some discrepancy on larger models.

Regarding tests with bodies of irregular geometries, Kleine et al. (2018) and Guedes et al. (2018) also worked with manifold models at IPT's Towing Tank, aiming at understanding the influence of geometric simplifications and modifications concerning their directional stability. A regression analysis could estimate the hydrodynamic coefficients from static and dynamic tests to feed in the equations of motion. The studies demonstrated acceptable reliability for the simple models, but in contrast, indicated a significant change in the manifold's maneuverability with the most complex shape. That indicates the importance of conducting experimental studies on models with unusual shapes, but at the same time, suggests that the lack of literature might be related to its specific applications.

Other devices with singular geometries are the torpedo anchors projected to moor drilling and production systems in the offshore exploration industry. They come in complex shapes and sizes (Fig. 9b) but are primarily designed to penetrate the seabed. Cenac (2011) presented a drag coefficient analysis on scale anchor model, with adjustable fins, through towing tank runs with a captive model. The drag showed some similarity compared to spheres and cylinders but limited to a small Reynolds number range. Additionally, Hasanloo, Pang and Yu (2012) and Fernandes et al. (2006) carried out free-fall experiments focusing on the installation of torpedo anchors. Both studies employed video tracking systems in deepwater basins on models with several configurations to estimate drag and directional stability coefficients, combining experimental procedures and mathematical models. Even though the innovative model testing arrangements, there were some limitations in extrapolating the results to full scale prototypes.

Figure 9 – Complex geometry bodies subject to hydrodynamic tests. (a) Deep water manifold model. (b) Reduced-scale model of Mark I OMNI-Max anchor. (c) Net fish model tested on flume tank

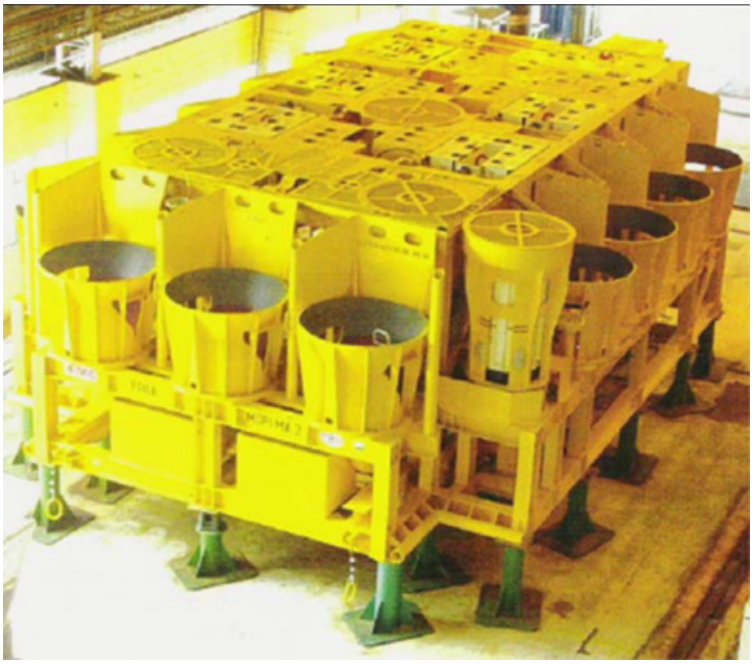

(a)

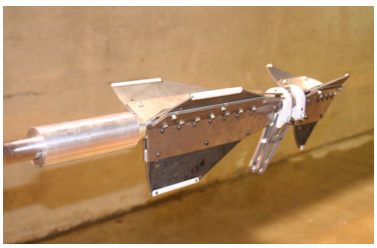

(b)

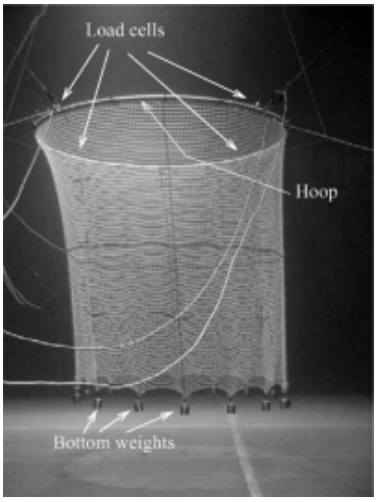

(c)

Source: Fernandes and Mineiro (2007), Cenac (2011), and Lader and Enerhaug (2005).

Hanging structures have an extensive application capability in Engineering. For instance, various cable problems paved the way for some well-known techniques, equations, and mathematical functions (IRVINE, 1981). Even the analytical mechanics of systems with a cable first approach can be model as such and contribute to their final engineering design (PESCE, 1997; SILVEIRA; MARTINS, 2004). Sea fish farming applications include the utilization of porous and flexible net cages, which are hanging structures that admit flow through and around them (Fig. 9c). The complex interaction between flow load pattern and their shape makes them pertinent to be experimentally explored (LØLAND, 1993). Løland (1991) performed hydrodynamic tests using models of net panels in several configurations to determine lift and drag forces coefficients as a function of solidity ratio and flow angle. From those results, a mathematical model was developed to calculate the total force and deformation on a net cage system, assuming that each net cage was a line fixed at the top, with bottom weights at the opposite extremity. That line could be divided into a set of panels, each subject to a stream velocity U and angle α as in Fig. 10. The total force on the net cage system was expressed as the sum of forces acting on each panel. Based on a two-dimensional approach, numerical results showed agreement with

Figure 10 – The lateral shape of a fishing net cage subject to a free stream and divided into net panels

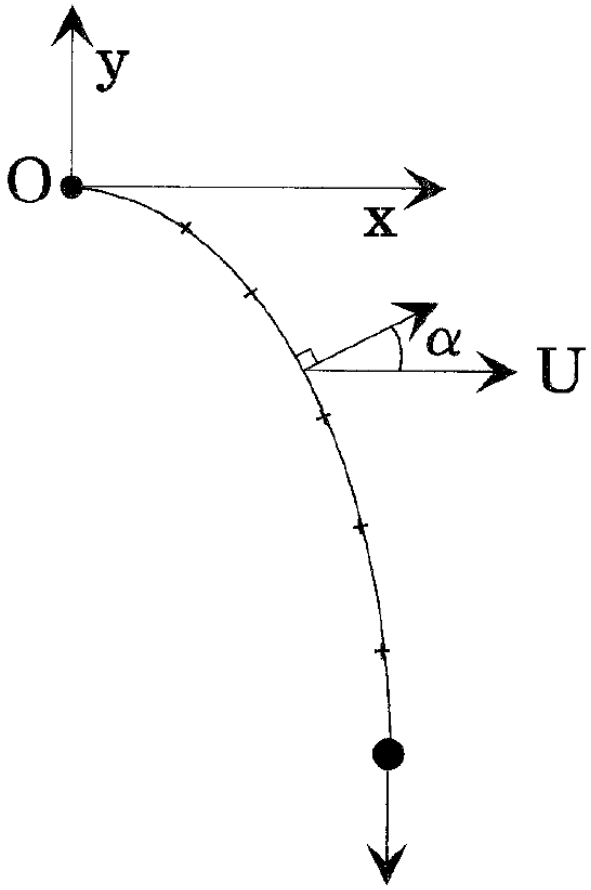

Source: Adapted from Løland (1991).

experimental measurements using net cage models, despite the three-dimensional effects presented in a fishing farm with several net cages.

An interesting study was conducted by Ådnanes (2011) comparing four distinct methods to predict forces and deformations on a hanging fishing net cage. In one of the methods, he assumed the net as a catenary curve and used previous lift and drag coefficients, from experimental data of tests performed by Løland (1991), to create a semi-empirical tool to calculated loads and deformation on nets in uniform current.

Experimental hydrodynamic techniques applied in bodies with complex geometries have applications that can guide towards their operational understanding. For simplification and practical purposes, analytic formulations to predict tension loads and shapes of lines of debris booms provide some estimates to design these systems. In the present study, we aim to provide new insights about forces and motion acting on scale log booms, allied with visual observation to understand the effect caused by wooden debris.

3 Theoretical formulation

The balance of forces on each module occurs by axial force through the modules until the attachment terminals. The source of forces is the hydrodynamic load on the structure and, in the case of log booms, its interaction with debris brought by the flow. This chapter discusses which parameters may influence the log boom modules' forces and what hypothesis can be assumed due to its geometric form.

3.1 Dimensional analysis

Experiments with reduced-scale models are a means to obtain more insights into the flow behavior around bodies. They complement analytical models on fluid-structure problems that are too complex, both geometrically and physically, to be solved. To reproduce a fluid-structure interaction problem in experiments, one has to determine which parameters govern the phenomena and how that information is obtained from the smallest set of experiments (BIRK, 2019).

Dimensional analysis is an important tool in the search for physical relationships in experimental and theoretical models. It employs a method for reducing the number and complexity of experimental variables which affect a given physical phenomenon by combining them into dimensionless parameters (BIRK, 2019; GANESAN, 2010). The theory is based on the Buckingham Π-theorem (BUCKINGHAM, 1914) and states that a phenomenon with n dimensional variables, that may be expressed in terms of k independent fundamental physical quantities, is physically represented by an equivalent expression involving a group of $i = j-k$ dimensionless parameters, generally called Π-terms. Essentially one assumes that any physically meaningful equation involving n variables, such as

$$x_1 = f(x_2, x_3, ..., x_j), \tag{3.1}$$

has the same physical dimension in both right-hand and left-hand side terms. Based on that, one can rearrange the equation into a set of dimensionless products of Π-terms like

$$\Pi_1 = \phi(\Pi_2, \Pi_3, ..., \Pi_i). \tag{3.2}$$

Log boom modules are part of a multibody structure and will be considered single pieces of an entire line. A log boom module consists of a rigid floating body subjected to the river flow. Analogously, Birk (2019) performed the dimensional analysis for a ship, also a floating body except that it moves through the flow and has a smoother shape. Hence, a similar approach seems reasonable to be employed here.

One of the most important and challenging steps in applying dimensional analysis to any given problem is identifying the variables involved. In terms of hydrodynamic resistance force F_R acting on a log boom module, the following variables are identified: density of water ρ, flow velocity u, the dimension of the log module represented by its characteristic length L_C, dynamic viscosity of water μ, acceleration of gravity g, module yaw angle β, and upstream visual debris length ℓ_D, therefore

$$F_R = f(\rho, u, L_C, \mu, g, \beta, \ell_D). \tag{3.3}$$

There are eight dimensional parameters ($j = 8$), represented by the following fundamental dimensions of length L, mass M, and time T in SI unities

F_R hydrodynamic resistance force $\left[\frac{\text{kg}}{\text{ms}^2}\right]$ or $[MLT^{-2}]$

ρ water density $\left[\frac{\text{kg}}{\text{m}^3}\right]$ or $[ML^{-3}]$

u flow velocity $\left[\frac{\text{m}}{\text{s}}\right]$ or $[LT^{-1}]$

L_C log boom characteristic length [m] or $[L]$

μ water dynamic viscosity $\left[\frac{\text{kg}}{\text{ms}}\right]$ or $[ML^{-1}T^{-1}]$

g acceleration of gravity $\left[\frac{\text{m}}{\text{s}^2}\right]$ or $[LT^{-2}]$

β module yaw angle in the calm water plane [rad] or [1]

ℓ_L upstream debris length [m] or $[L]$

The fundamental physical quantities involved are M, L, and T, i.e., $k = 3$. Therefore, the required number of Π-terms is 5. To apply the Π-theorem, k repeating variables must be selected among the original variables list and combined with each of the remaining variables to form the Π-terms. Variables ρ, u, and L_C are chosen because they cover the dimensions of mass, time, and length, and they are dimensionally independent. That means that repeating variables cannot themselves be combined to form a dimensionless product (MUNSON et al., 2009). The Π-terms must be formed by multiplying one of the nonrepeating variables by the product of the repeating variables, each raised to an exponent that will make the combination dimensionless. Based on that, to form the first Π-term one has

$$\Pi_1 = F_R \rho^a u^b L_C^c. \tag{3.4}$$

Since this combination is to be dimensionless, it follows that

$$(M^0L^0T^0) = (MLT^{-2})(ML^{-3})^a(LT^{-1})^b(L)^c. \tag{3.5}$$

Combining the corresponding terms, the following can be written:

$$1 + a = 0 \qquad (for \quad M), \tag{3.6}$$

$$1 - 3a + b + c = 0 \qquad (for \quad L), \tag{3.7}$$

$$-2 - c = 0 \qquad (for \quad T), \tag{3.8}$$

resulting in $a = -1$, $b = -2$, $c = -2$ and, therefore

$$\Pi_1 = \frac{F_R}{\rho L_C^2 u^2}. \tag{3.9}$$

The process is repeated for the remaining nonrepeating variables in order to find out the remaining Π-terms. The following ones are obtained:

$$\Pi_2 = \frac{\mu}{\rho L_C u}, \tag{3.10}$$

$$\Pi_3 = \frac{gL_C}{u^2}, \tag{3.11}$$

$$\Pi_4 = \beta, \tag{3.12}$$

$$\Pi_5 = \frac{\ell_L}{L_C}. \tag{3.13}$$

Based on 3.2, the result of the dimensional analysis is expressed as

$$\frac{F_R}{\rho L_C^2 u^2} = \phi\left(\frac{\mu}{\rho L_C u}, \frac{gL_C}{u^2}, \beta, \frac{\ell_L}{L_C}\right), \text{ or} \tag{3.14}$$

$$F_R = \rho L_C^2 u^2 \phi\left(\frac{\mu}{\rho L_C u}, \frac{gL_C}{u^2}, \beta, \frac{\ell_L}{L_C}\right). \tag{3.15}$$

From an incompressible fluid hypothesis and since force is expressed on both sides of Eq. 3.15, right-hand side can be thought of as integral of dynamic pressure and shear stress over a wet area S, previously described as L_C^2. Moreover, the dimensionless terms are

rearranged and rewritten as four dimensionless parameters: Reynolds number Re, Froude number Fn, yaw angle β, and debris length factor δ. Then, 3.15 is finally expressed as

$$F_R = \frac{1}{2}\rho S u^2 C(Re, Fn, \beta, \delta), \tag{3.16}$$

where C is function of 4 dimensionless parameters, with some of them producing more or less effects.

Reynolds number governs the dynamic similarity of inertial and viscous forces (BIRK, 2019). It is a measure of the ratio of the inertia force on an element of fluid to the viscous force on an element, and it is generally essential in all types of fluid problems (MUNSON et al., 2009).

A closer look at a log boom module geometry characterizes it as a sharp-edged body (Fig. 11). Its form tends to cause flow separation, and once geometric and kinematic similarities are kept, its breakaway points are fixed, and Reynolds number variation may cause no significant changes in terms of resistance force (KHOSHNEVIS; MAMOURI; MIR, 2015). Unlike a body like a log boom, elliptic cylinders, being smoothly rounded, present a laminar-turbulent transition effect in the boundary layer that changes separation depending on Reynolds number (RATHAKRISHNAN, 2007). Sharp-edged bodies tend to cause flow separation regardless of the boundary layer's nature (FERNANDES et al., 2010); hence shear forces have secondary importance relative to pressure loads. Therefore, scaling drag forces from model to full scale are usually insensitive to Reynolds number effects (FALTINSEN, 2005). In contrast, Larose and D'Auteuil (2006) and Schewe and Larsen (1998) have conducted tests on cross sections of bridge decks, also considered bodies with sharp edges, and concluded that the effect of Reynolds number on the drag forces is not negligible. This discussion seems to converge on how to classify a body as a sharp-edged one and how "quantitatively sharp" the body needs to be, which is not the focus of this study.

Froude number is a measure of the ratio of inertial to gravitational forces on an element of fluid. It will generally be important in problems involving free surface flows, where gravity effects such as waves can no longer be ignored. Typical problems would include the flow of water around ships, flow through rivers or open conduits (MUNSON et al., 2009).

The purpose of conducting model tests is to understand the general phenomenon and transfer physical quantities measured at model scale to the full scale design. Three required similarities must be achieved to regulate the conversion of model test results into full scale results: geometric, kinematic, and dynamic. Geometric similarity implies the similarity of shape and a constant ratio of any length in one system to another system's corresponding length, usually known as the scale factor. That also involves assessing

Figure 11 – Log boom module highlighting some of its sharp edges

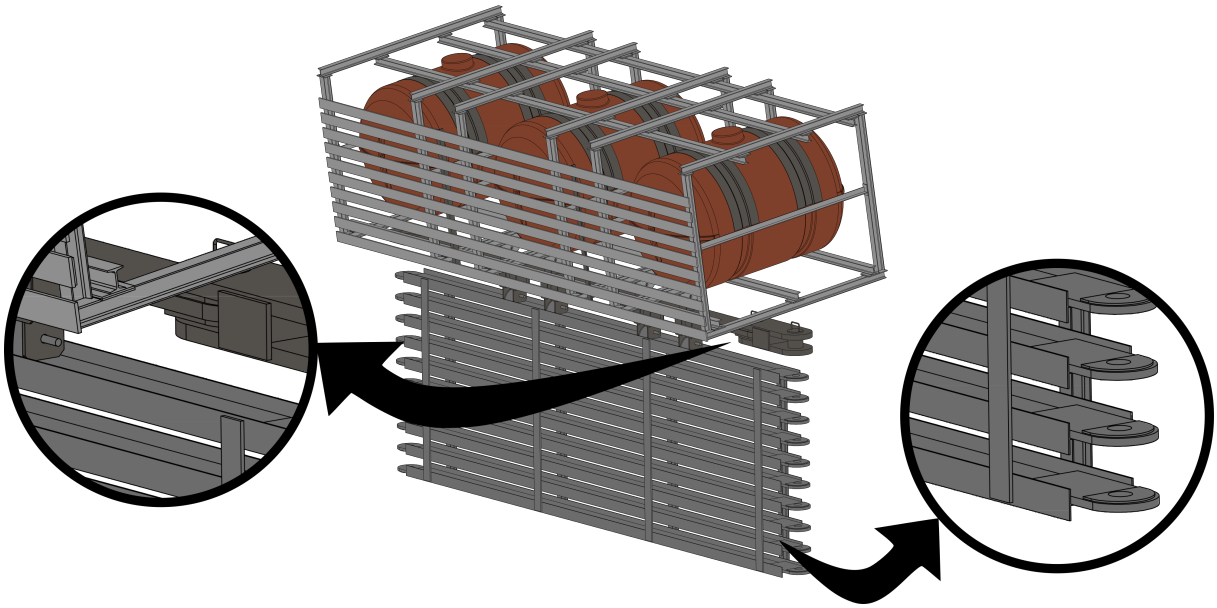

Source: Author.

whether the facility's geometrical limitations influence the model test results or not. Kinematic similarity refers to the similarity of streamline patterns, in which fluid particles should not only take similar geometric paths but should also maintain an equivalent time scale (ZOHURI, 2015). Dynamic similarity requires that forces in full and model scale have the same direction and a constant ratio. Froude and Reynolds numbers are two important governing parameters, and to achieve complete dynamic similarity would require reproducing their values at model and full scales, at the same time, which is impossible (BIRK, 2019). On the other hand, a partial dynamic similarity is valuable and doable in the log boom problem on a Froude number similarity approach.

From the dimensional analysis, module yaw angle β presented itself as a dimensionless parameter, which means that a dimensionless variable becomes a dimensionless Π-term. Only the module yaw angle is considered since a two-dimensional approach has been assumed. Its effects on the surface forces seem intuitive, and literature presents many studies with several shapes of bodies, in which the angle related to the flow is the main variable (BLEVINS, 1984; HOERNER, 1992). From a force diagram, the resistance force is the combination of drag and lift components with respect to the flow direction, acting upon the module surface that is yawed at a certain β angle (Fig. 12). Nevertheless, it is important to remember that the unbalance of forces generates a moment M_z around the z-axis, which is also affected by β. The magnitude of forces follows a trigonometric law,

Figure 12 – Forces and moment, generate by a upstream flow, acting on the plane for a single log boom module

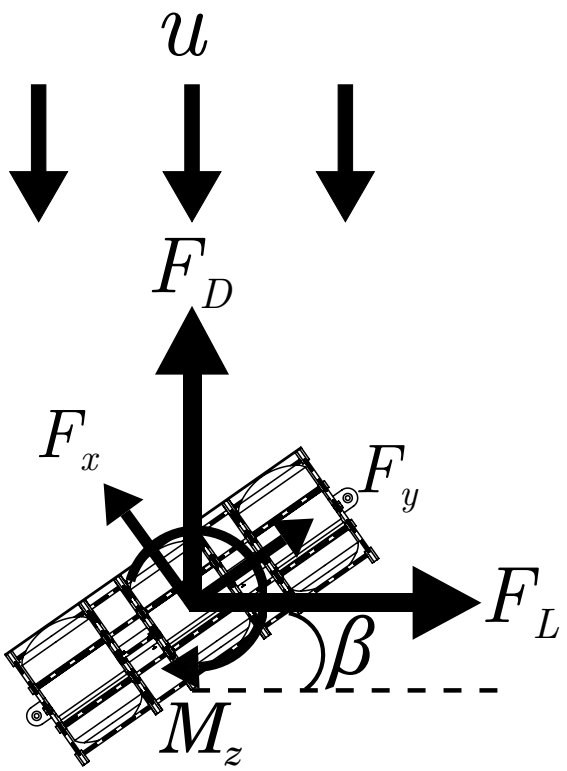

Source: Author.

giving

$$\begin{aligned} F_R^2 &= F_D^2 + F_L^2 \\ F_D &= F_x cos(\beta) + F_y sin(\beta) \\ F_L &= -F_x sin(\beta) + F_y cos(\beta). \end{aligned} \tag{3.17}$$

Looking at Fig. 1, it is reasonable to infer that the effects caused by debris are either hard to define or measure. The last term, $\delta = \ell_L / L_C$ considers the one-dimensional accumulation effect of debris on a log boom module, which is assumed to corroborate significant effects on a log boom line. Debris occupy a three-dimensional space, but their accumulation pattern is only seen on the waterline plane and can be reduced to the accumulation length ℓ_L. On the other hand, laboratory measurements can provide some understanding about debris arrangement on a module along its depth and relate it to the flow velocity and how that would affect module resistance response. Hartlieb (2017) says that the backwater effect caused by a debris jam at spillways and racks has the same fundamental dependence of what one calls "debris jam compactness," which is the ratio of height to length of a debris jam. From that hypothesis, one concluded that the higher the Froude number and density ratio of debris and water, the more compact is the debris jam. In a floating structure like a log boom, the debris compactness might reach some limit

value, in which debris start to pass underneath it and affect its load response.

3.2 Catenary

Looking at Fig. 2 more carefully, we see lines of log booms protecting the intake regions of Santo Antonio HPP and directing debris to the spillway gates. From a two-dimensional point of view, considering the portion of the lines we see above the waterline, their shapes on the water surface resemble hanging cables. However, in this case, instead of being defined by gravity, their geometric form comes from the interaction with water and debris (Fig. 13). When subject to a controlled uniform flow, the shape of a line of log booms can be simplified to a catenary-like one.

Any chain or cable, neglecting its flexural rigidity, supported at its ends and hanging under its weight, when static balanced, assumes a curve shape called catenary (PAPINI, 2010). Taking a two-dimensional catenary, with mass per unit length m (Fig. 14), with extremities at P_1 and P_2 and length segment s. Placing the main axes at the inflection point and considering a symmetric curve with respect to the y-axis, the static equilibrium of forces, for this segment, on the two directions gives

$$T\cos\phi = T_0, \tag{3.18}$$

$$T\sin\phi = mgs, \tag{3.19}$$

where T and T_0 are the tension at the right and left extremity of the segment s and T_0 is also the horizontal component of T. Dividing Eq. 3.19 by 3.18 yields

$$\tan\phi = \frac{mgs}{T_0} = \frac{dy}{dx}. \tag{3.20}$$

The ratio

$$a = \frac{T_0}{mg} \tag{3.21}$$

makes it possible to write

$$\frac{dy}{dx} = \frac{s}{a}. \tag{3.22}$$

If a planar curve is defined as $y = f(x)$, being $f(x)$ continuously differentiable, the arc length s_{1-2} between two points p_1 and p_2, which are part of $f(x)$, is given by

$$s_{1-2} = \int_{p1}^{p2} \sqrt{1 + \left(\frac{dy}{dx}\right)^2}\, dx. \tag{3.23}$$

Figure 13 – Satellite picture of Santo Antônio HPP (top), showing several log boom lines; one of the lines is highlighted (middle), where its shape resembles a catenary-like curve due to stream and debris accumulation. A scale section of the log boom line is tested along IPT's Towing Tank (bottom)

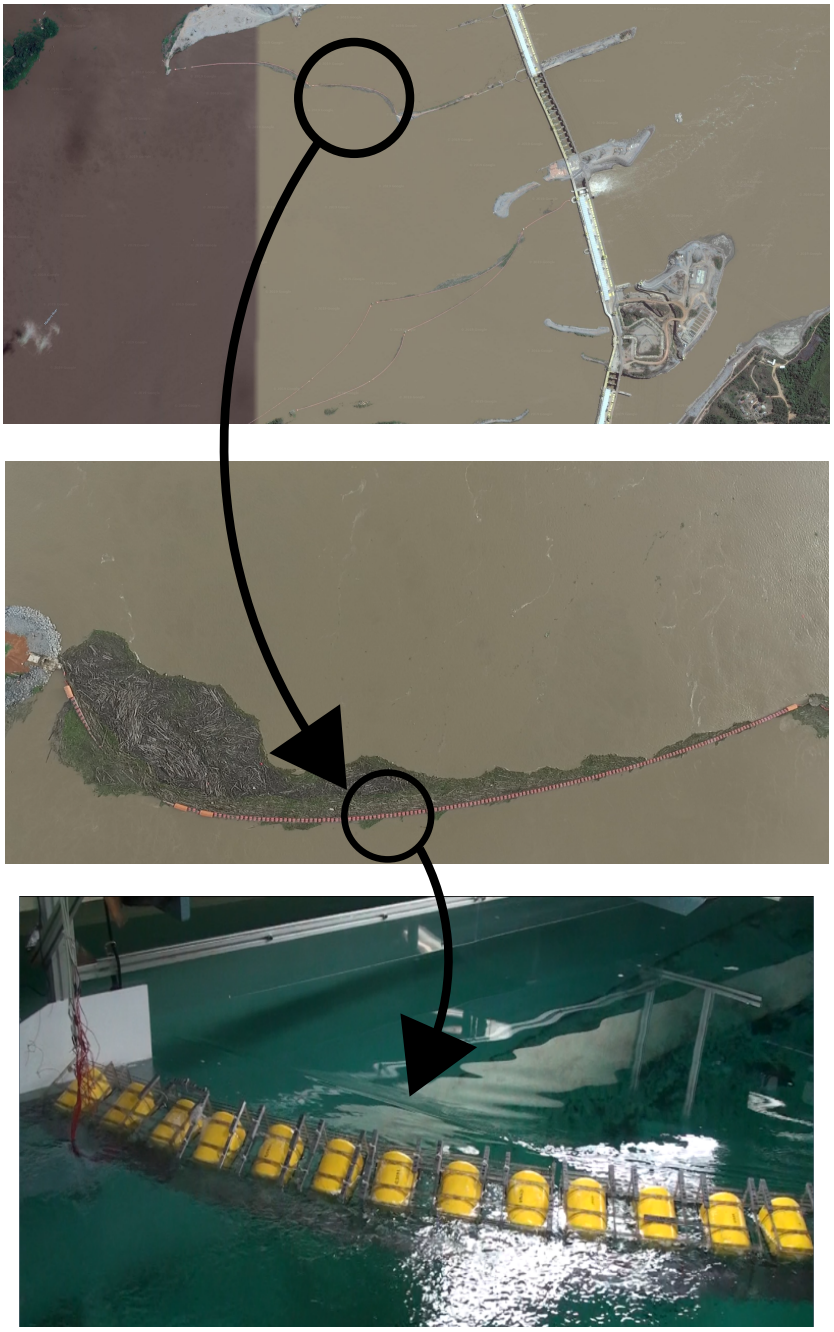

Source: Author.

Figure 14 – Diagram of forces acting on a static catenary segment

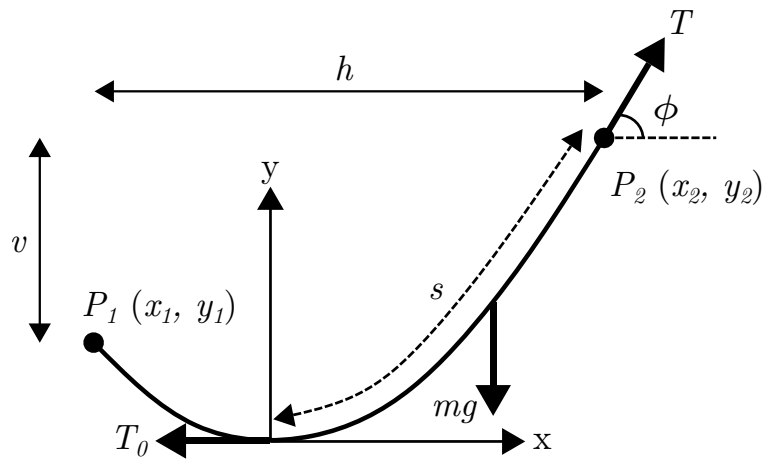

Source: Author.

Combining Eq. 3.22 and 3.23 gives

$$\frac{ds}{dx} = \sqrt{1 + \left(\frac{s}{a}\right)^2} = \frac{\sqrt{a^2 + s^2}}{a}, \tag{3.24}$$

which, after some manipulation, results in

$$\frac{dx}{ds} = \frac{a}{\sqrt{a^2 + s^2}}. \tag{3.25}$$

By integrating the previous equation, the length s is defined as

$$s = a \sinh\left(\frac{x}{a}\right). \tag{3.26}$$

Using Eq. 3.22 an 3.26 it is possible to obtain a function $y = f(x)$ that describes the catenary shape

$$y = a \cosh\left(\frac{x}{a}\right). \tag{3.27}$$

The parameter a, necessary to define the catenary curve, was initially defined as function of T_0 and mg. On practical applications, those variables are not known beforehand. Once the curve satisfies Eq. 3.27 and calling h the horizontal and v the vertical distance from P_1 and P_2, defined by the coordinates (x_1, y_1) and (x_2, y_2) respectively, the height difference can be written as

$$v = a \cosh\left(\frac{x_2}{a}\right) - a \cosh\left(\frac{x_1}{a}\right), \tag{3.28}$$

and the catenary lenght, described by Eq. 3.26, from P_1 to P_2 is

$$s = a \sinh\left(\frac{x_2}{a}\right) - a \sinh\left(\frac{x_1}{a}\right). \tag{3.29}$$

Squaring Eq. 3.28 and subtracting it from Eq. 3.29, applying some hyperbolic trigonometric identities, produces

$$\sqrt{s^2 - v^2} = 2a \sinh\left(\frac{h}{2a}\right). \tag{3.30}$$

Equation 3.30 is only dependent of geometric terms, and a can be numerically obtained. In other words, the geometric form of a catenary-like line subject to a uniform load can be determined once its holding points and length are known.

The line of log booms does not constitute a gravity-load catenary, but instead, it is a catenary-like shape due to hydrodynamic forces. This catenary model will be employed in the present study to estimate the shape of experiments with truncated lines of log booms floating on the water surface plane.

4 Experiments with a line of log booms

This section presents the development of the experimental approach. Once this study originated from a technological project conducted at IPT, the experimental methods and techniques are presented chronologically. Even presented like that, the followed steps presented a logical order, in which was necessary to understand the behavior of the system assembled as a line and then study a unitary part of this line afterward.

Initial tests were designed to understand the load pattern and dynamic behavior of a truncated log-boom line and also to qualitatively analyze how it would react in the presence of debris, making the 1st round of experiments. In order to collect more data about the motion and log accumulation, a subsequent series of experiments was conducted, measuring module heave and chassis rotation (2nd round of experiments).

A schematic diagram is shown in Fig. 15, highlighting the aspects developed in the IPT project and the scope of the present investigation. It becomes clear that the present study builds on prior understanding acquired during the first phase of the IPT project. Nonetheless, it extends the experimental investigation in another direction: the detailed investigation of a single log boom's behavior.

4.1 Methods and results of the 1st round of experiments

First experiments intended to reproduce the log booms' circumstances on Santo Antônio HPP. Hence, scale models were built to understand how they would perform as close as possible to operating conditions. At this stage, the system was designed to measure loads in the anchorage regions and module components (CASTRO; KATSUNO; DANTAS, 2017; CASTRO et al., 2017). This first battery of tests also observed some peculiarities on the log boom modules, especially their motion behavior.

4.1.1 Experimental facility

Tests were carried out at IPT, specifically on the Towing Tank of the Laboratory of Naval Architecture and Ocean Engineering (NAVAL). This towing basin is 280m long, 6.6m wide, and 4m deep, shown in Fig. 16. It is equipped with a towing carriage system, which reaches velocities up to 3.5m/s, covering its entire length.

All scale models and attachment frames construction, measurement devices assembly, and calibration procedures were executed at the prototyping, workshop, and instrumentation laboratory sections.

Figure 15 – Present investigation and IPT's R&D project structure diagrams. The solid line circled steps represent activities developed during project at IPT, while dashed line circled steps represent the scope of this work

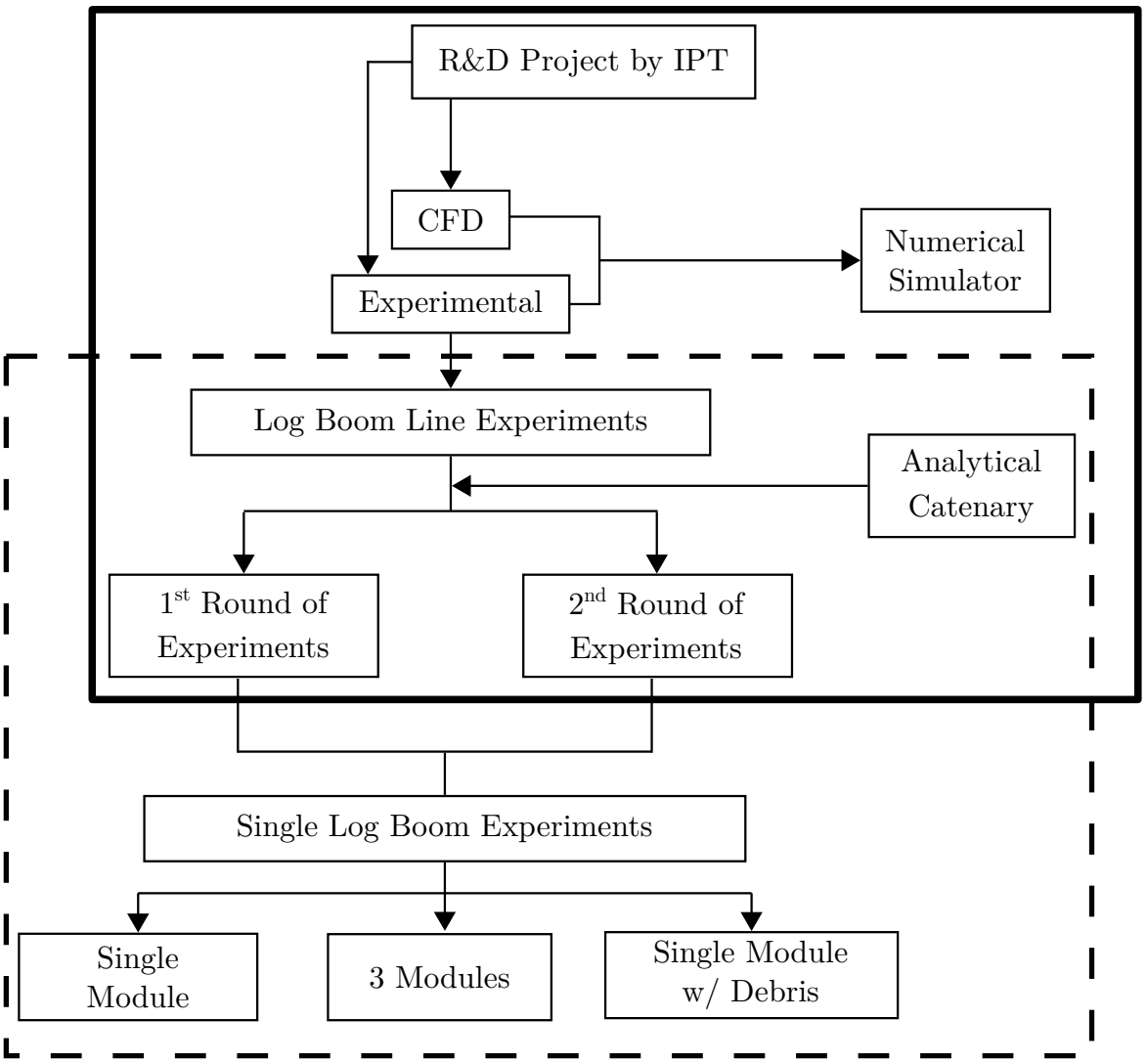

Source: Author

4.1.2 Model

Models of log booms at a 1:10 scale were chosen considering the towing tank's physical limitations, model handling, assembly, and quality of hydrodynamic load measurements. This fact also made the manufacturing process less arduous, especially on detailing. Since most of the parts in a module are I-beams, its pieces were manufactured using laser cutting techniques on thin polycarbonate sheets, except for the buoys, 3D printed, and the aluminum anchoring system. Its final design and details are shown in Fig. 17. The truncated model consisted of five to eight modules fixed on its extremities and towed along the tank.

Figure 16 – IPT's Towing Tank

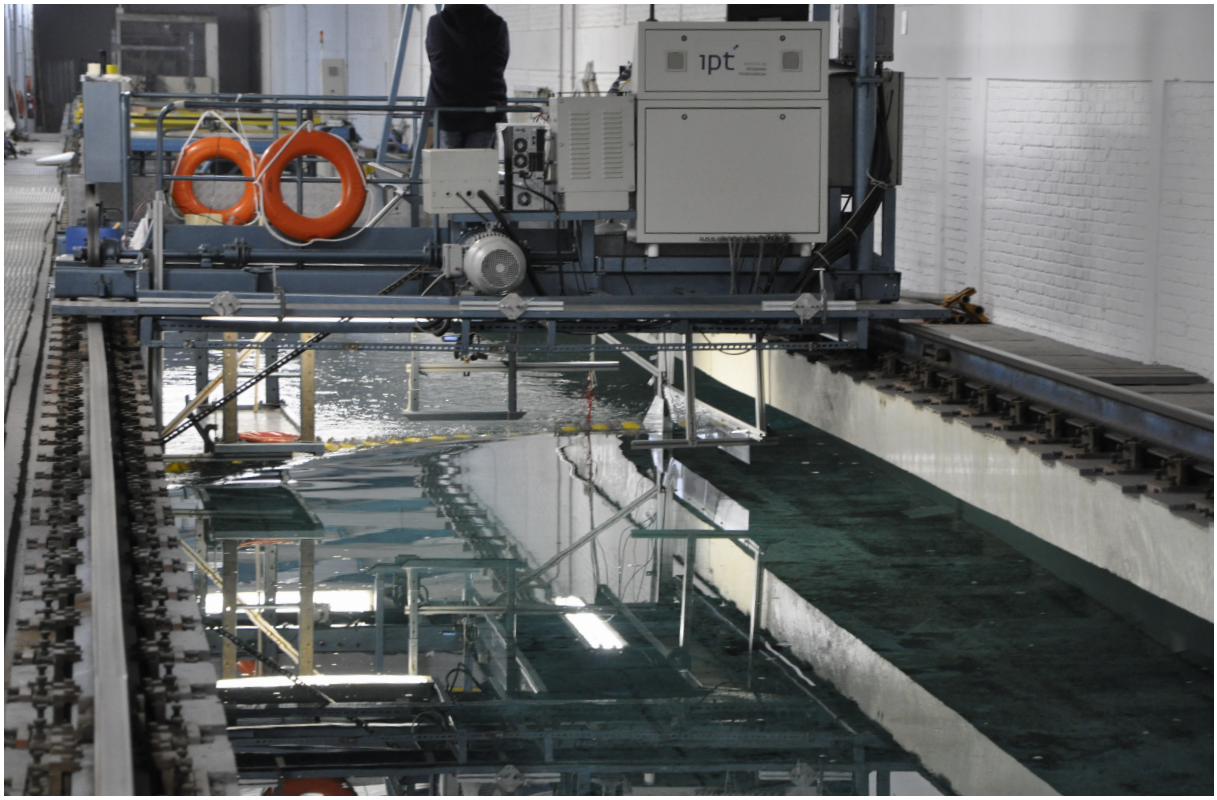

Source: Courtesy of IPT.

Figure 17 – Manufactured scale module (left) and main dimensions (right)

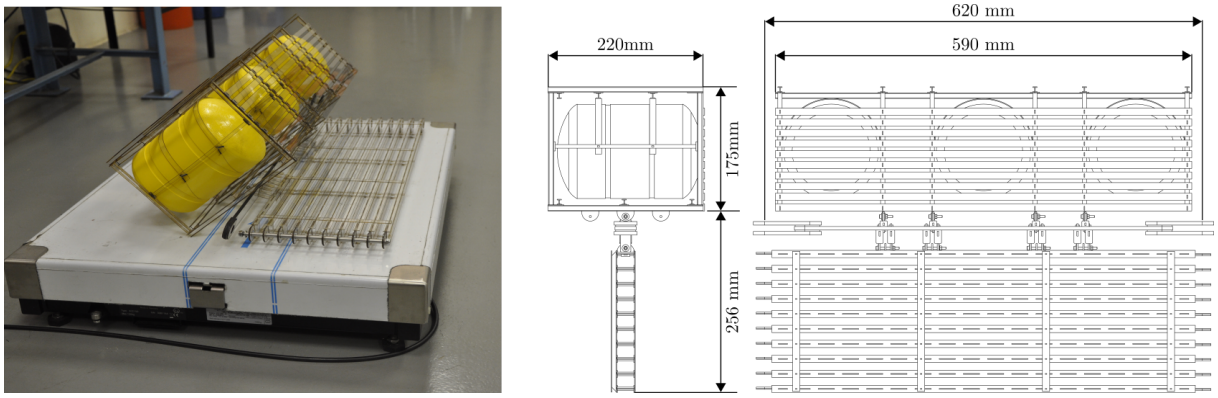

Source: Courtesy of IPT.

Figure 18 – Uniaxial load cells assembled at the model extremity

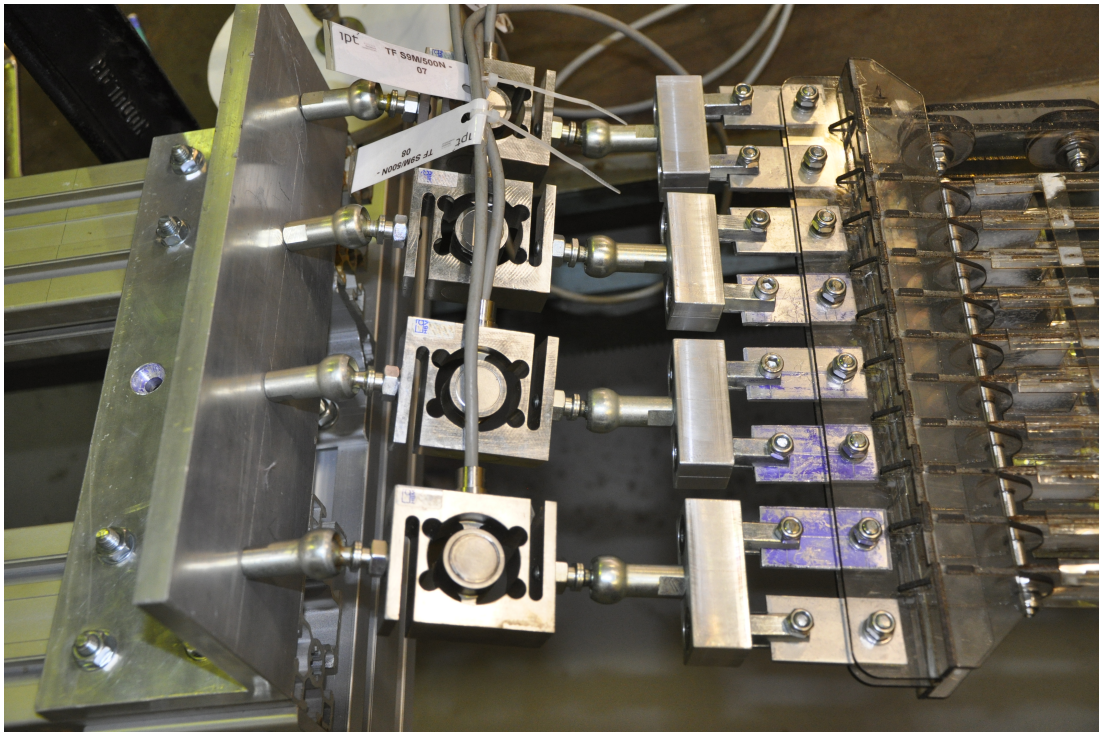

Source: Courtesy of IPT.

4.1.3 Measurement techniques

The measurements focused on the external forces acting on a truncated log-boom line's extremities. Eight S-Type S9M uniaxial load cells, produced by HBM, were used. They have a nominal measurement limit of 500N, and four of them were allocated on each side, as seen in Fig. 18. They measured tension and compression, whether their responses were positive or negative, respectively. A data acquisition system by Lynx (model A2161 and A2164) was used to condition signals and convert them into digital format.

4.1.4 Set up

From Computer Aided Design (CAD) models and knowing the density of all elements, it was possible to find out the weight distribution of a log boom module and estimate draft and trim values for the hydrostatic configuration. Ballast weights were set on top of the model, altering the model frontal area as minimum as possible.

As an actual log boom line assumes a curvature on the free surface due to water flow, hence the towing structure was designed to allow the line to alter its shape and then its reference angle to the free stream. T-slot profiles were set to allow the line's extremities to move transversely and longitudinally and lock the line during experiments. A pair of end plates was fixed on the sides and towed together to reduce interference from measuring devices and support structures and control flow incidence. Tests were planned to maximize

the number of runs without modifying its geometrical format, considering the devices' hard access.

A Froude number (Fn) similarity was adopted, assuming it as a surface-flow problem with a sharp-edged floating body, where the model is expected to have a low dependency on Reynolds number. Towing velocities u_M at the model scale were obtained from river stream velocities u_R, calculated from Froude number similarity law and function of the scale factor $\lambda = L_R/L_M$

$$\begin{aligned} Fn_M &= Fn_R \\ \frac{u_M}{\sqrt{gL_M}} &= \frac{u_R}{\sqrt{gL_R}} \\ u_M &= \frac{u_R}{\sqrt{\lambda}}, \end{aligned} \tag{4.1}$$

where L_M and L_R are characteristic lengths of scale model and real prototype, respectively.

Line nominal angle and Froude number were adopted as test variation parameters. Nominal angle (θ), formed by a straight line connecting extremities and a line perpendicular to the incoming flow direction, was defined by the number of modules along with transversal (d_T) and longitudinal (d_L) distances. A schematic representation is shown in Fig. 19. While the left side was fixed, the right side was able to translate to adjust θ.

From the previous analytical catenary formulation, the model line's geometry is ideally and primarily assumed as a catenary-like shape on the waterline plane, which is influenced by the stream and debris affecting the line's structural response. That assumption worked as an estimation for the truncated line inclination. Based on that, and once its length is known, anchorage points and expected shapes could be analytically predicted, along with the expected position for each module of the line, allowing the model to be placed appropriately.

4.1.5 Results

This section brings results for the 1st round of experiments and first impressions that guided the decisions taken to conduct the study. Each test condition was repeated at least once.

A schematic representation of line shapes for these experiments is shown in Fig. 20. Asterisks represent articulations, and their entire length was considered, including the load cells, placed as first and last elements of each line (Fig. 18).

To ensure that the instrumentation could produce reliable results, the symmetrical configuration ($\theta = 0°$) with five modules was assumed as a reference case and, by definition, should produce similar load results on both anchorage points. Figure 21 shows the resistance force, i.e., the simple sum of forces on the load cells on each side, for multiples runs without

Figure 19 – Schematic representation for the 1st round of log boom experiments

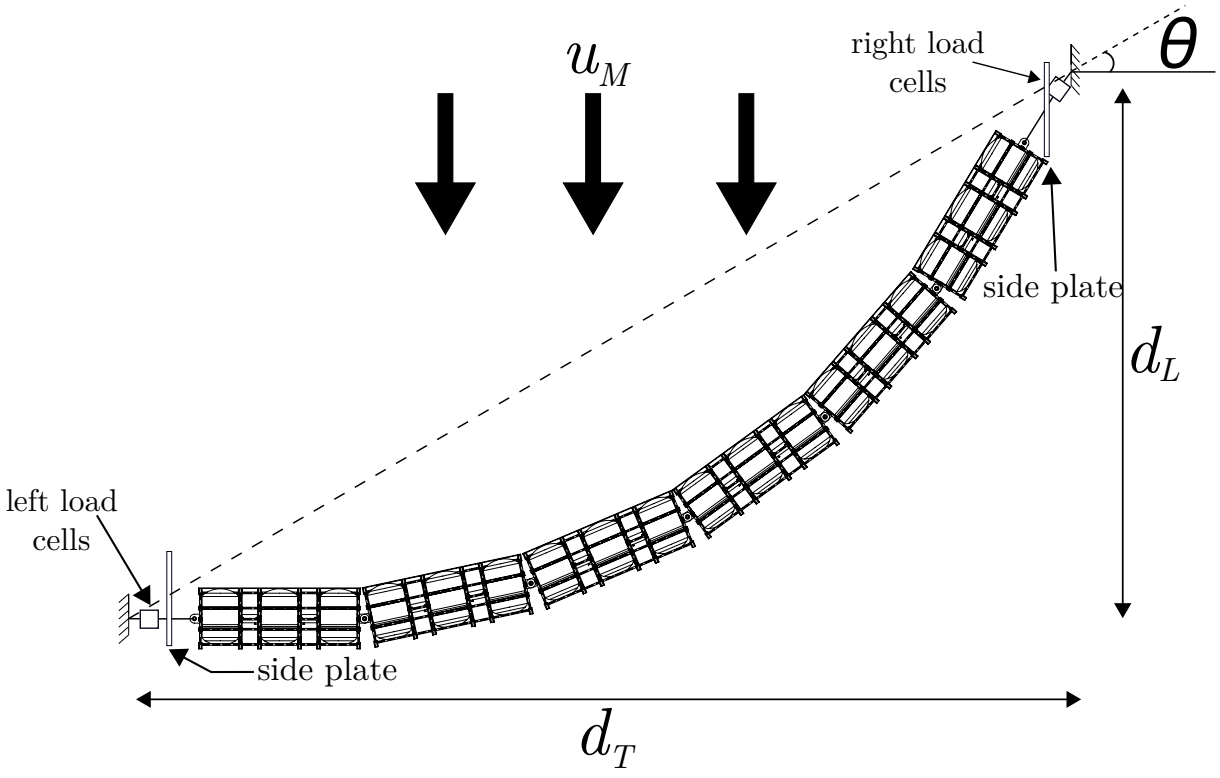

Source: Author

debris, for five modules increasing Fn. Results show equivalent resistance values on both sides, with a quadratic behavior with respect to Fn.

The effect of the line nominal angle θ is seen in Fig. 22 and 23 by the variation of modules amount. Results are presented as the total resistance (R_T) measured on load cells and in terms of a non-dimensional coefficient (C_T) calculated as

$$C_T = \frac{R_T}{\frac{1}{2}\rho u_M^2 n L_M D_s}, \tag{4.2}$$

where n and D_s stand for the number of modules and hydrostatic draft, respectively.

Even with more modules, it was possible to observe a reduction in the total load with the increase of incidence angle θ, which becomes more evident for higher Fn. However, from a certain Fn upwards and given their inclination with respect to the flow, they tended to rotate backwards its upper chassis and heave downwards completely (Fig. 24), which increased their wet surface together with the hydrodynamic resistance. For the tested scenarios, low θ values combined with the increased wet area play a more important role in the total measured force than the number of modules at the line with increased θ. Additionally, the upstream anchorage point presented higher loads than the opposite side, which is expected by the line's catenary-like aspect on the water surface.

Figure 20 – Geometrical representation of model lines in the waterline plane, for the 1st set of experiments based on the catenary formulation

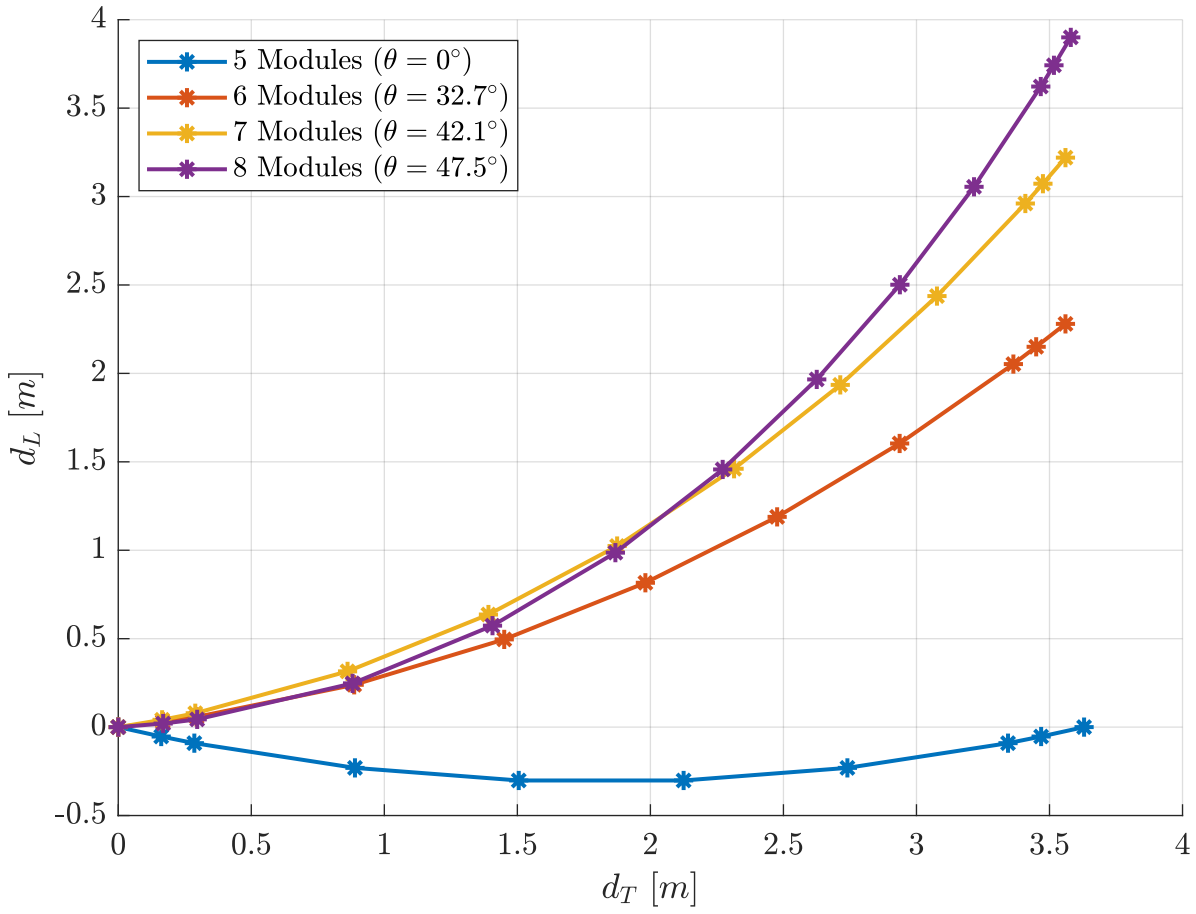

Source: Author

4.1.6 Conclusion

The 1st round of experiments was intended to measure forces on truncated lines of log booms for some number of modules and nominal angles in a flow without debris. The total resistance presented results inversely proportional to its nominal angle (θ), where low values of θ mean high values of total resistance, even with fewer modules. Simultaneously, heave and trim motion were observed in the model with the increase of Fn.

Following tests will investigate the load response of a line in the presence of debris and measure the heave and trim motion of some modules.

Figure 21 – Total resistance (R_T) as a function of Fn for the 5-module symmetrical configuration ($\theta = 0°$) with no debris

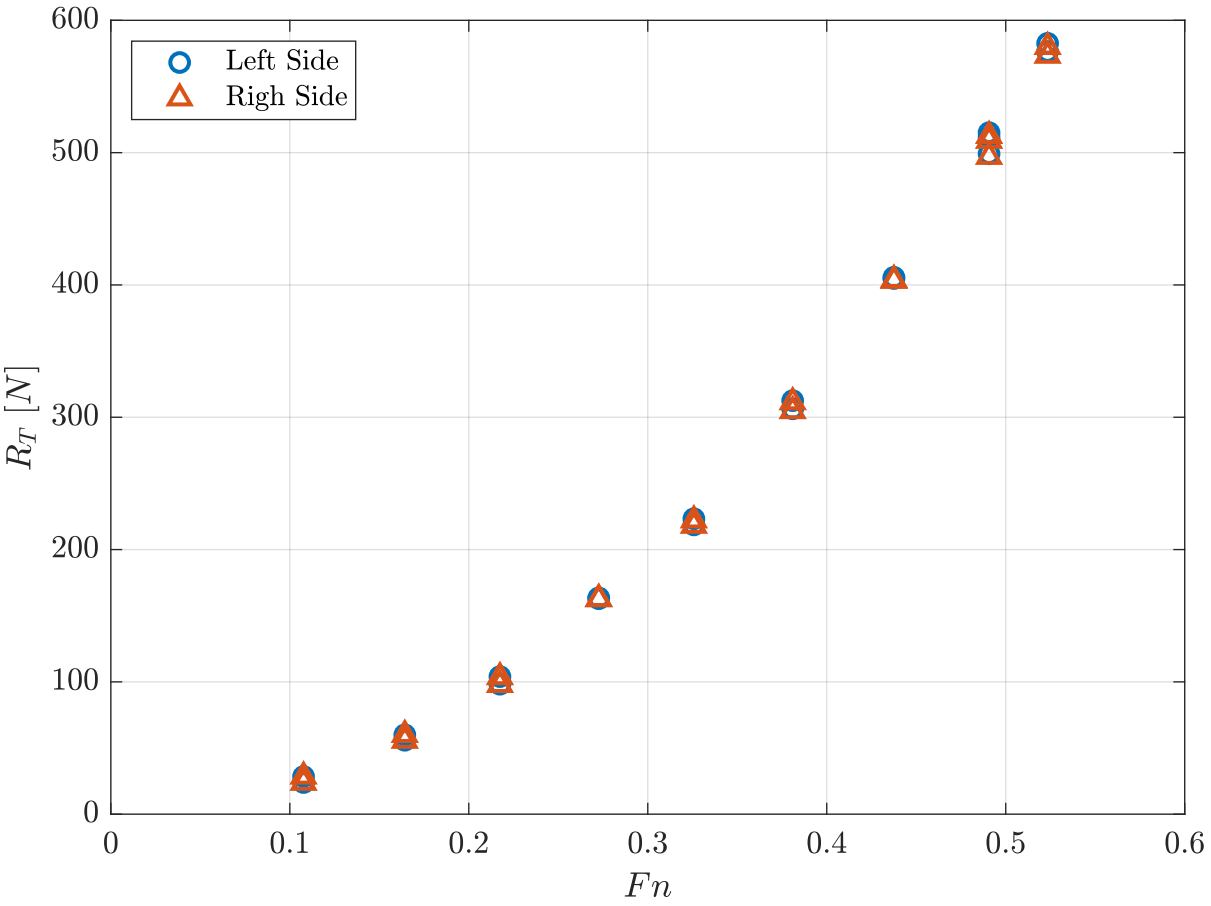

Source: Author

Figure 22 – Total resistance on left and right extremities as a function of Fn, for each configuration

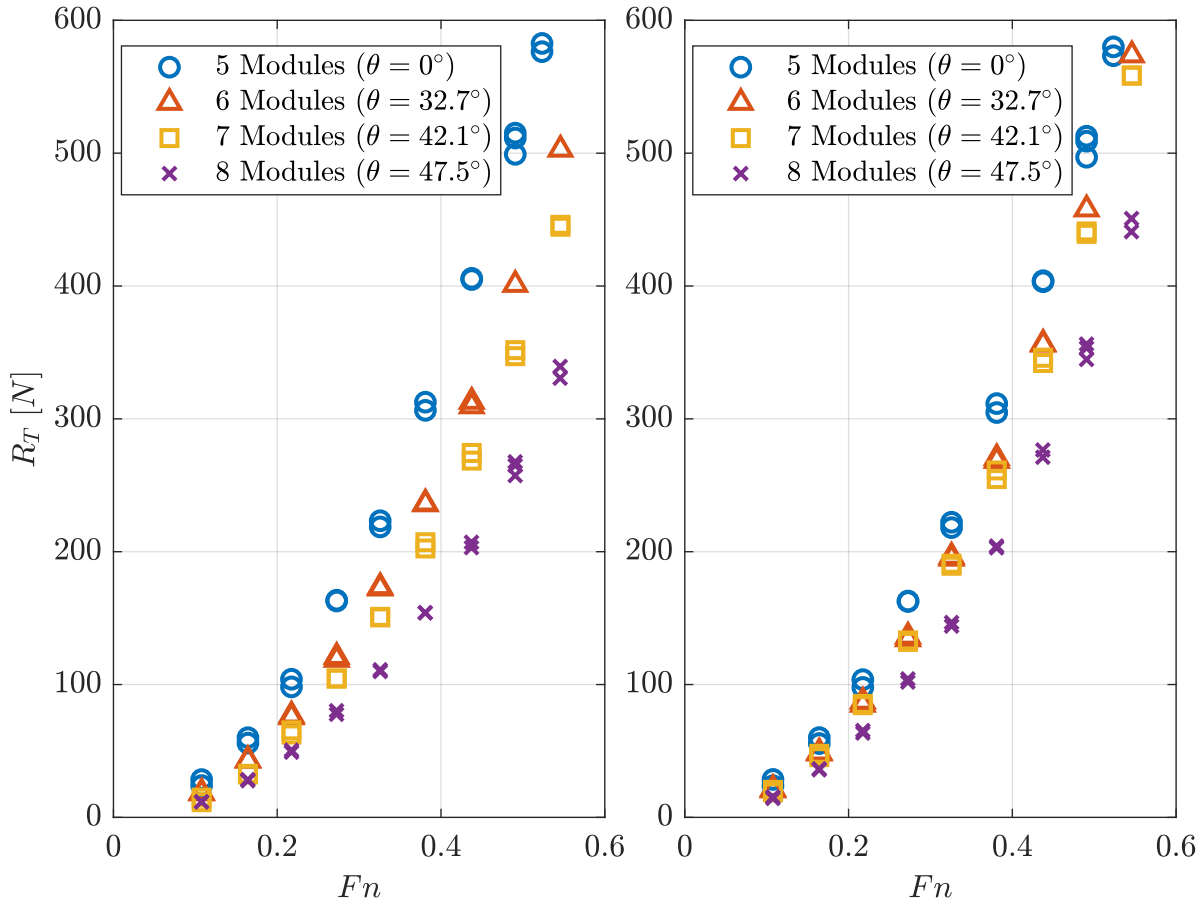

Source: Author

Figure 23 – Coefficient of total resistance on left and right extremities as a function of Fn, for each configuration

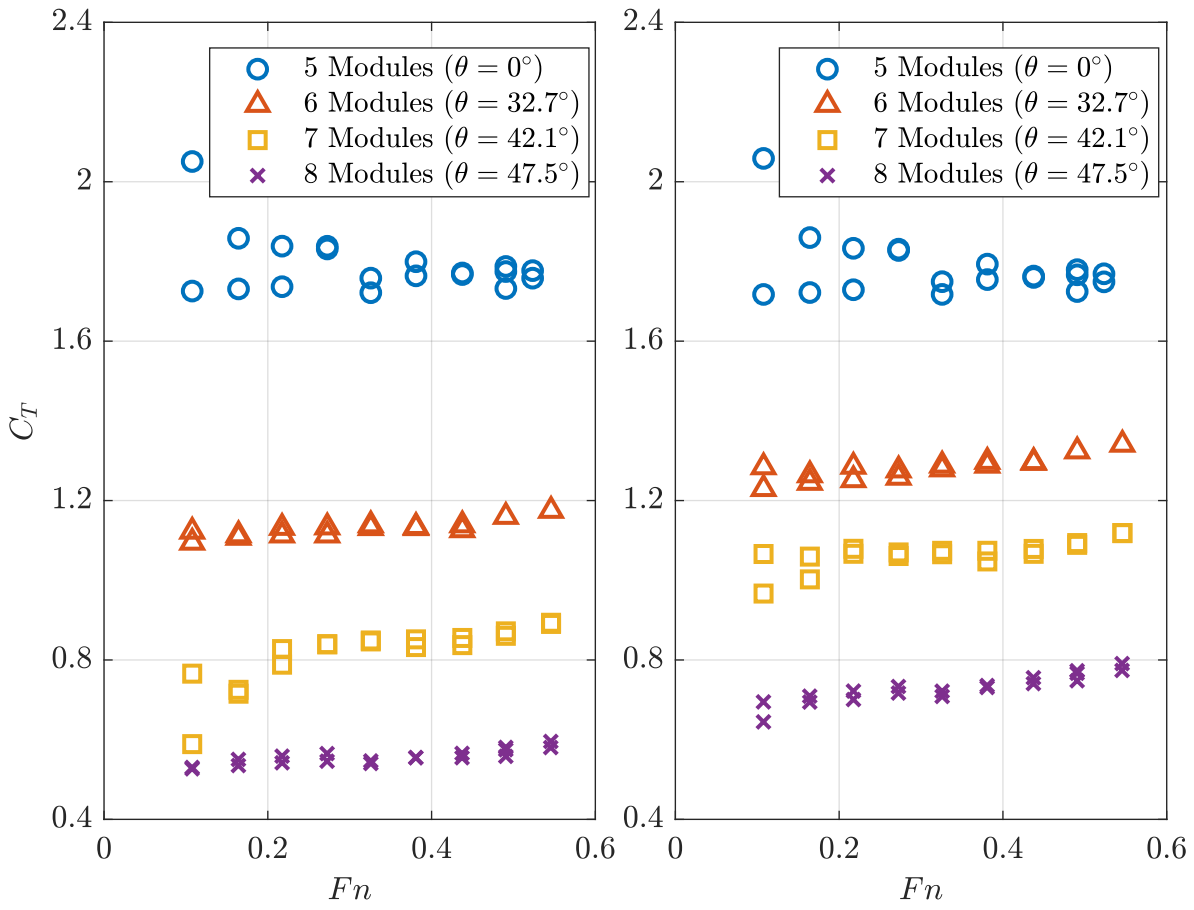

Source: Author

Figure 24 – Experiments conducted on the 1st round with several Fn values. The chassis tends to rotate and the entire module heaves downwards

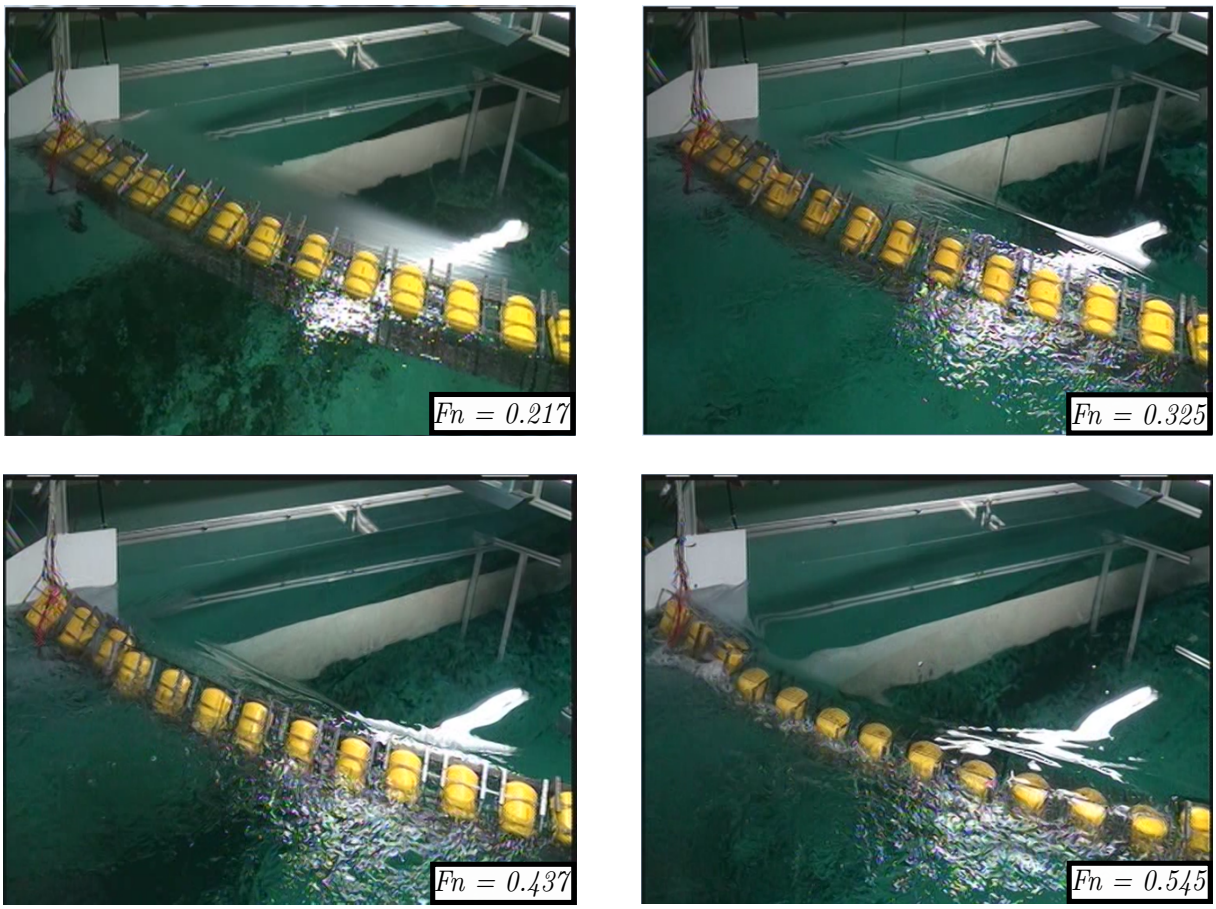

Source: Author

Figure 25 – Side and parametric view of an adapted module with spherical targets at static position

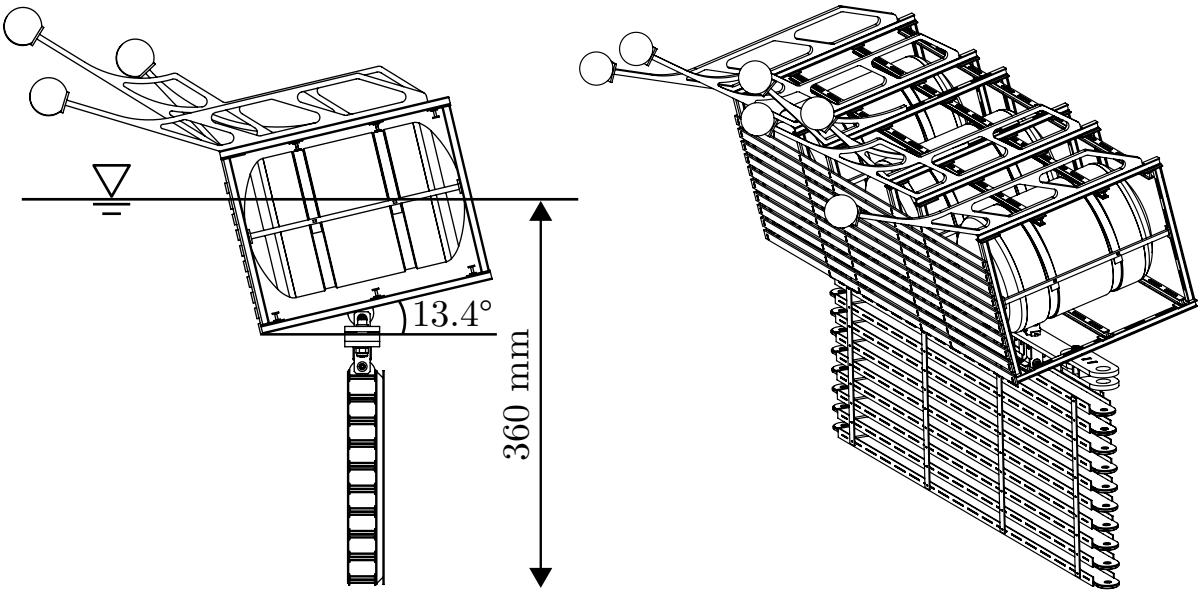

Source: Adapted from Dantas (2018).

4.2 Methods and results of the 2nd round of experiments

From the first group of experiments and given its operational significance, vertical translation of modules and rotation of chassis were interpreted as a coupled motion, influenced by the flow velocity and angle, as seen in Fig. 24. This 2nd round of tests was designed to investigate that phenomenon and track loading on the line extremities with five distinct volumes of debris retained by the line. Aside from these changes, this sequence of tests resembled the previous one methodologically.

4.2.1 Model

The log boom model did not undergo any major modifications, except for installing a motion tracking system, which uses spherical reflexive targets settled on top of the chassis of two modules, located in the center and at the upstream end of the truncated line. Due to its submersion tendency, external rods were installed to place the targets, preventing them from getting wet, which could affect measurements. Figure 25 shows the model after modification, at its static draft (D_s) and chassis pitch angle (α).

4.2.2 Scale debris

Cylindrical pine-wood rods were used to simulate the effect of debris given their simple volume estimation and the fact they are less susceptible to get waterlogged comparing

Table 1 – Specifications, amounts, and volume of debris during 2nd round of experiments

Ø [mm]	16					23					32							
length [mm]	200	300	400	600	900	200	300	400	600	900	200	300	400	600	900	total pieces	total volume [m³]	% of total volume
D_0	0	0	0	0	0	0	0	0	0	0	0	0	0	0	0	0	0	0%
D_1	49	69	49	18	17	49	69	49	18	17	23	32	23	9	8	499	0.075	16%
D_2	98	138	98	37	34	98	138	98	37	34	46	64	46	17	16	999	0.151	33%
D_3	196	277	196	74	68	196	277	196	74	68	92	129	92	34	32	2001	0.303	66%
D_4	393	553	279	74	68	393	553	279	74	68	183	258	137	34	32	3378	0.459	100%

Source: Author

to natural wood sticks. Five different lengths (up to 900mm) and three different diameters (up to 32mm) were adopted. Debris accumulation over the model line was investigated by running out tests considering five increasing log jamming levels located upstream. Table 1 describes quantities and characteristics of the scale debris.

4.2.3 Measurement techniques

The modules' motion was tracked by three infrared cameras from Qualisys, model Oqus 500, through the reflective targets previously mentioned. With a proper calibration procedure, it was possible to accurately capture the rigid body's motion in six degrees of freedom. Limited by the number of cameras, the goal was to measure the steady pitch and heave motions for two modules, assumed as rigidy body motions.

Four new S-Type S9M uniaxial load cells, with a load limit of 1000N, were added to each side to promote a more detailed measurement and determine which components were being more structural required during the tests. Moreover, to more faithfully represent a real prototype line of log booms, structures used to anchor the line to the pillars installed upstream Santo Antônio HPP, here called tie rods, were 3D printed and connected to the extremity of the modules and then attached to the load cells. Their calibration process with the tie rods is shown in Fig. 26.

4.2.4 Set up

Using the same apparatus from previous tests, θ, Fn, and debris concentration were now taken as variables. Acrylic panels were fixed on the sides of the towed frame to guide wooden debris towards the line. Debris were randomly disposed at the upstream region of the model and dragged along with it as it was towed along the tank. Schematics in Fig. 27 shows the main components of the setup in tests with debris. At this time, experiments were conducted with 5 and 7 modules, and only two modules — central and lateral — had their motion tracked.

Figure 26 – Tie rods in real size (left) being installed and calibration check adjustment of those in scale (right), with 8 load cells at each side

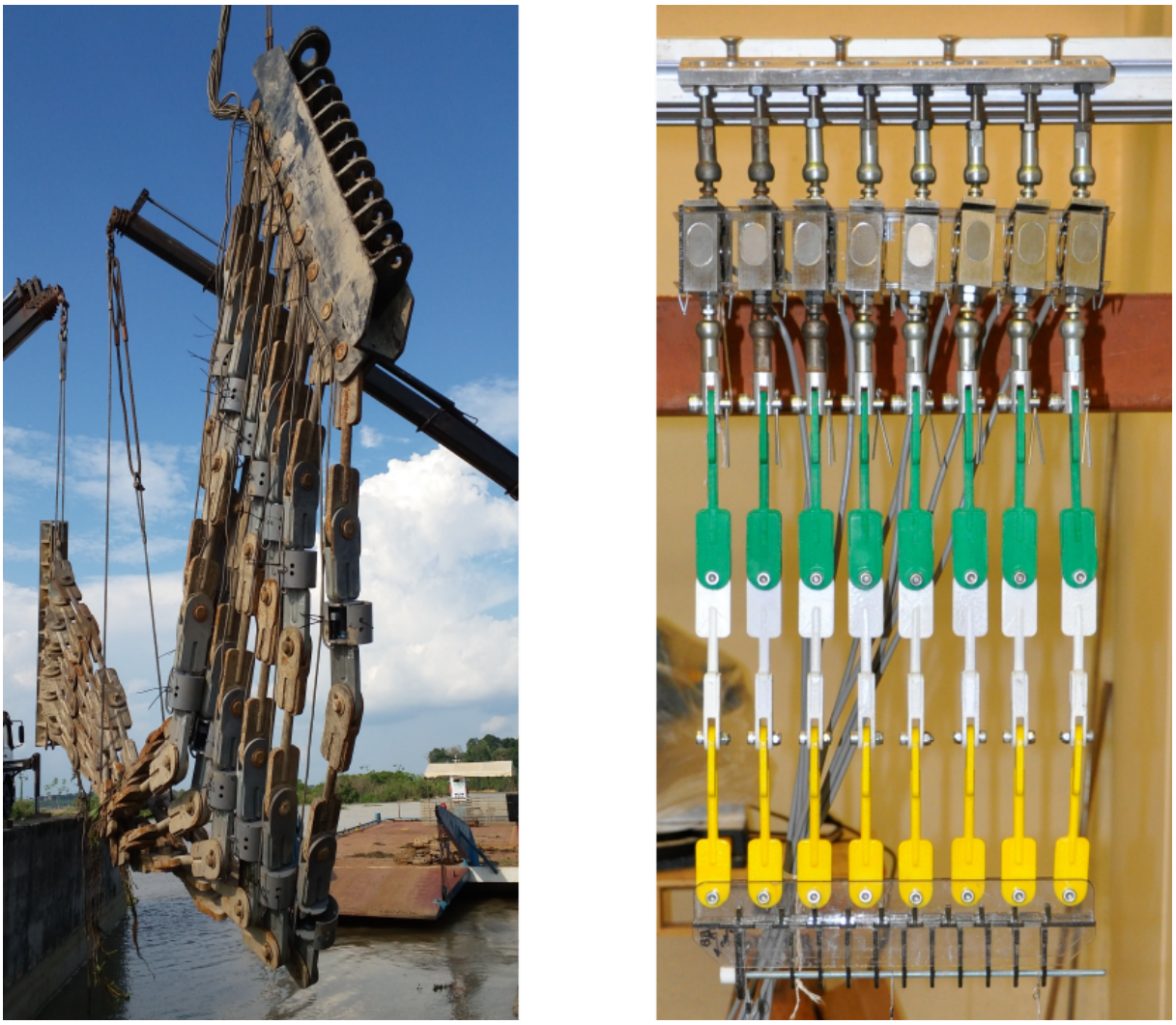

Source: Dantas (2018).

4.2.5 Results

This section brings results for the 2nd round of experiments, focusing on modules motion and the effect of debris accumulation on the model. Each test condition was repeated at least once.

The expected line shapes, due to upstream flow only, for these experiments are shown in Fig. 28, based on the catenary formulation. Dotted lines represent tie rods, and load cells were placed as the first and last elements of each line (Fig. 26). Central and lateral modules are highlighted. Yaw angles for central and lateral modules on the 7-module configuration were expected to be higher than that for five modules.

Heave motion (H) over hydrostatic draft (D_s) as a function of Fn for a flow with

Figure 27 – Schematic representation for the 2nd round of log boom experiments

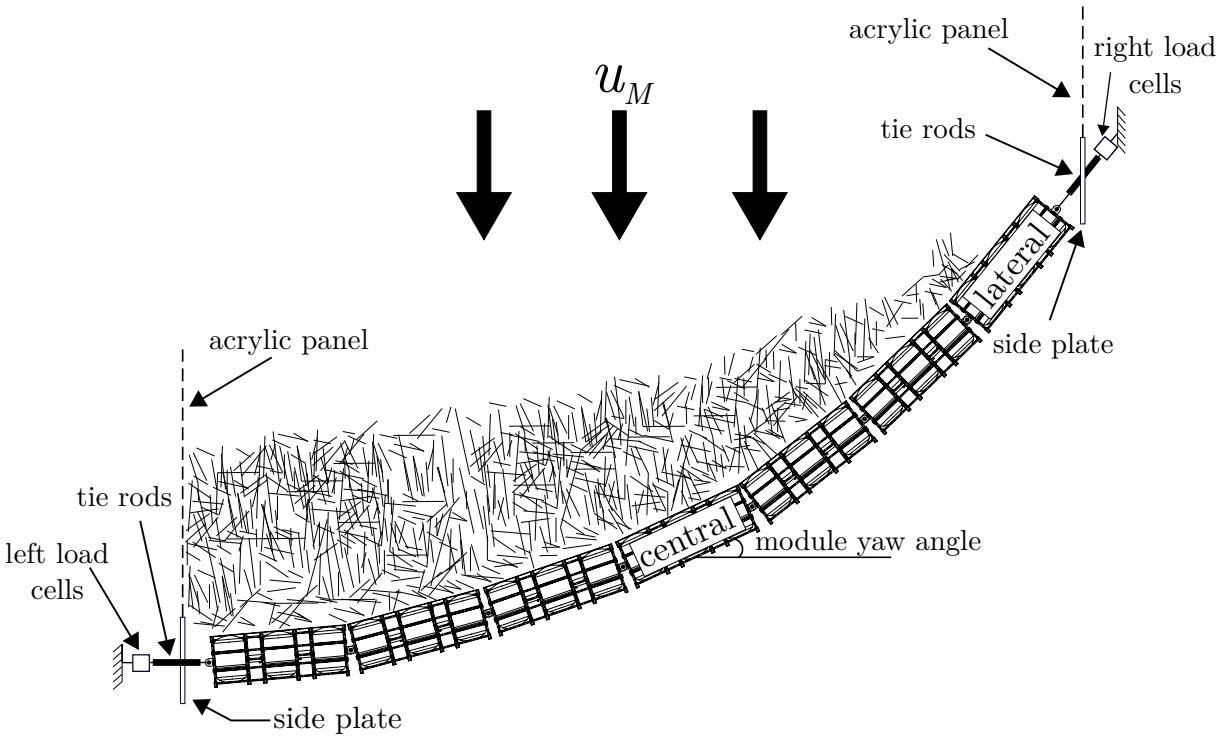

Source: Author.

no debris is presented in Fig. 29. Results represent steady-state heave ratio values in which positive results indicate heave motion downwards. Modules with different yaw angles (β) presented low increases of the draft for $Fn < 0.5$ (less than 10%). After that range, modules with low yaw angles — 5-module central and lateral — presented a nonlinear increase of draft with respect to Fn. The central module got fully submerged, excepted for the reflective targets, at the highest tested Fn. On the 7-module configuration, the central module presented the same increase behavior, but at $Fn > 0.6$. The module with the highest expected β — 7-module lateral — did not present a significant change in H/D_s compared to the other three modules.

Figure 30 shows module pitch angle, in degrees, as function of Fn for the instrumented bodies, without debris. Pitch angle (α) is referenced at the static equilibrium condition, shown in Fig. 25, in which negative values represent clockwise rotation, assuming the side view of Fig. 25 as reference. Pitch motion was inversely proportional to the module yaw module (β), having a nonlinear behavior with respect to Fn for $Fn > 0.5$ on the 5-module configuration, which is very similar to heave. This effect tended to reduce for modules with higher β values, represented on the 7-module configuration.

Figures 31 and 32 present the resistance behavior of the line with five modules for all debris accumulation levels. Non-dimensional values follow the formulation presented

Figure 28 – Geometrical representation of model lines in the waterline plane, for the 2nd set of experiments

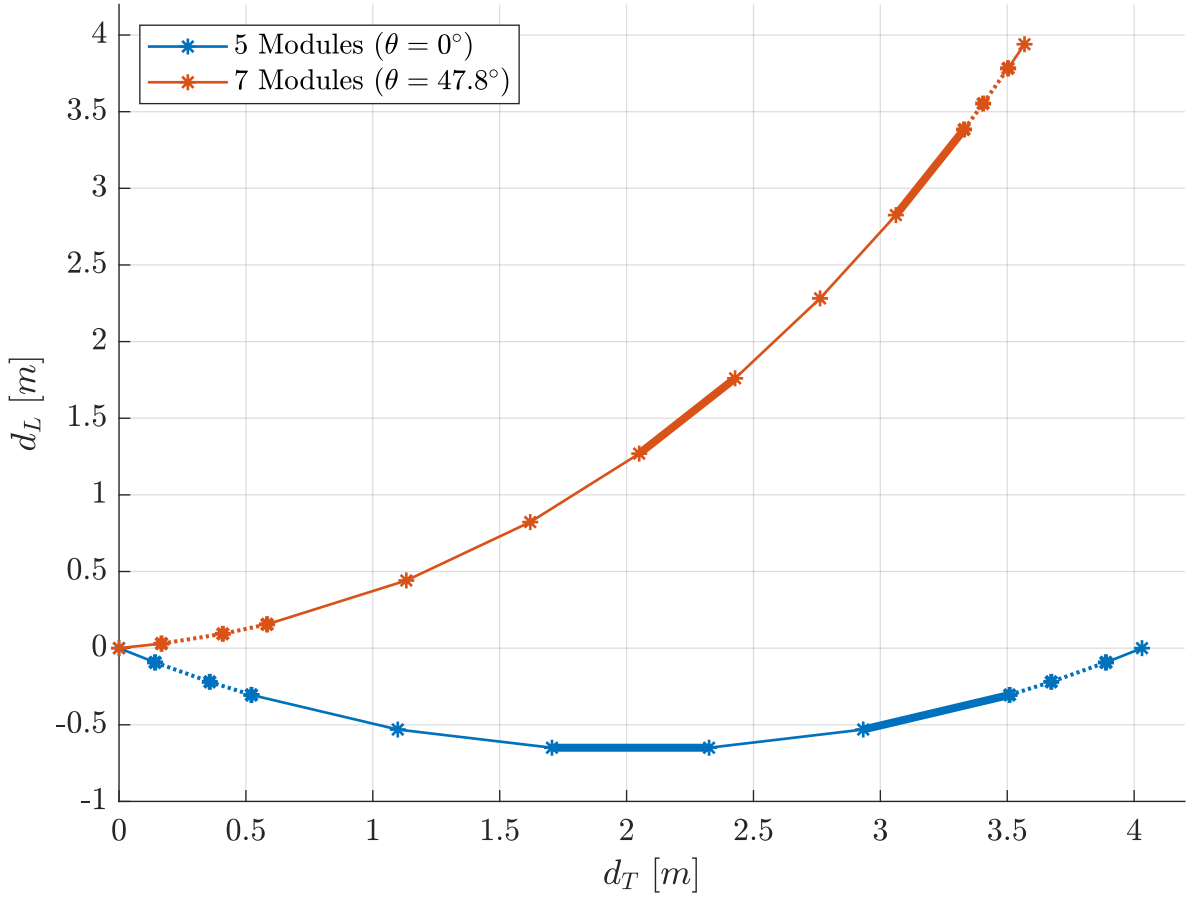

Source: Author.

in Eq. 4.2. There are some changes in measured forces with respect to the volume of debris. Force behavior has been higher in some of the D_2 and D_3 tests for the highest Fn values. However, a direct relationship in which higher volumes of debris implied higher forces could not be observed. That is because in Fig. 32 values occupied the regions below and above the reference curve that represents experiments without debris. That variation might be related to the fact that this configuration ($\theta = 0°$) tends to heave downwards almost entirely, leaving enough space for debris to pass above the line and, as Fn gets higher, to start to compact onto the line and some part of it pass underneath the model, shown in Fig 33.

In the 7-module configuration (Fig. 34 and 35), force response presented higher values at the upstream right end, as expected, even in the presence of debris. Also, results presented less variety compared to the symmetric configuration of five modules, which is seen by the number of values above the blue reference line. Debris accumulation levels D_3 and D_4 increased the force response, seen at most of the regions above the reference

Figure 29 – Heave downwards over static draft (H/D_s) as a function of Fn for tests without debris

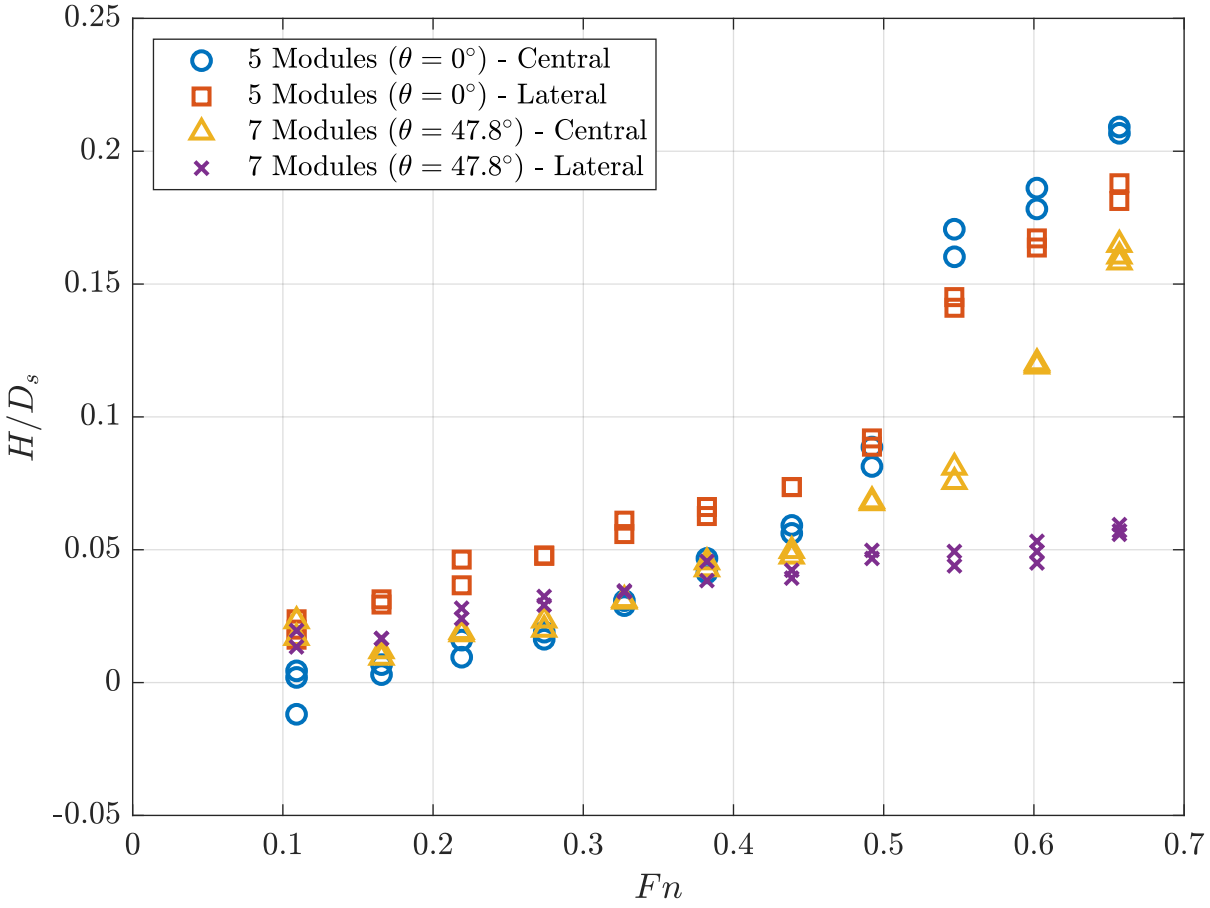

Source: Author.

curves in Fig. 35.

Because of the log boom line's inclination, debris tended to move to the left side, i.e., the downstream end (Fig. 36), sometimes reaching some of the load cell loads, affecting their measurement. As the total resistance force was composed by the simple sum on the load cells, negative results at low Fn values for certain load cells do not necessarily indicate a compression behavior on the line as a whole. On the other hand, the right end presented a tension behavior for most of the Fn values.

The presence of debris affected the motion of the line, sometimes avoiding the sinking behavior of the line, but in a random way. Motion measurements were done in test with debris and are discussed by Castro and Dantas (2019).

It is important to note that debris accumulation did not seem to meet any local pattern, characterized by data variability of force response, even in a laboratory-controlled condition. This effect should be more significant on the real size log boom, mostly because debris come from all direction and the velocity profile is not precisely known.

Figure 30 – Pitch angle (α) as a function of Fn for tests without debris

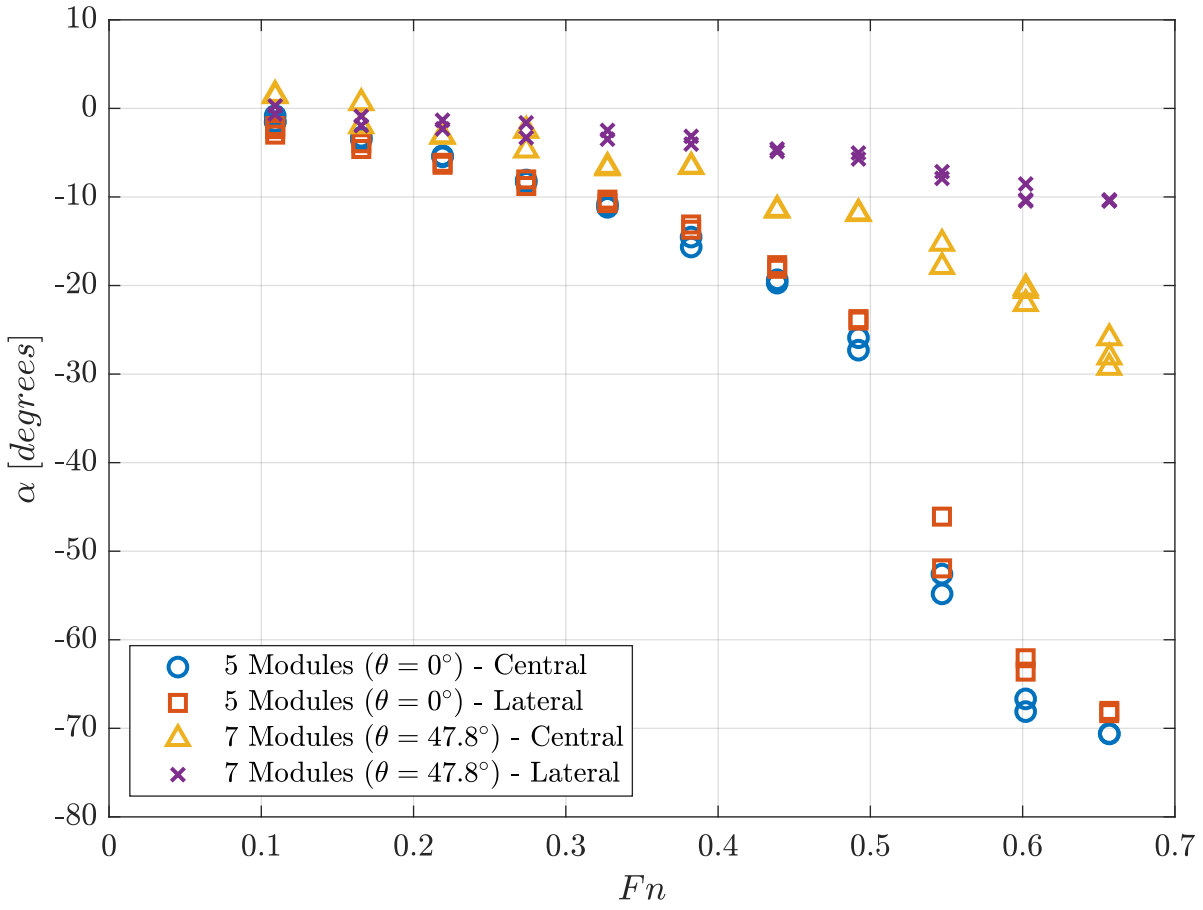

Source: Author.

4.2.6 Conclusion

In the present section, tests showed a coupled motion of pitch and heave motion for the truncated line, which seems to be present in a log boom line subject to uniform flow. The magnitude of these motions was associated with the module yaw angle (β) and Fn, where the highest values of Fn induced part of the model's submersion. $Fn \leq 0.3$ represented less than 5% of draft change and less than 10° in terms of pitch angle modification in tests without debris.

Total resistance on a truncated line model has been measured, with distinct nominal angles (θ) and debris accumulation levels. The incidence of large volumes of debris affected the resistance force. The 5-module configuration ($\theta = 0°$) increased total resistance at some runs in scenarios with high Fn values but with a significant variation. Meanwhile, the 7-module configuration ($\theta = 47.8°$) presented minor result variation, where high volumes of debris led to higher resistance values for most of the runs compared to scenarios without debris.

Figure 31 – Total resistance on left and right ends as a function of Fn, for tests with debris accumulation levels, in a 5-module configuration ($\theta = 0°$)

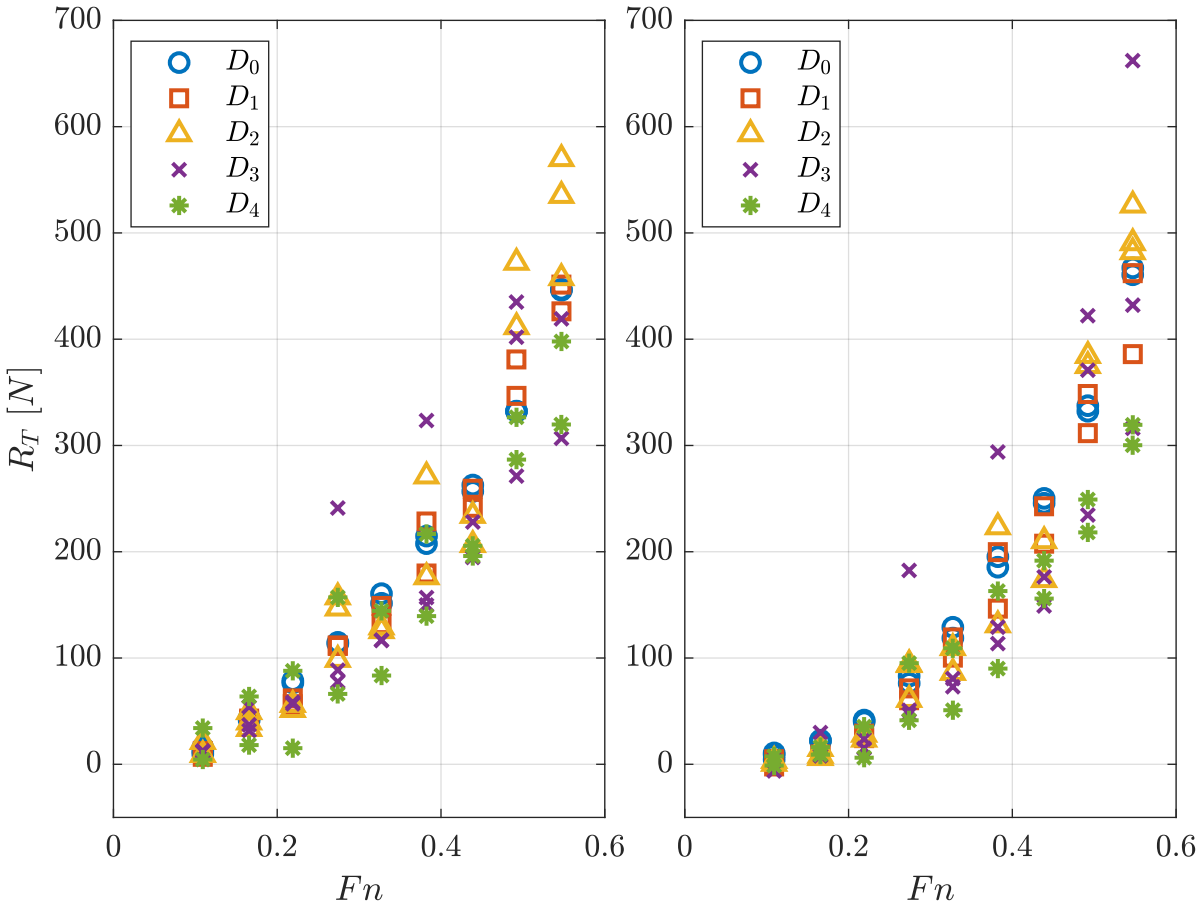

Source: Author.

Even had been randomly distributed at the upstream region of the line, debris accumulated close to the downstream end. It is important to notice that effect, even though qualitatively. As modules are pieces of the log boom line, the effect of debris on the force behavior might produce more conclusive results if analyzed individually. The next chapter will investigate a single module's force behavior, with the interference effect of adjacent modules and effects caused by wooden debris.

Figure 32 – Comparison among coefficients of total resistance on the left and right ends as a function of Fn, for tests with debris accumulation levels, in tests with five modules ($\theta = 0°$). The highlighted curve represents tests without debris on that configuration

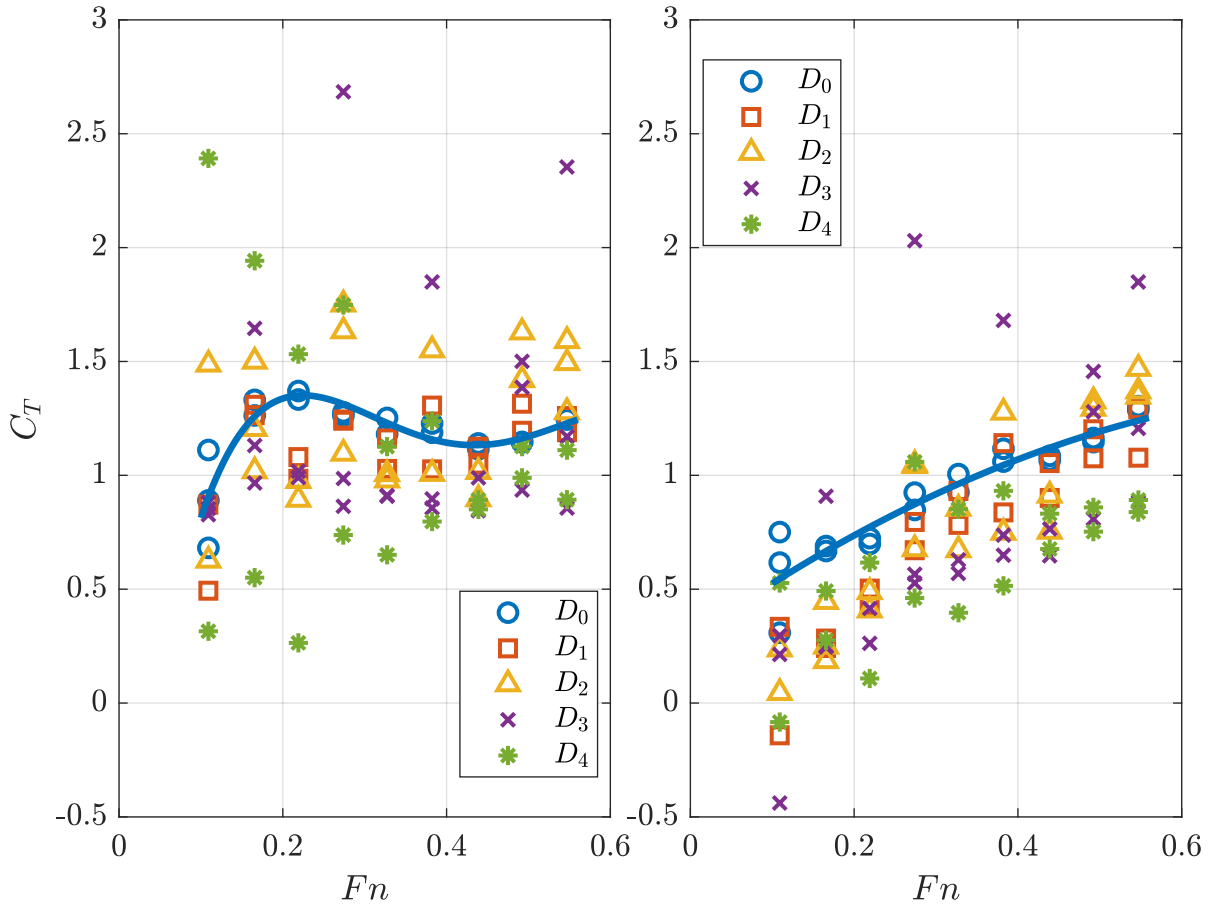

Source: Author.

Figure 33 – Emerged and submerged view of tests with debris

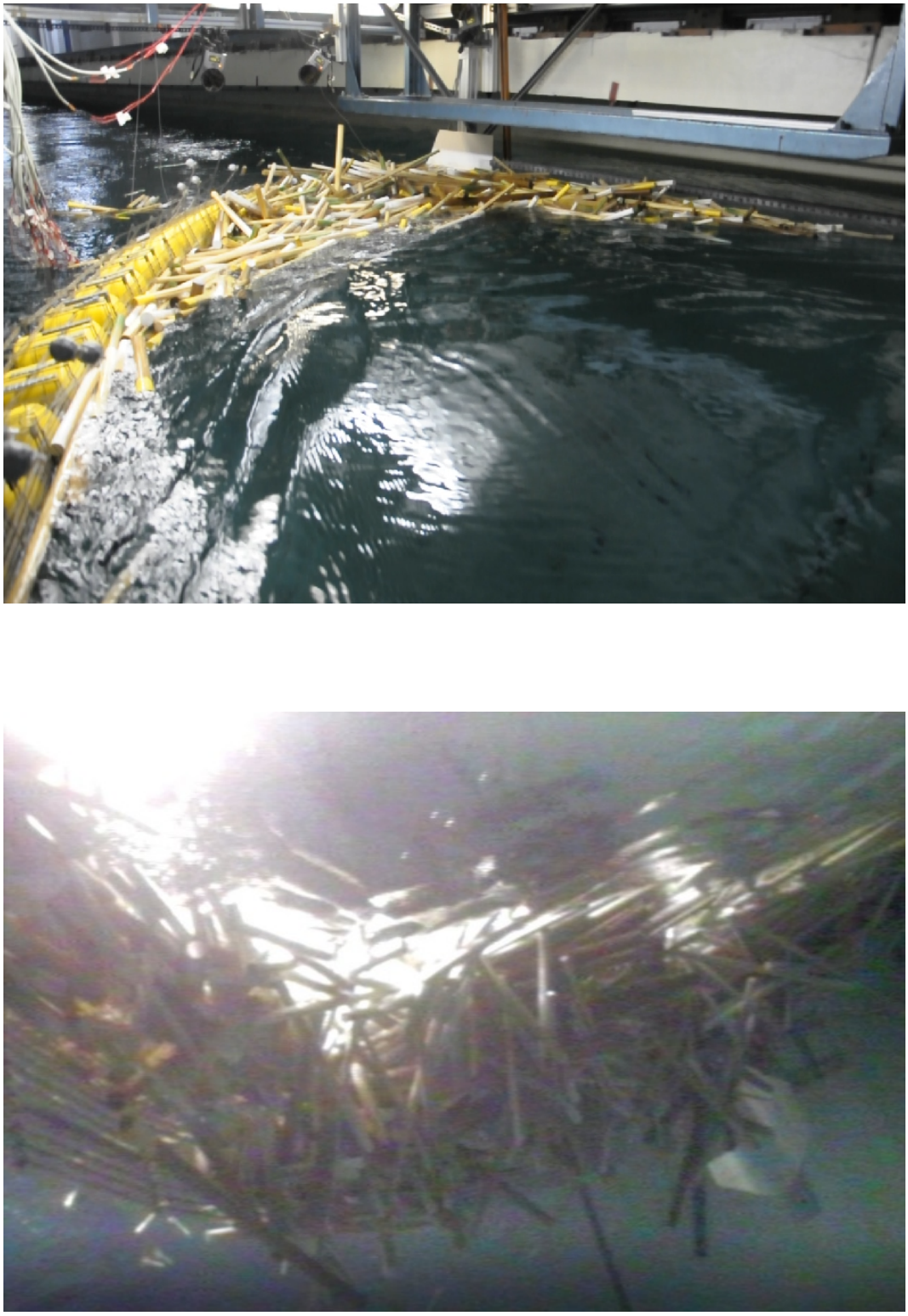

Source: Author.

Figure 34 – Total resistance on left and right ends as a function of Fn, for tests with debris accumulation levels, in a 7-module configuration ($\theta = 47.8°$)

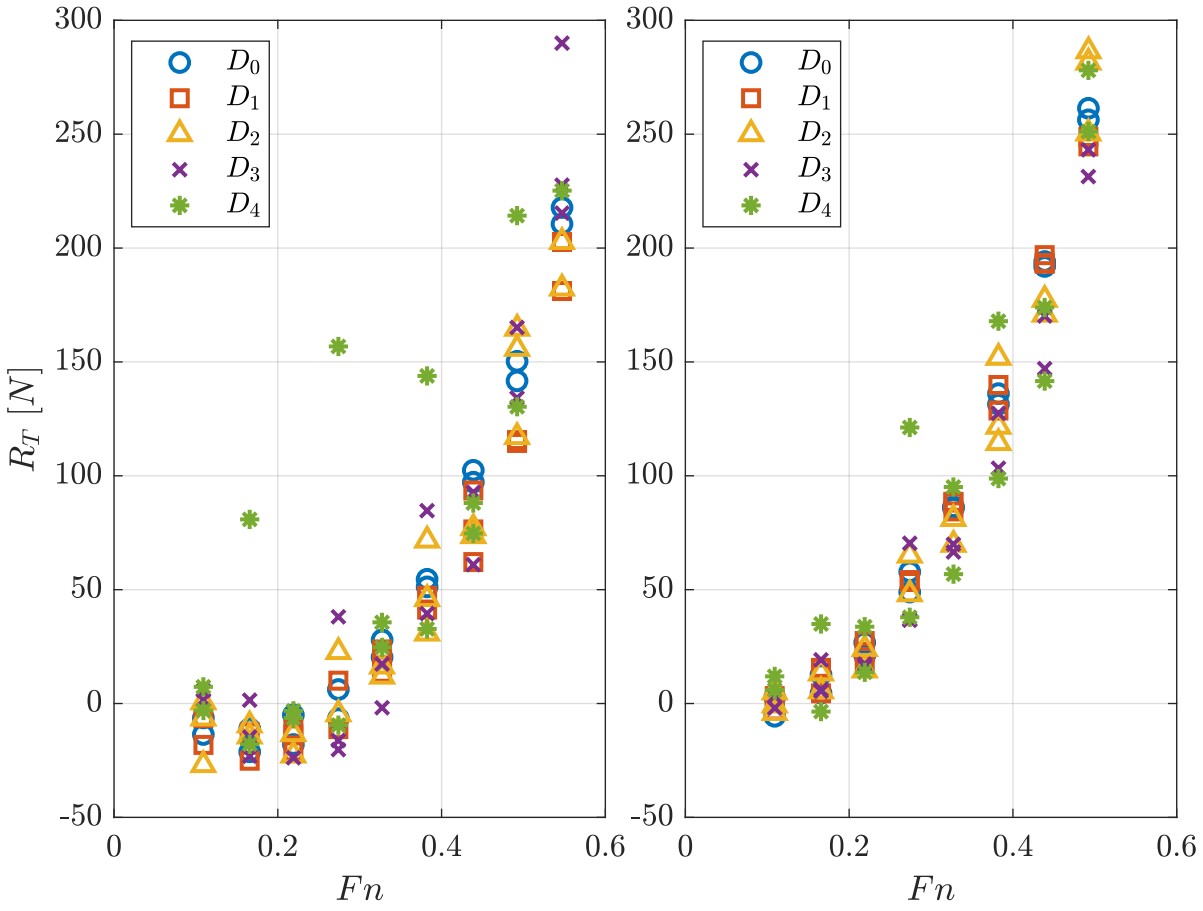

Source: Author.

Figure 35 – Comparison among coefficients of total resistance on the left and right ends as a function of Fn, for tests with debris accumulation levels, in tests with seven modules ($\theta = 47.8°$). The highlighted curve represents tests without debris on that configuration

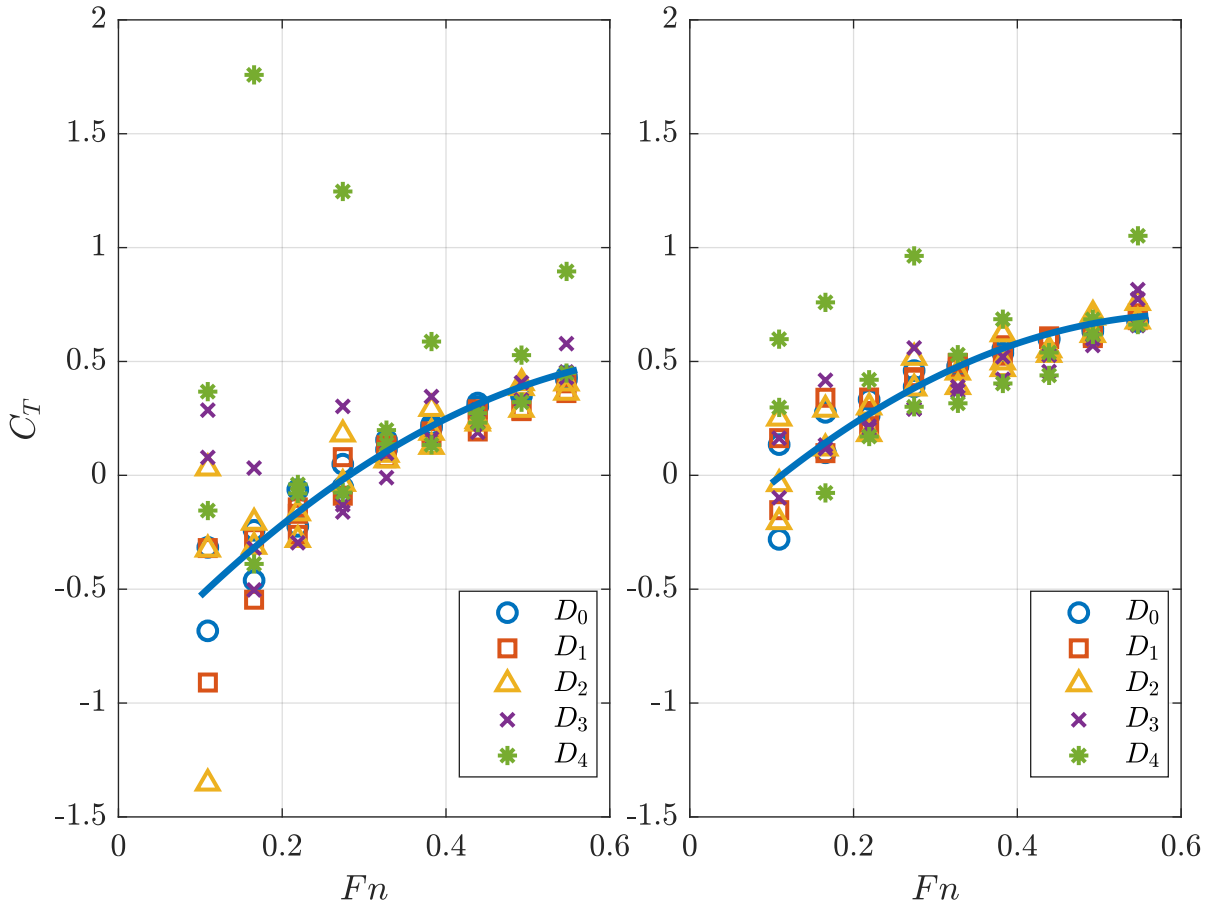

Source: Author.

Figure 36 – Test with debris on the 7-module configuration. Debris tended to occupy the downstream end, given the shape of the line

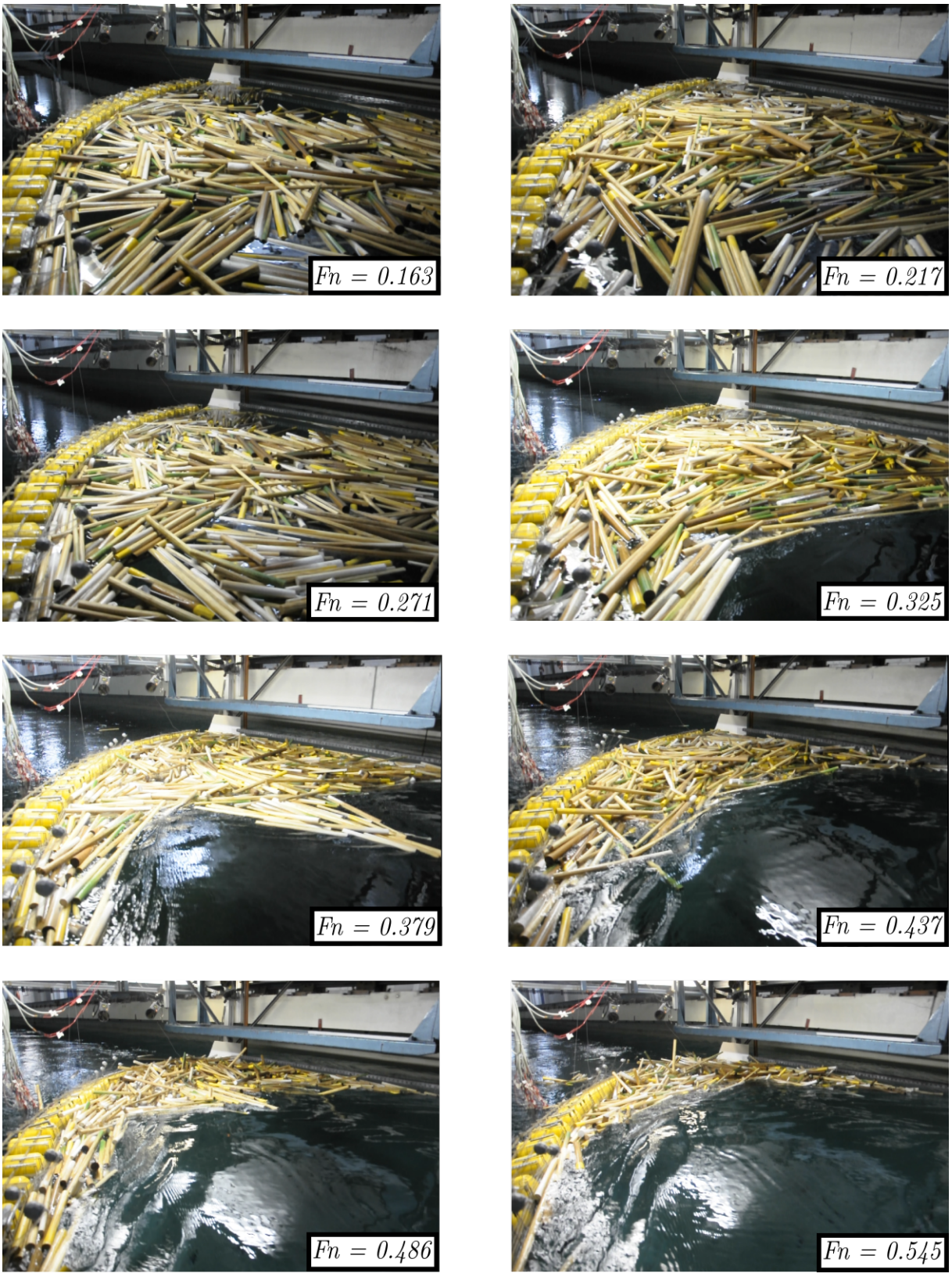

Source: Author.

5 Single log boom experiments

Based on the results of the previous tests, experiments using captive scale modules have been designed to understand the following phenomena:

- The hydrodynamic loads on the individual body of a line of log boom (single module).
- The interference effects from adjacent bodies (three lined up modules).
- How debris are spatially distributed upstream of the log booms, and how debris affect the resistance response (single module with debris).

Following hydrodynamic tests consisted in the 3rd round of experiments.

5.1 3rd round of experiments

Previous tests have shed some light on the behavior of the log boom. In terms of its dynamics, we can state that the heave and pitch behavior at high Fn are issues to be addressed appropriately. Furthermore, line inclination angle θ has been a variable that affected model resistance and log accumulation. At the local module, line inclination is represented by the module yaw angle β. In order to gather information on the hydrodynamic loads acting on the modules, a new experimental apparatus has been assembled to measure forces and moments on a single scale model at varying Fn and β.

This last round of experiments was conducted at both IPT and NDF facilities. The main objective was to obtain the hydrodynamic resistance of a single module and the interference effect of neighboring modules with and without debris. The expected results will be taken in terms of drag, lift and moment non-dimensional coefficients

$$C_D = \frac{F_D}{\frac{1}{2}\rho u_M^2 A}, \tag{5.1}$$

$$C_L = \frac{F_L}{\frac{1}{2}\rho u_M^2 A}, \tag{5.2}$$

$$C_M = \frac{M}{\frac{1}{2}\rho u_M^2 A L_M}, \tag{5.3}$$

where A and L_M are adopted as the reference area and length of the model, respectively.

Figure 37 – NDF's Water Channel

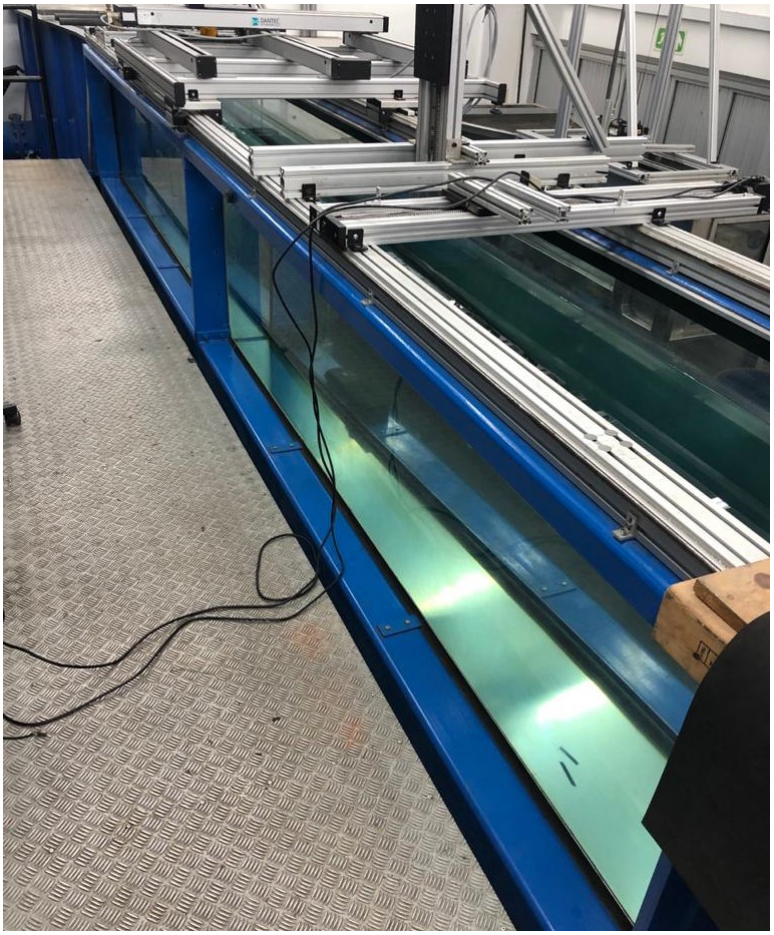

Source: Author.

5.1.1 Experimental Facility

While some tests of the third campaign took place at the much wider IPT's Towing Tank, to avoid blockage effects, the other part of the experiments was performed at the recirculating Water Channel of the NDF research group at Escola Politécnica of the University of São Paulo. The channel has a test section that is 0.7m wide, 0.9m deep, and 7.5m long (Fig. 37), with transparent sidewalls and bottom, allowing for the use of flow visualization techniques. The upper part is equipped with a model attachment rig. The free stream can reach velocities up to 1.0m/s. Its particulars were valuable to conduct tests with scale debris, mainly in terms of flow observation. A detailed description of the recirculating water channel was presented by Assi (2005).

5.1.2 Model

One of the challenges to conduct hydrodynamic experiments with an individual log boom module without anchoring its ends and representing only its natural motion (pitch and heave) would be to restrain the other degrees of freedom. Since the motion behavior

depends on Fn, it was decided to fix a limit for it and to perform tests in a captive model, i.e., locking its degrees of freedom, on a two-dimensional static approach. The followings changes had been done on the model to attend this hypothesis:

- To couple a top structure to attach the model on a rig. Since the model pieces are fragile, given their thickness, it consists on a polycarbonate plate to hang the module uniformly. Besides that, an aluminum wedge was installed to offset the hydrostatic pitch angle.
- To lock the reinforced beam to the grid with a lateral axis. Also, to attach four corner brackets along the model width to either lock the grid rotation movement and mitigate its larger-scale vibrations.

It is important to notice that since most of the model pieces were made from 1mm-thick polycarbonate sheets, they became naturally flexible for some small movements. This movement did not have much expression and were neglected. A schematic representation is shown in Fig. 38.

5.1.3 Measurement Techniques

Force and moment measurements were performed using a six degrees-of-freedom load cell, Mini58 SI-700-30 model, produced by ATI. It consisted of a compact and monolithic cylinder transducer, as presented in Fig. 39. The load cell was mounted on top of the model, as close as possible to the waterline plane projection center.

5.1.4 Set up

The model was set up on a rig, adapted to fit on both IPT and NDF facilities. The rig had a protractor attached to it, and the yaw angle could be manually adjusted. The model was assumed symmetric, varying β from 0° up to 90°, only in the counterclockwise direction.

The first step was to measure the hydrodynamic forces and moments, in terms of non-dimensional coefficients, experienced by the single captive module varying upstream velocity u_M and yaw angle β, without debris. Measured forces were assumed to be acting on the waterline plane, under a static regime, with Fn ranging within limited experimental scale values. From previous section results, we concluded that $Fn \leq 0.3$ did not represent a significant heave and pitch motion experience by the modules, so we assumed that might not represent a significant change on the project area of the model, and then was chosen as the limit value for the further experiments. Moreover, this value was close to the acceptable limit force expected for the model and the 6DOF load cell's safe operation.

Figure 38 – Model schematic representation for the 3^{rd} round of log boom experiments. Free stream flows in the x-axis direction

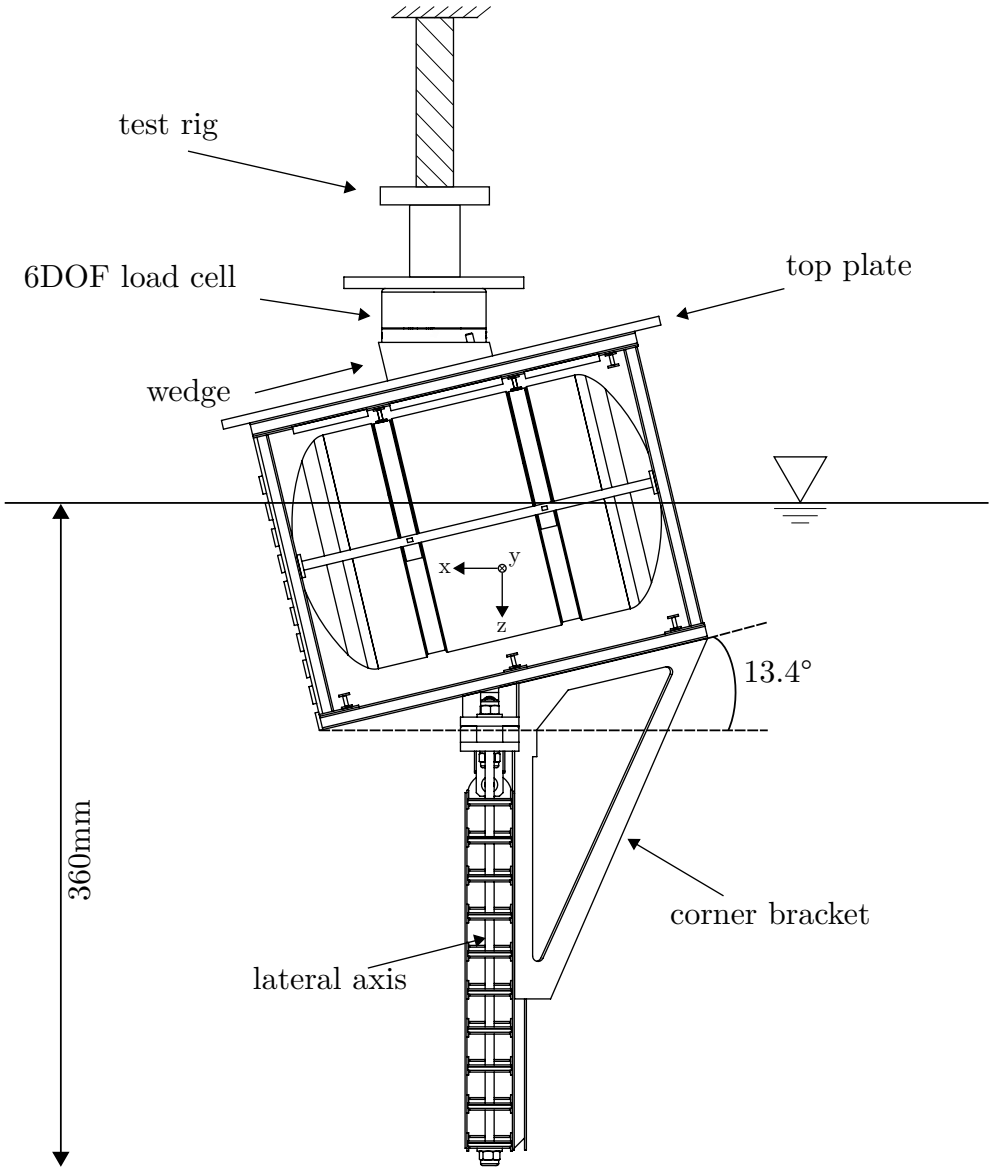

Source: Author.

Figure 39 – 6DOF load cell during calibration checkup

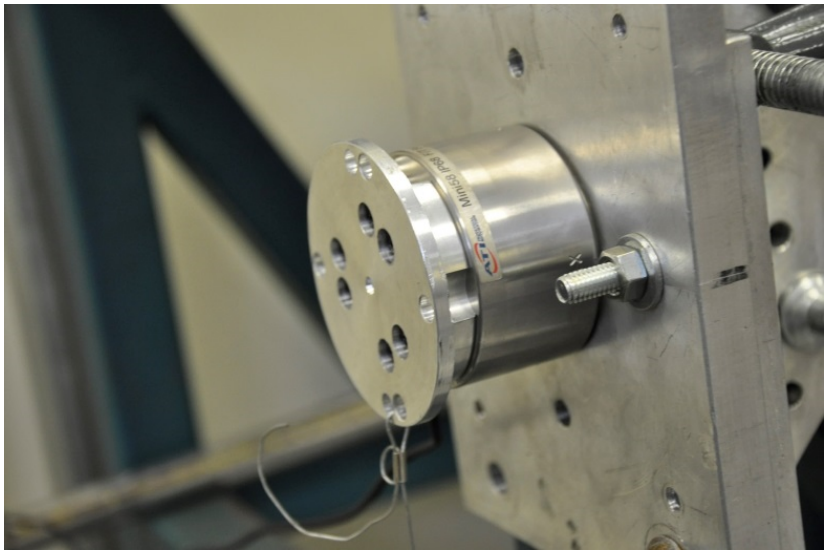

Source: Author.

Figure 40 – Basic schematics of single module test (left) and 3 modules (right) test at IPT's Towing Tank

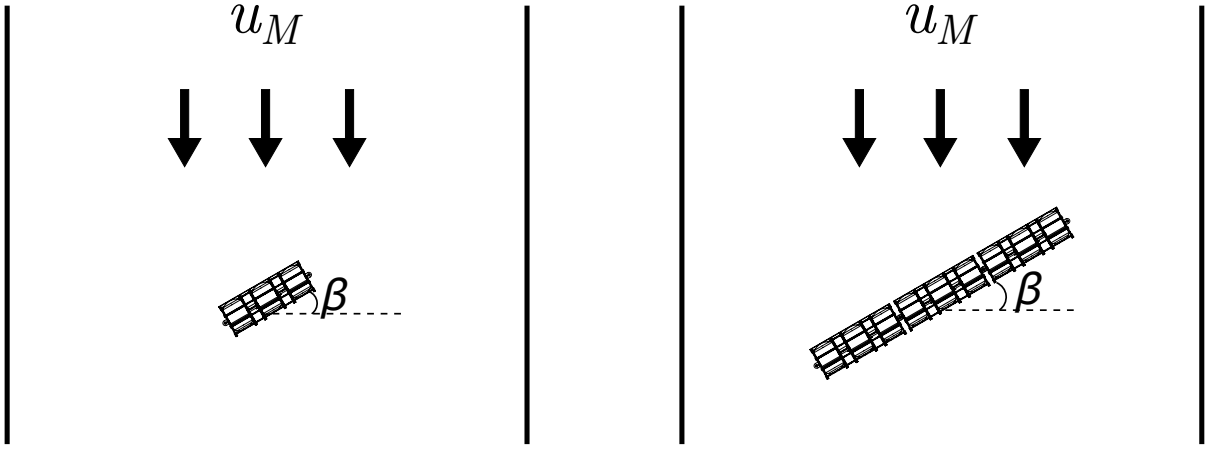

Source: Author.

A log boom line comprises several identical bodies arranged side by side. One can only assume that the hydrodynamic interference effect on neighboring modules must be taken into account. Therefore, the second step was interested in measuring the same variables but considering the interference of adjacent bodies. Three modules were positioned in a row, facing an upstream velocity u_M and varying their yaw angle β. Schematics of these two steps are seen in Fig. 40.

The same arrangement of tests with a single module was used during tests with and without debris at the NDF laboratory. Wooden rods used as debris had the same diameter (32mm), which least absorbed water and had less mass variation. An average density was adopted (800kg/m^3), so the volume of debris could be varied through tests by

Figure 41 – Basic schematics of test with scale debris at NDF's Water Channel on top view (left) and side view (right)

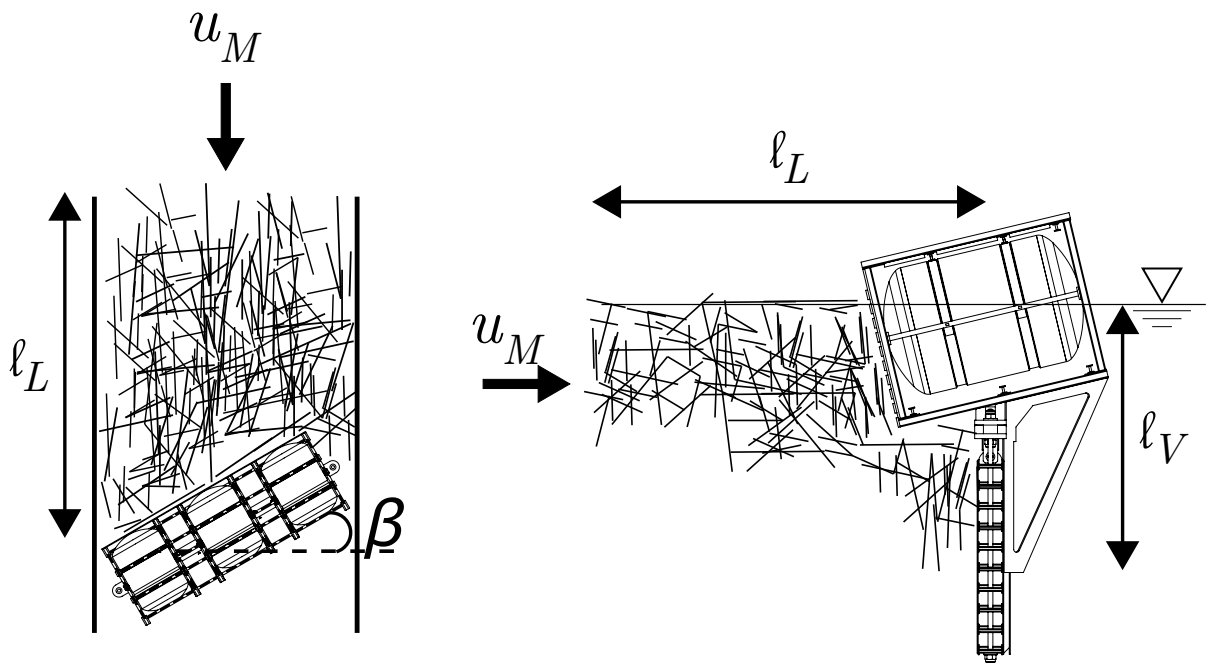

Source: Author.

weighing their mass. They varied from W_0 (no debris) up to W_4, increasing the mass of debris to 8kg, 12kg, 16kg, and 20kg. As in the 2nd round of experiments, wooden debris were randomly disposed at the upstream region of the model.

Two cameras were set up on the water channel's top and lateral to record the experiments. Rulers were placed on the two views to estimate the distance of log accumulation in the longitudinal (ℓ_L) and vertical (ℓ_V) direction. The schematics of tests with debris are shown in Fig. 41.

The water channel dimensions allowed the use of its sidewalls as constraints for the debris floating on the water. This condition did not represent the actual operation scenario, but in this case, these walls could be interpreted as symmetry plans with other log booms with upstream debris on them, in which debris can only move underneath them. Due to the model width, its yaw angle β could only be varied up to 45°. Angles beyond that allowed the debris to pass alongside the model, which did not serve the experiments' purpose.

Table 2 – Equations obtained from tests with one module at IPT's Towing Tank and their R^2. β is given in degrees and ranges from 0° to 90°

Coeficcient	Equation	R^2
$C_D(\beta)$	$C_D = 1.038\cos^3(0.5702\beta)$	0.9401
$C_L(\beta)$	$C_L = -0.1708\sin(3.304\beta - 12.88°) - 0.01628$	0.9395
$C_M(\beta)$	$C_M = 0.09245\sin(1.825\beta) - 0.03143$	0.9267

Source: Author.

5.1.5 Results - Single module at IPT

This section presents the results of the single-module configuration tested at IPT. A scenario with one log boom module does not represent an operational situation once multiple log boom bodies are used together during operation. However, as a reference, it is helpful to study the effects caused by the wake interference of nearby bodies. A picture of the single captive model during experiments is presented in Fig. 42.

Figure 43 shows the hydrodynamic load coefficients as a function of twelve module yaw angles and seven different Froude numbers. In order to determine a unique relation between coefficients and β independent of Fn, fitting curves were drawn along with 95% prediction interval (PI) curves that show a range that likely contains the value for the non-dimensional coefficient for a given specific value of β. Each test condition was repeated at least once.

For drag coefficient (C_D), a cosine behavior is observed, where maximum results are observed for $\beta < 15°$. On the other hand, lift coefficient (C_L) assumes a sine shape, with maximum absolute values at β around 30°, and minimum ones for β around 0° and 60°. As expected, a log boom module presents a bluff body behavior in terms of drag coefficient, being at least two times greater than lift on absolute values. Additionally, the moment coefficient (C_M) also presents a sine aspect with a maximum at $\beta = 45°$, but in this case, much less intense when compared with drag and lift.

As it could be noted for the tested Fn range, there were small variations of the non-dimensional coefficients, making it possible to fit a curve for each one of them. Within this variation, it seems reasonable to reduce the data to equations that give the hydrodynamic response of a scale log boom module as a function of its yaw angle. They are presented in Tab. 2, as well as their coefficient of determination (R^2).

Figure 42 – Single captive log boom model on IPT's Towing Tank

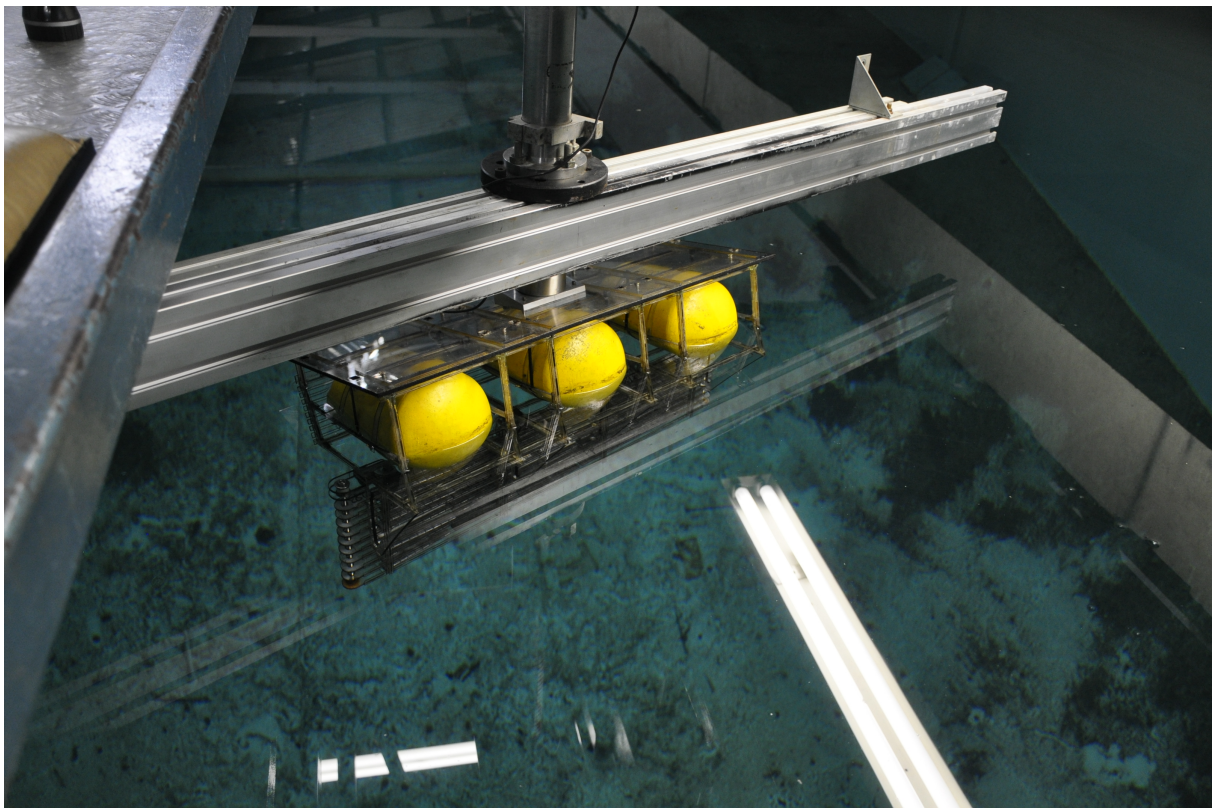

Source: Author.

Figure 43 – Drag coefficient (top), lift coefficient (middle), and moment coefficient (bottom) as a function of module yaw angle for 1-module experiments at IPT

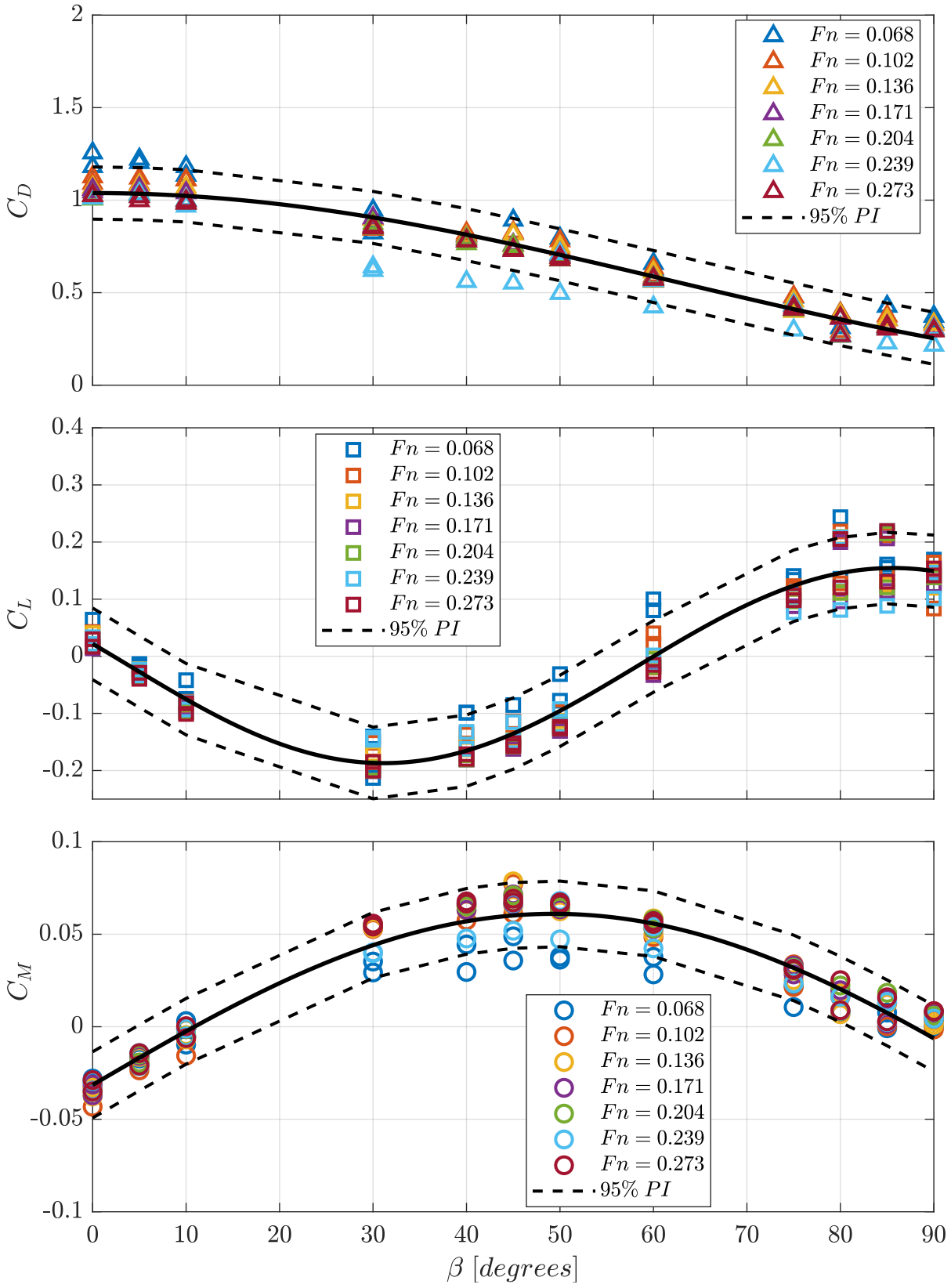

Source: Author.

Table 3 – Equations obtained from tests with three modules and their R^2. β is given in degrees and ranges from 0° to 90°

Coeficcient	Equation	R^2
$C_D(\beta)$	$C_D = 1.21\cos^{4.241}(0.6081\beta)$	0.9571
$C_L(\beta)$	$C_L = -0.1087\sin(3.954\beta - 44.97°) - 0.07433$	0.9263
$C_M(\beta)$	$C_M = 0.06906\cos(1.813\beta) - 0.03045$	0.9118

Source: Author.

5.1.6 Results - Three modules at IPT

This section presents results for the 3-module configuration tested at IPT. It emulates a portion of a line of log booms in which all bodies have the same β. The goal was to capture interference effects on the loads caused by adjacent bodies. Figure 44 shows a picture of this apparatus during experiments.

Figure 45 shows results of the hydrodynamic load coefficients as a function of twelve module yaw angles and for seven different Froude numbers. In order to determine a unique relation between coefficients and β independent of Fn, fitting curves were drawn along with 95% prediction interval (PI) curves. Each test condition was repeated at least once.

For drag coefficient (C_D), a cosine behavior is seen, but in this case, with greater values when compared to Fig. 43 for $\beta < 30°$. Lift coefficient (C_L), as before, also assumed a sine shape, with maximum values at β around 40°, and minimum ones for β around 0°, 70°, and 90°. Moment coefficient (C_M) presented a sine aspect with maximum values around 45°. Again, the small variation, on the coefficients with Fn, made it possible to fit those curves, which are presented in Tab. 3.

Looking at the equations and comparing graphs, it is possible to note some differences between tests with one and three modules. They were arranged in Fig. 46. Drag is higher at $\beta < 40°$ due to flow velocity increasing caused by the adjacent modules' blockage. For $\beta > 40°$, their wake interference generated a drag reduction, probably to a deficit in velocity, compared to the free stream. When it comes to lifting, approximately at the region of $\beta = 40°$, the wake interference becomes relevant, leading to a more smooth curve at $\beta = 70°$, which means a lift reduction. The moment did not experience significant changes caused by the wake interference, leading again to smaller values when compared to drag and lift.

Using the expected line shapes of the 1st round of experiments (Fig. 20), which were based on the analytical catenary formulation, we estimated the yaw angle β of each module.

Figure 44 – Single captive log boom model with adjacent bodies on IPT's Towing Tank

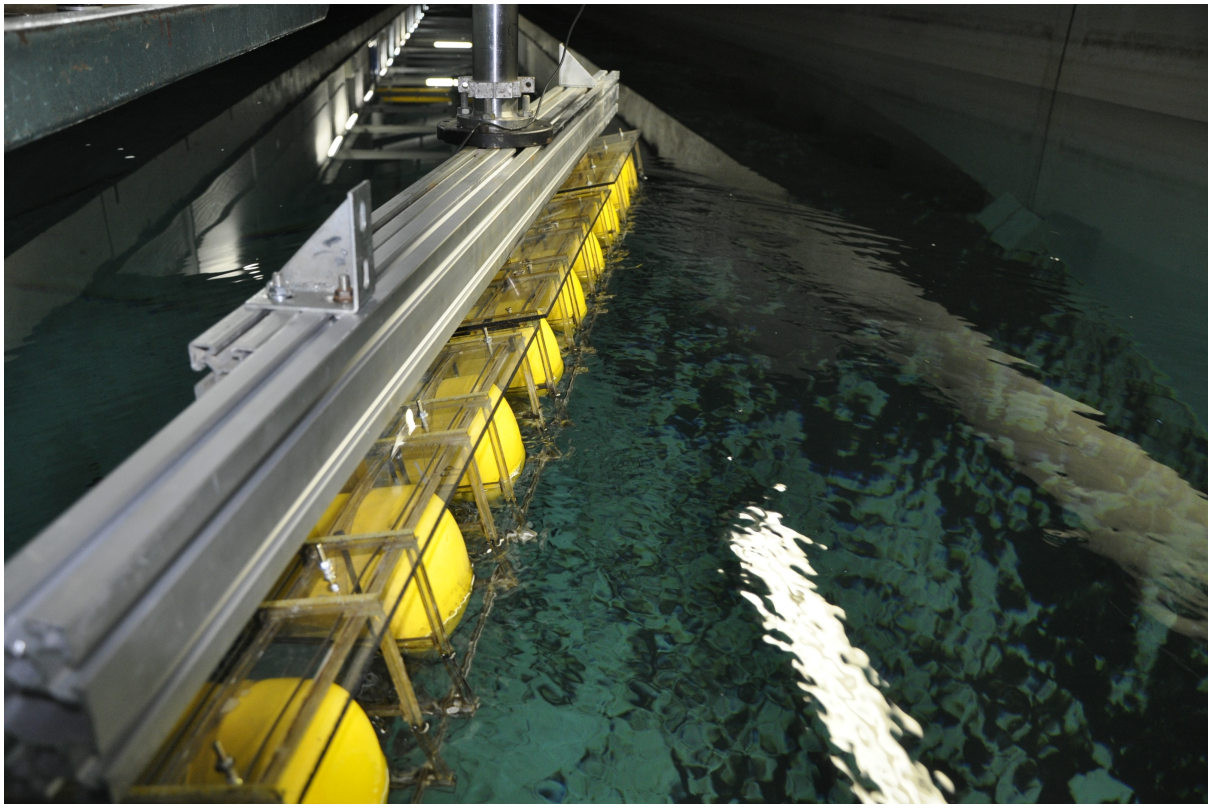

Source: Author.

With the equations that describe the forces acting in a log boom module as a function of β (Tab. 2 and 3), it was possible to estimate the total resistance on the end of a truncated line for each scenario tested in the 1st round of experiments. The estimation only considered drag and lift contributions, similar to Ådnanes (2011) and Løland (1991), summing the forces in each direction for each module assuming that both ends' total resistance was aligned to the modules at the left and right ends. The comparison is seen in Fig. 47. The differences indicated that the tested lines did not have an exact catenary-like shape, mainly at the more inclined scenarios where the lift component reaches its highest values. However, the 5-module configuration presented more similarity because the modules had small β values. Drag acts with more intensity than lift at this range, which corroborates to the catenary formulation that has only the same weight force for each segment of the line acting as its external force component (Fig. 14). The effect of adjacent modules' blockage produced most of the difference between the formulation with one and three modules.

Figure 45 – Drag coefficient (top), lift coefficient (middle), and moment coefficient (bottom) as a function of module yaw angle for 3-module experiments at IPT

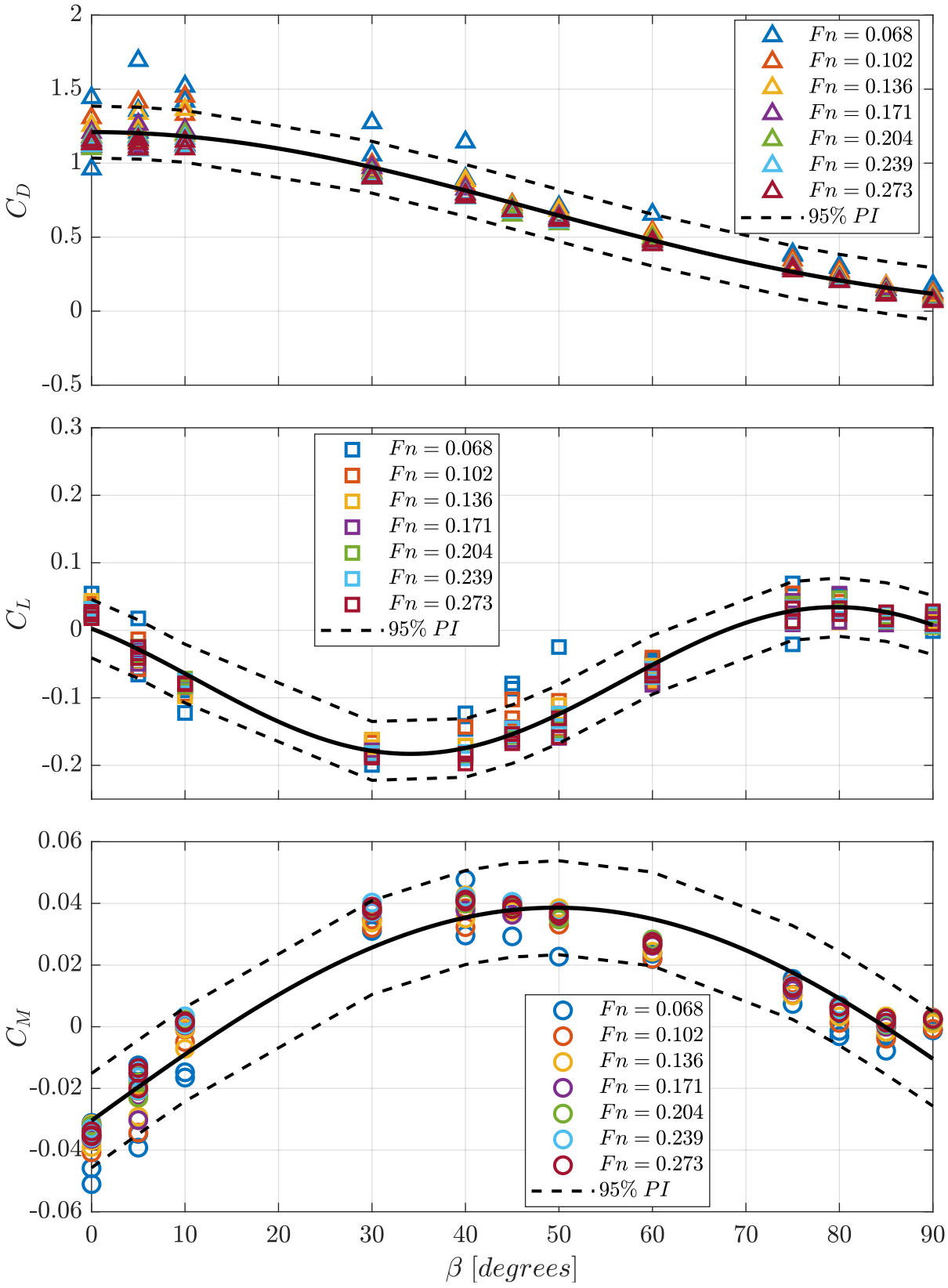

Source: Author.

Figure 46 – Drag, lift, and moment coefficients fitting curves for configuration with one and three modules

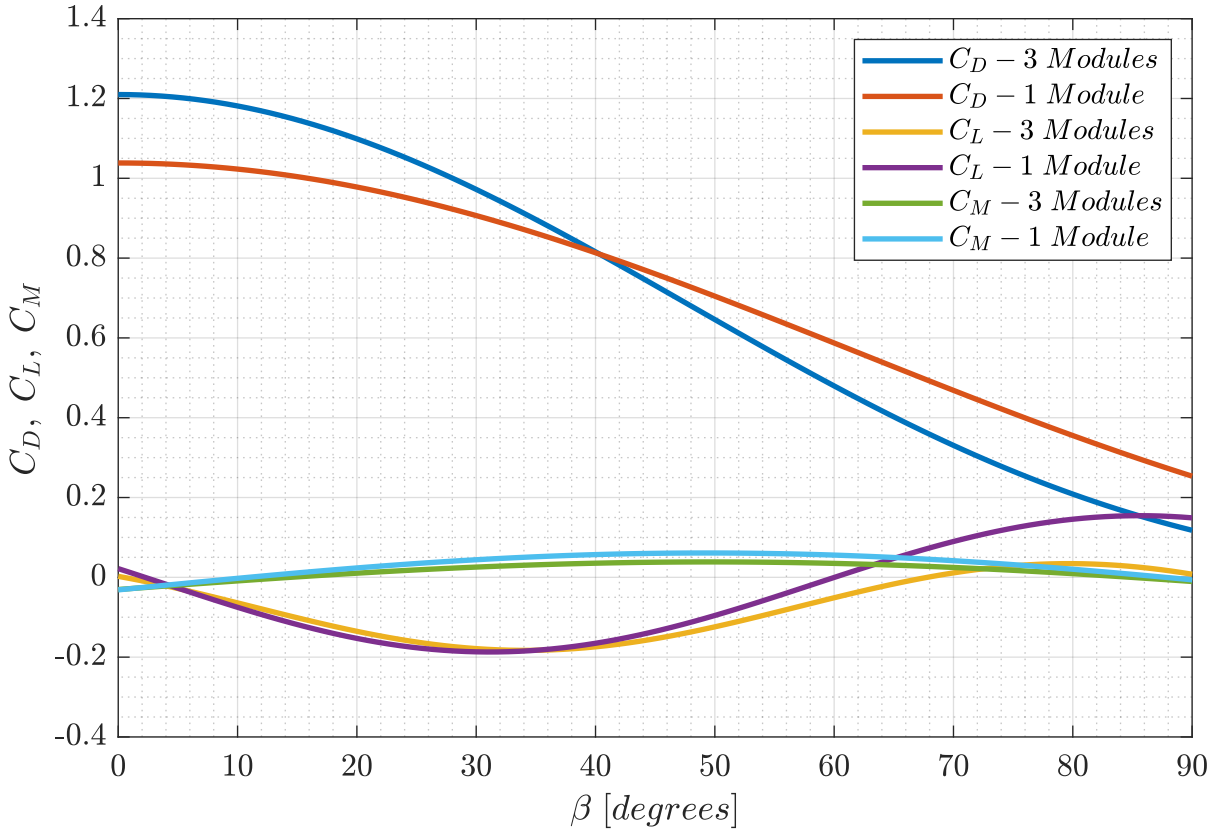

Source: Author.

Figure 47 – Force comparison among experiments of the 1st round of experiments and the catenary model with equations found at tests with one and three modules

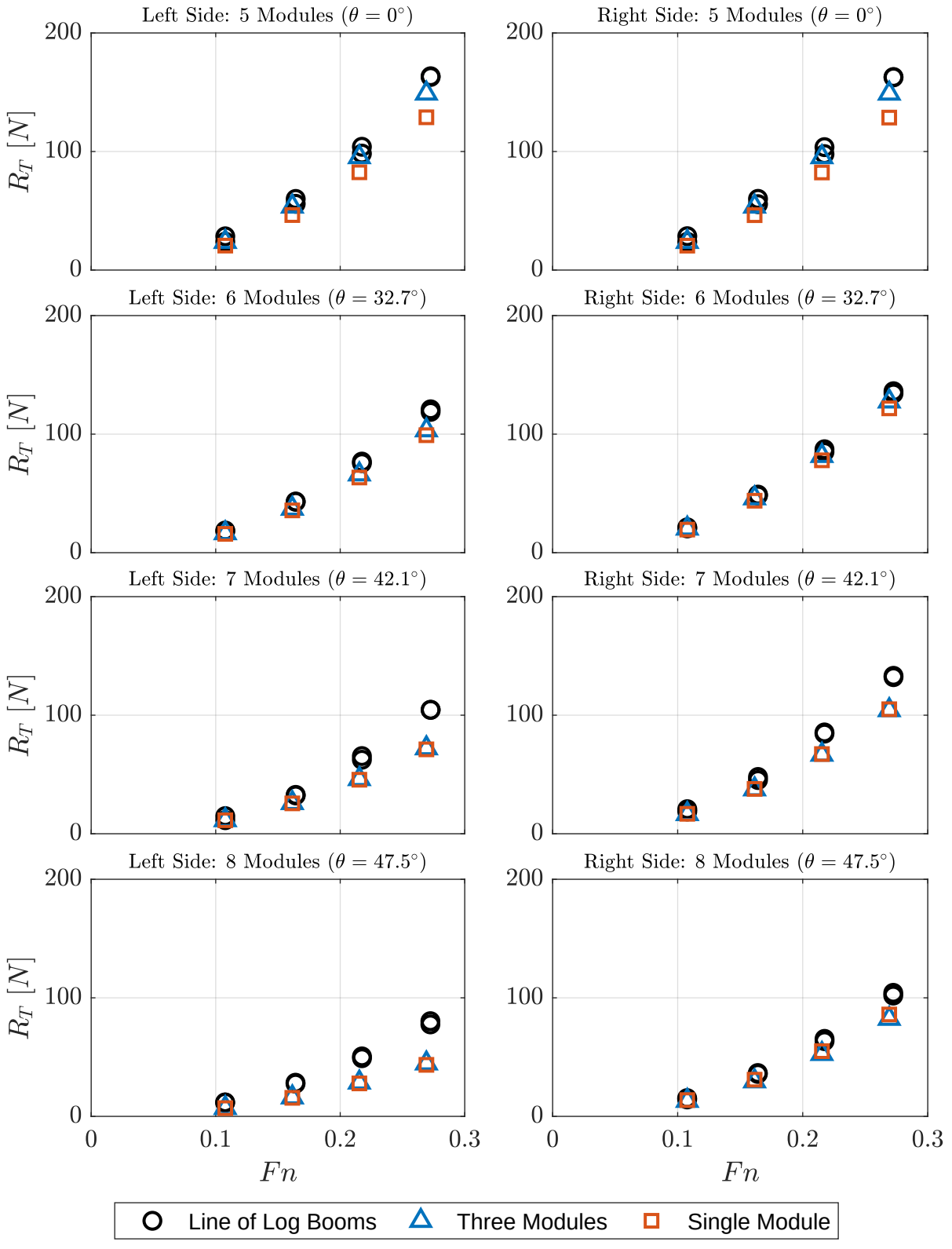

Source: Author.

Figure 48 – Single captive log boom model on NDF's Water Channel

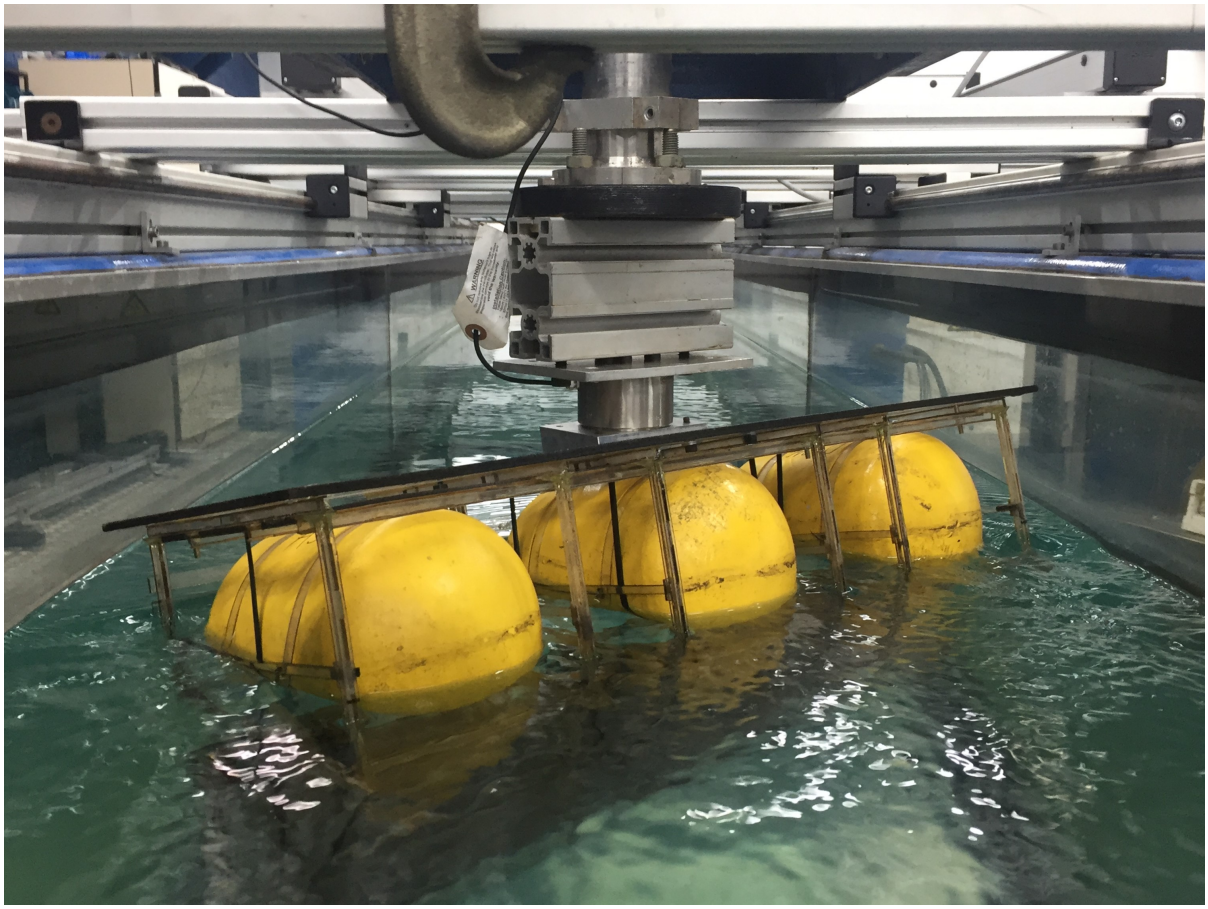

Source: Author.

5.1.7 Results - Single module at NDF

This section presents the results of tests conducted at NDF's Water Channel. A picture of the model during these experiments is presented in Fig. 48.

The first step was to conduct tests without debris as a reference case. Figure 49 shows results of non-dimensional coefficients as a function of twelve module yaw angles for seven different Froude numbers. Fitting curves were drawn, to explore the independence of Fn, together with 95% prediction interval curves. Each test condition was repeated at least once.

Looking into the equations of Tab. 4 and comparing to Fig. 43, for all coefficients, an even smaller variation with Fn was observed. Regarding drag results, a similar tendency was observed, except they were visibly higher for $\beta < 60°$. Similarly, lift and moment curves presented some resemblance when compared to Fig. 43. Their differences become noticeable at $30° < \beta < 30°$.

The observed distinction among results was caused by the channel blockage and a consequent local flow velocity increase. The variation in the velocity is mainly affected by

Figure 49 – Drag coefficient (top), lift coefficient (middle), and moment coefficient (bottom) as function of module yaw angle for 1-module experiments at NDF

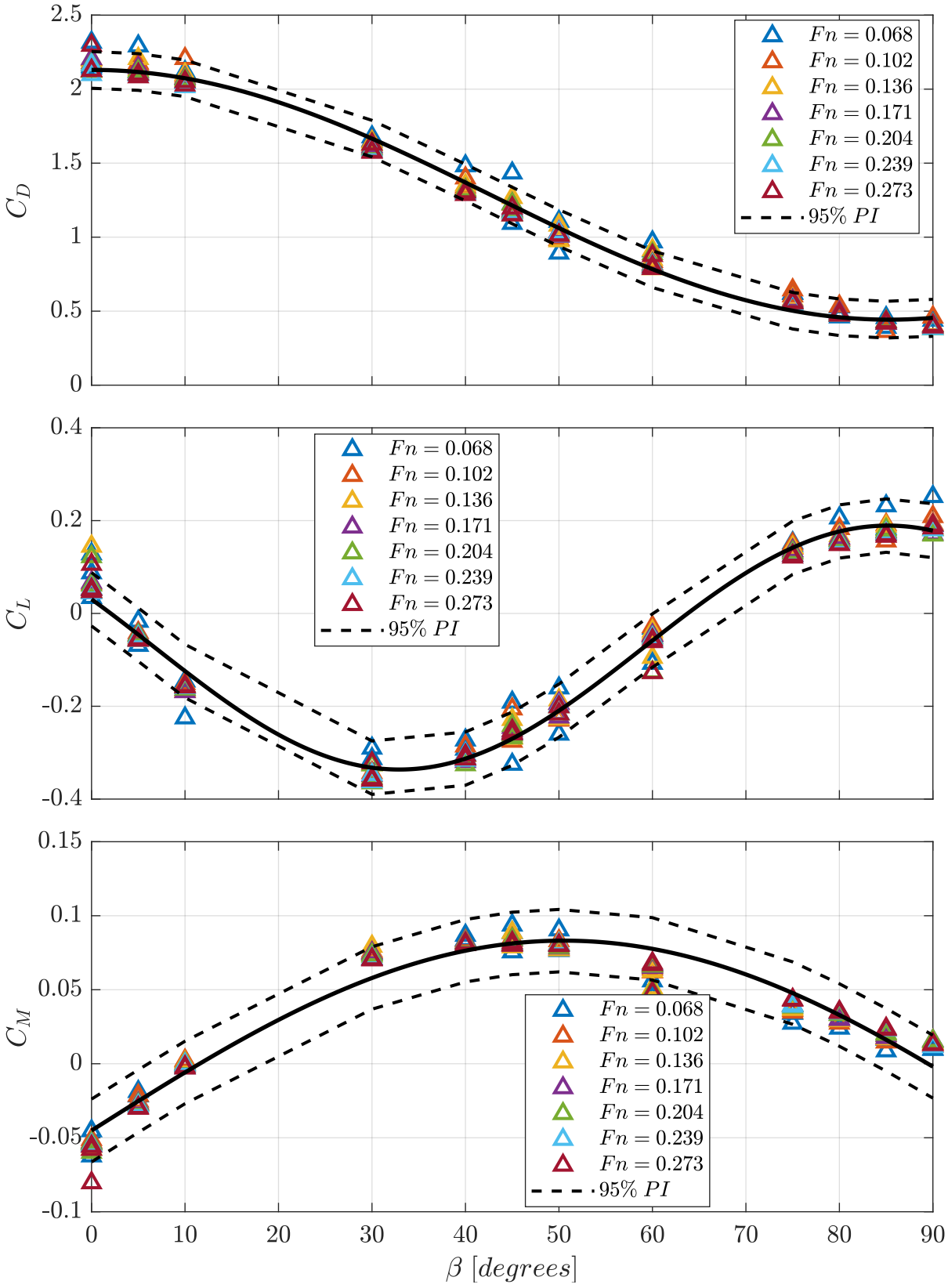

Source: Author.

Table 4 – Equations obtained from tests with 1 module on NDF's Water Channel and their R^2. β is given in degrees and ranges from 0° to 90°

Coeficcient	Equation	R^2
$C_D(\beta)$	$C_D = 0.8438 \cdot \cos(2.109 \cdot \beta) + 1.286$	0.9909
$C_L(\beta)$	$C_L = -0.2628 \cdot \sin(3.443 \cdot \beta - 23.33°) - 0.07352$	0.9777
$C_M(\beta)$	$C_M = 0.1283 \cdot \sin(1.782 \cdot \beta) - 0.04513$	0.9453

Source: Author.

the blockage ratio, defined as

$$BR = \frac{A_b}{A_c} \tag{5.4}$$

where A_b and A_c are the submerged projected area of the log boom model and the cross-sectional area of the water channel, respectively. It is important to note that resistance variation is also affected by the body's length and velocity and the geometries of the body and the channel. Typical blockage correction for open channel tests involve geometries of slender bodies, such as ships or ellipsoids of revolution (ITTC, 2011; DURGUN; KAFALI, 1991). In the case of a scale log boom module, Eq. 5.4 produces several values once there is a variation on yaw angle. Using CAD tools and, given the similarity between the designed and built model, submerged cross-sectional area was estimated as a function of β and shown in Fig. 50

Based on the continuity equation, a simple velocity increase formula is given by:

$$\Delta u = \frac{u_M BR}{1 - BR} \tag{5.5}$$

To compensate the blockage effect, a correction method was applied on tests conducted on NDF's Water Channel. The method only altered the reference local velocity on the body using Eq. 5.5. Then the non-dimensional coefficients were recalculated (Eq. 5.1, 5.2, and 5.3) considering the increase on flow stream velocity. Figure 51 shows the blockage correction for drag, lift, and moment coefficients as function of β, for $Fn = 0.273$. Considering the body's high blockage ratios, the method shows a reasonable accuracy since most discrepancies were balanced out. This may indicate that the dynamic effect of debris can be isolate from the channel natural blockage.

Figure 50 – Submerged projected area as a function of module yaw angle

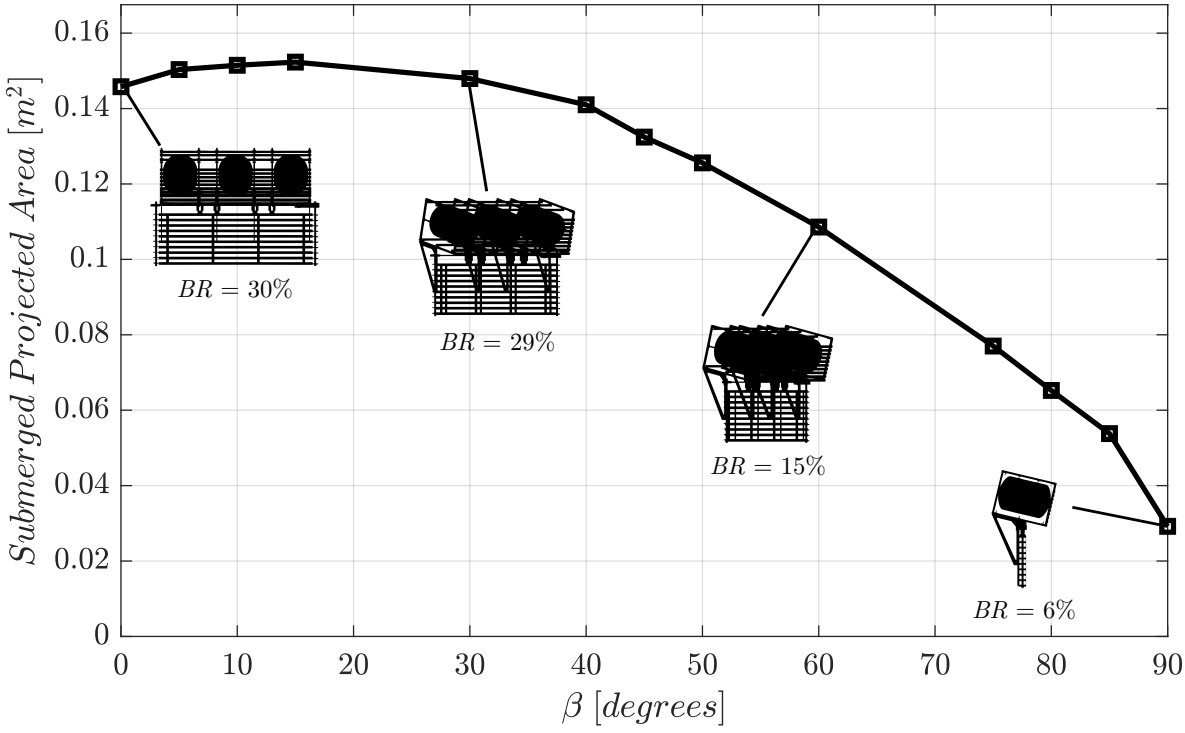

Source: Author.

Figure 51 – Comparison among C_D (top), C_L (middle), and C_M (bottom) as function of module yaw angle for 1-module experiments at NDF and IPT for $Fn = 0.273$, and the blockage correction results

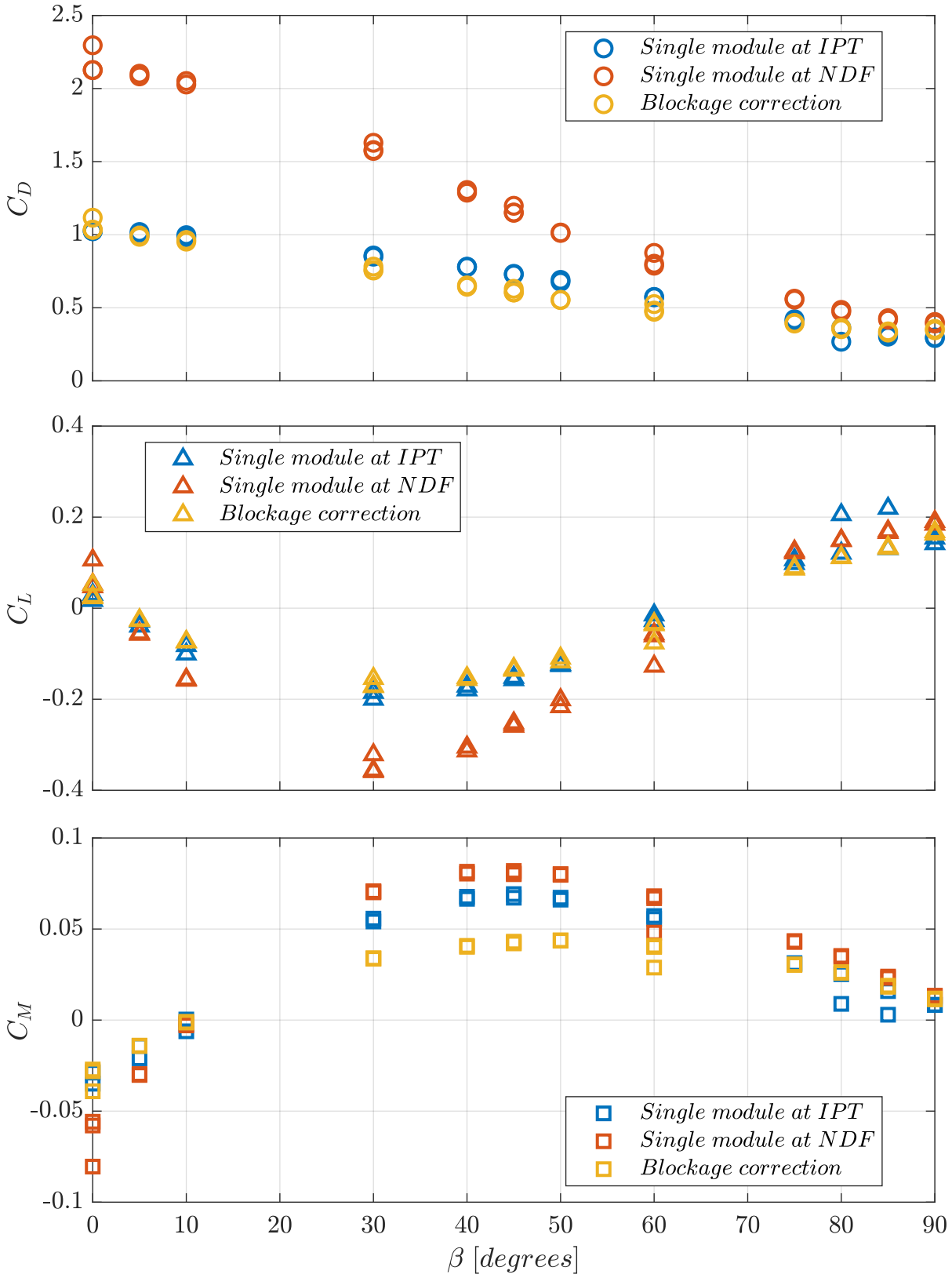

Source: Author.

5.1.8 Results - Single module with debris at NDF

This section presents the main results from experiments conducted with debris in the water channel at NDF. It is important to note that studies to check debris containment systems' performance, such as log booms, are based on visual observation. Also, given the randomness of the debris accumulation, a scenario with the same volume or amount of debris would not produce the same visual results. As a design criterion, Kennedy and Lazier (1965) measurements have produced valuable results of the log-stopping capacity of scale boom lines as a function of the free stream velocity and their angle to the current. These variables were adopted at this study in terms of Fn and β, and checking their relation with geometrical parameters as debris accumulation measured at longitudinal and vertical direction, here called ℓ_L and ℓ_V (Fig. 41).

The first observation was that low Froude numbers did not significantly affect debris kinematics. That means that debris would not move in the channel and stick to the sidewalls, instead. Because of that, efforts here were concentrated on $Fn > 0.203$, with more effects seen for $Fn = 0.273$ and $Fn = 0.306$. Again, the load cell limitation marked out the limits of the experiments.

Figure 52 brings the ℓ_V/ℓ_L ratio with the increase of Fn, for all the volumes of scale logs. Those measurements were taken from analysis of the visual records of tests, like in Fig. 53. Those values correspond to the model set at $\beta = 0°$, and in the case of the top view, measured at the central line of the picture. It is possible to observe that ℓ_L reduces as the logs begin to be pushed against the module, and depending on the volume of debris, to stuck on the module grid, increasing ℓ_V value. The ratio ℓ_V/ℓ_L increases with Fn for every different amount of debris, a behavior described by Hartlieb (2017) and called debris jam compactness. Besides, that debris jam compactness relation might also be associated with the mass of debris tested, since W_1 and W_2 reached higher values than W_3 and W_4 at the highest Fn.

Figures 54 and 55 present a comparison among tests with different debris volumes, in terms of drag and lift coefficients, as a function of β. Moment coefficient results were neglect here, once they did not present a significant magnitude compared to C_D and C_L. As the values presented some variation, fitting curves were also drawn for each debris accumulation level.

At $Fn = 0.273$, C_D highest values occurred at $\beta = 0°$, similar to Fig. 49. Drag coefficient had some increase for the lowest volume of debris W_1 compared to the condition without debris W_0. Conditions W_2, W_3, and W_4 had the same behavior but with less intensity. The debris compactness ratio ℓ_V/ℓ_L, shown in Fig. 52, had the greatest value for W_1 at $Fn = 0.273$, which seems to increase the model blockage and, by consequence, the drag for that condition. Looking at Fig. 55, C_D had a increase for all level of debris

Figure 52 – ℓ_V/ℓ_L ratio as a function of Froude number for the four volumes of debris accumulation at $\beta = 0°$

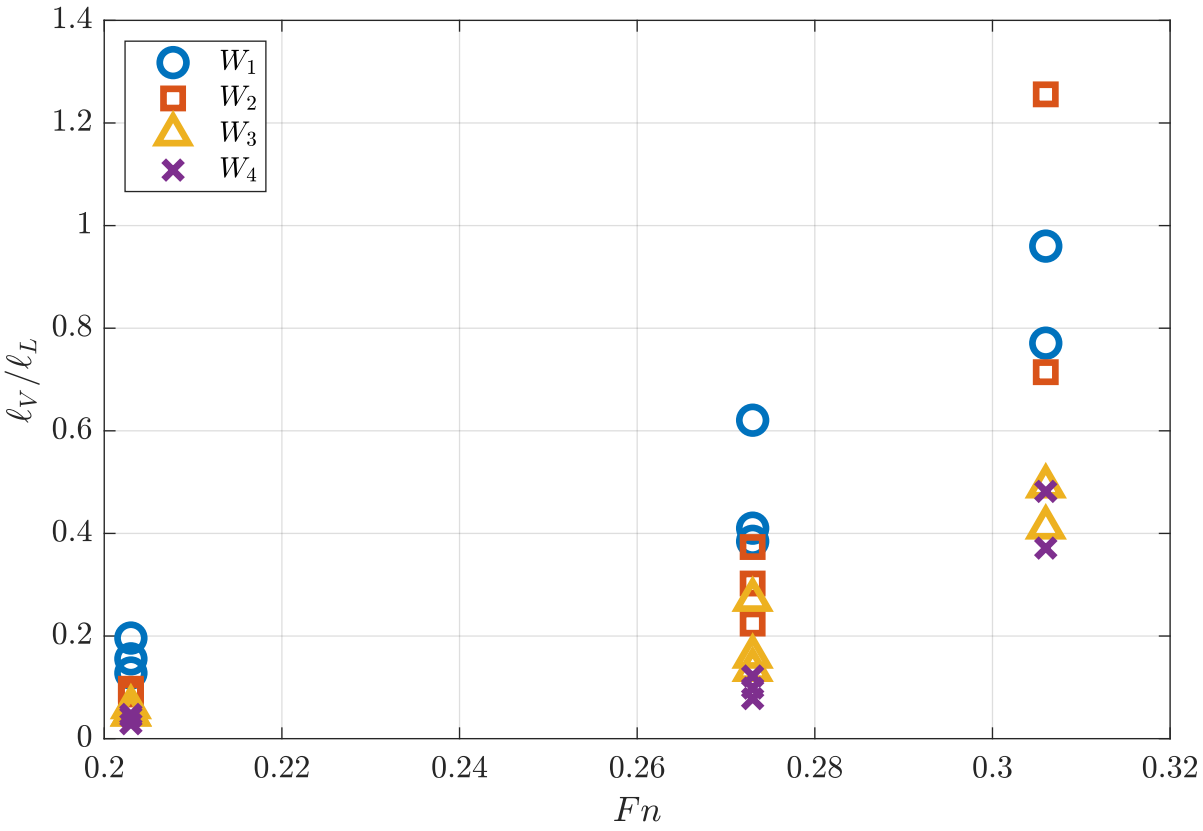

Source: Author.

accumulation compared to W_0, and for this condition ($Fn = 0.306$) all ℓ_V/ℓ_L results are greater or equal than 0.4.

For $Fn = 0.273$, C_L response presented a small variation in the presence of debris. For some accumulation levels, that reduced the lift response. On the other hand, C_L results presented a large variation for $Fn = 0.306$ as β was increased. On both Fn, drag C_D presented a response almost ten times bigger than C_L.

As in the tests performed with the truncated line (Fig. 31 and 34), an increased volume of debris did not represent an immediate increase of forces at its anchorage ends. However, that may be associated with the ℓ_V/ℓ_L ratio, especially when debris gets jammed on the model's grid.

5.1.9 Conclusion

The results presented in this section focused on forces and moments acting on a log boom module. The experiments were performed using a captive model hypothesis that forces and moments on a line of log booms could be reduced to the water surface. Furthermore,

Figure 53 – Side and top view for the debris accumulation level W_3, for $Fn = 0.273$ (top) and $Fn = 0.306$ (bottom)

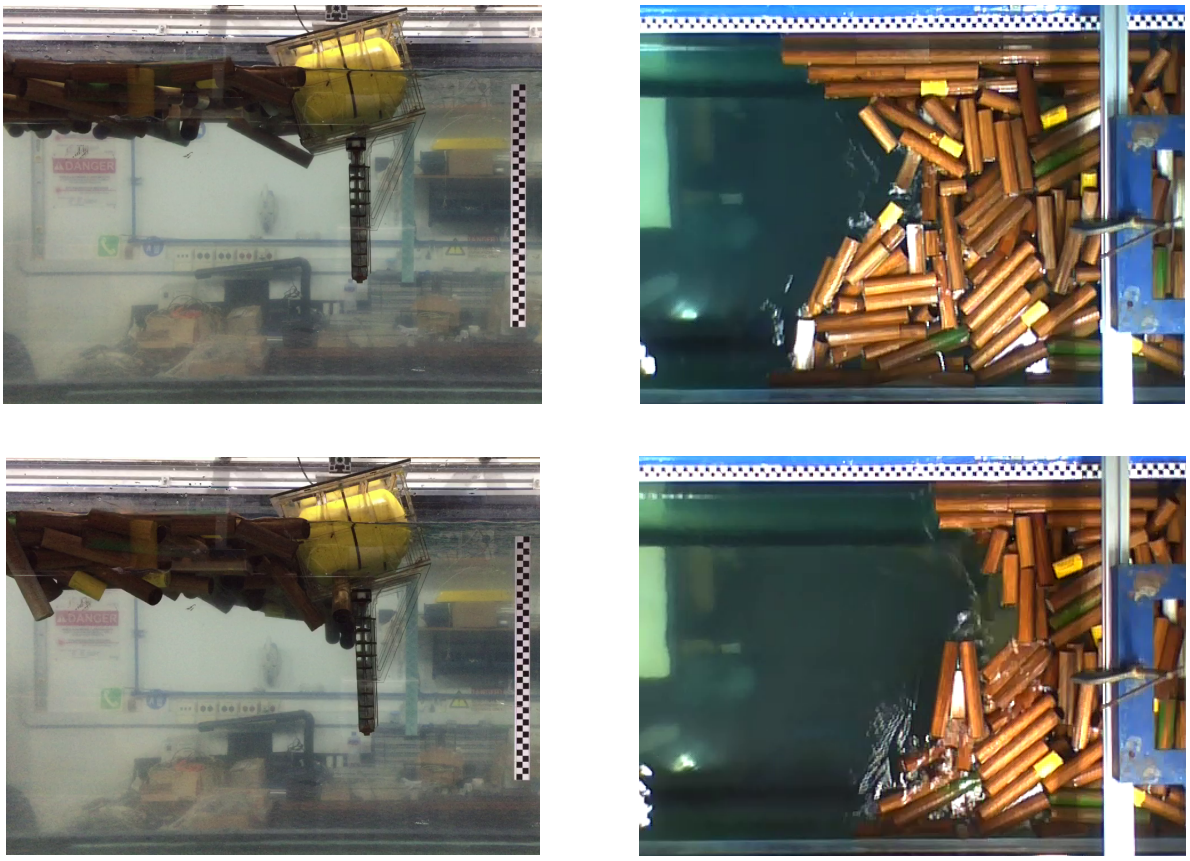

Source: Author.

single log boom experiments had a limited range of Froude number ($Fn \leq 0.3$), based on the small motion behavior of a log boom module, and yaw angle ($0° \leq \beta \leq 90°$), assuming the model was symmetric.

It was possible to achieve equations to represent C_D, C_L, and C_M as a function of β that could be assumed as independent of Fn, given their slight variation. For all conditions (single module, 3-module, and with debris), the log boom model presented more significant drag behavior than a lift one for most of the β range. The log boom module geometry did not generate high values of moment, being at least fifteen times lower than drag for the same Fn and β.

The interference generated by the wake of adjacent modules was noticed, with reductions in C_D and C_L for $\beta > 40°$, which gives some support that an inclined line of log booms could present lower values of tension at its ends, as seen in the 1st round of experiments.

The load comparison among tests with the truncated line and the single module formulations has shown some similarity with and without adjacent bodies. It is important to remember that assuming the lines have a catenary shape works as a first guess. The

Figure 54 – Drag and lift coefficients as a function of module yaw angle for all level of debris at $Fn = 0.273$

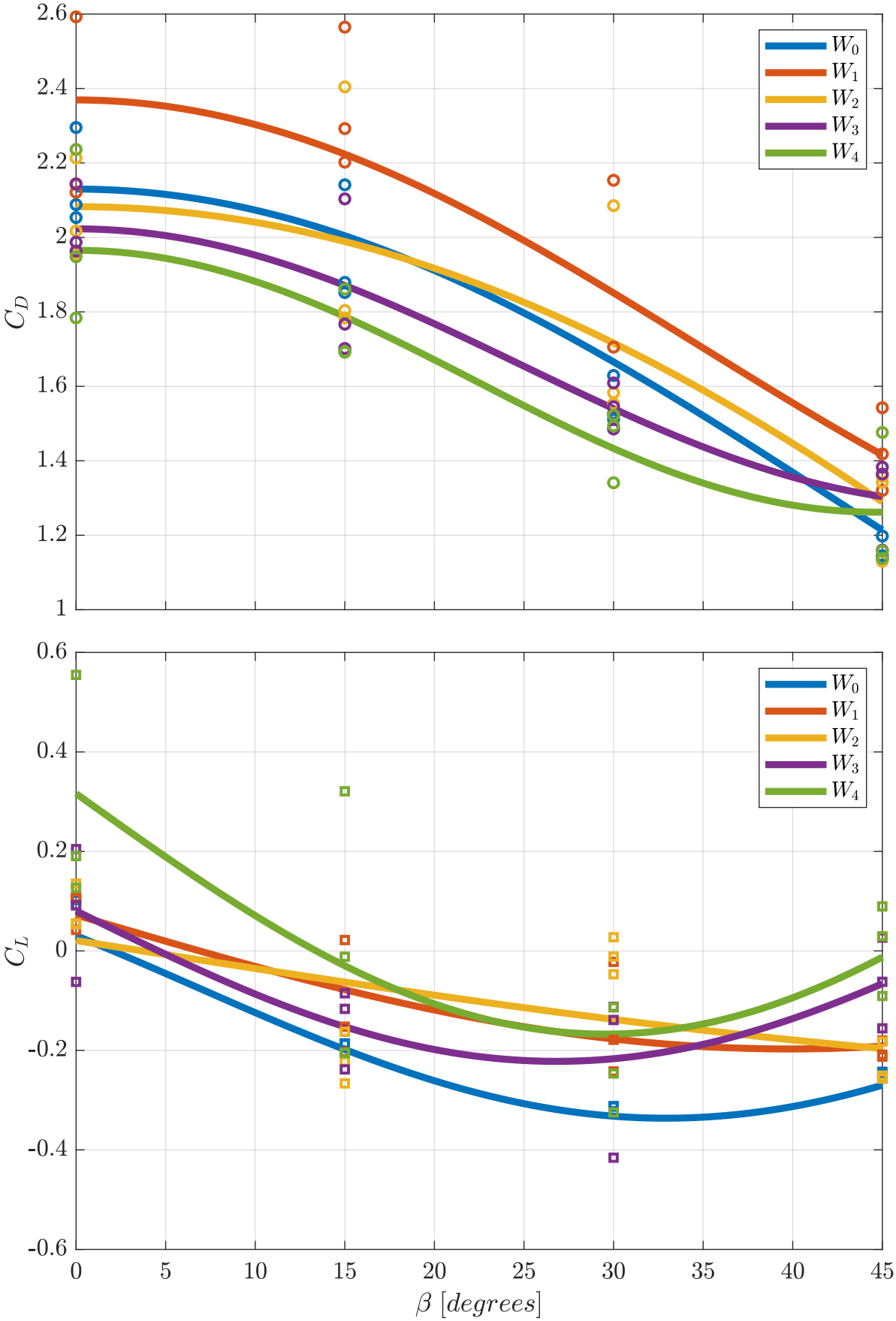

Source: Author.

Figure 55 – Drag and lift coefficients as a function of module yaw angle for all level of debris at $Fn = 0.306$

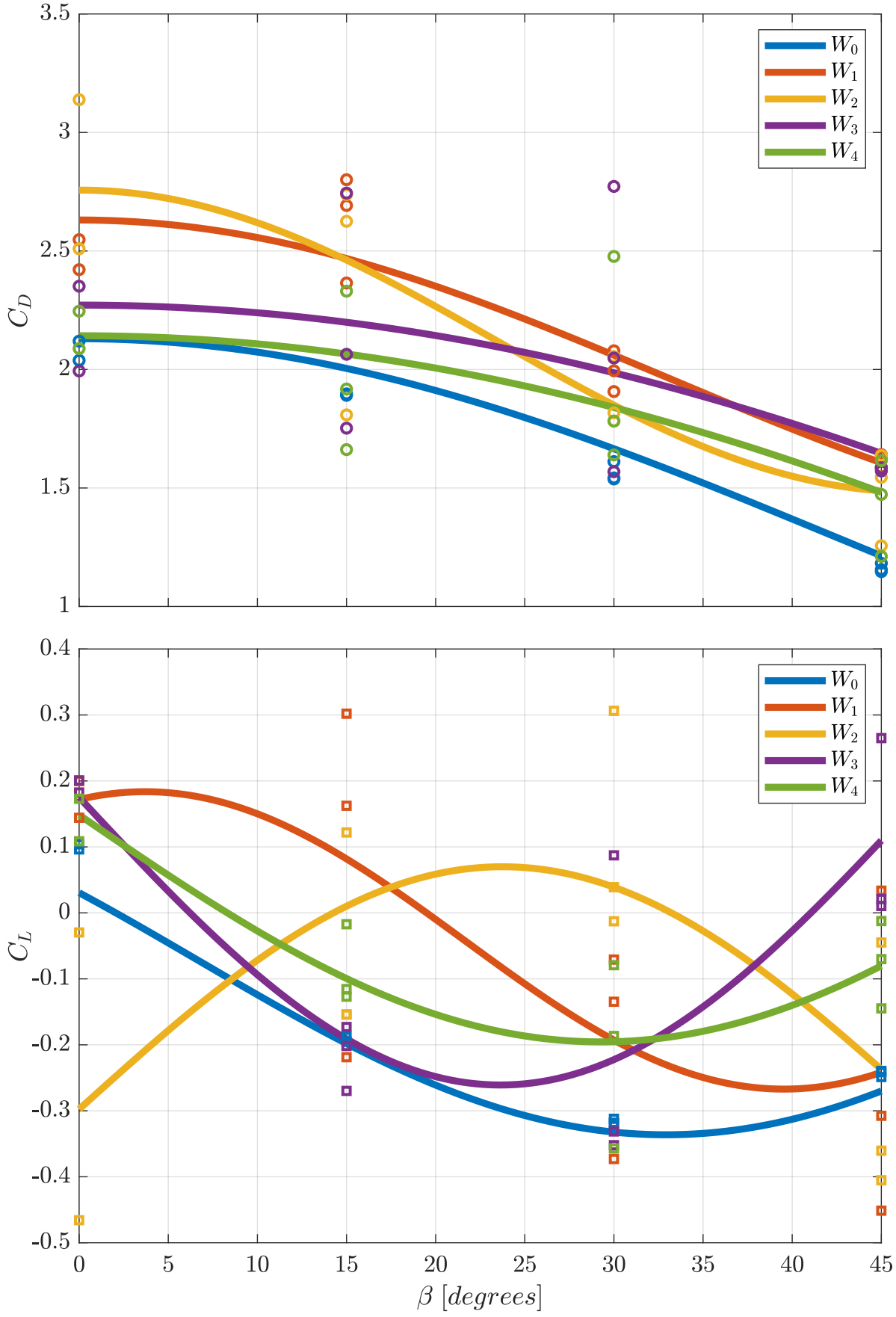

Source: Author.

differences among methods may intensify as we compare more inclined lines at Fn of higher magnitudes. The external force on the catenary formulation – its weight – has only one direction and the same magnitude for each part of the line, which was not seen in the line of log booms.

Tests at the NDF's Water Channel without debris presented higher magnitudes because of the blockage effect. A correction method based on the velocity increase was successfully applied.

The presence of debris increased the drag response while produced minor changes on the lift behavior at $0 \leq \beta \leq 45°$. Drag results seemed to be associated with debris compactness ratio ℓ_V/ℓ_L, which increased as a function of Fn and were characterized by the blockage on the grid caused by the wooden debris.

6 Conclusion

This study proposed using experimental techniques to understand the dynamic behavior of log booms employed at Santo Antônio hydropower plant, using a static approach. Models were designed, built, adapted, and tested to represent its original behavior as a line and a single body, with and without debris, adding up to approximately 400 test conditions performed at IPT and NDF.

The first part of the tests simulated the scale log booms as a truncated line and measured forces at its ends, varying the number of modules and nominal angles (θ), without debris. Tests without debris showed a total resistance (R_T) that is proportional to the Froude number (Fn) and inversely proportional to its nominal angle (θ), even in a configuration with fewer modules. Moreover, heave and trim motions were observed as Fn was increased.

The second part of the tests simulated a similar model, with and without debris. A few adaptations to track the motion of the line's central and lateral modules were made. For tests without debris, results showed a coupled motion of pitch and heave for the instrumented bodies, that is associated with Fn and the yaw angle (β) of the individual modules. The highest values of Fn induced part of the model's submersion. $Fn \leq 0.3$ produced less than 5% of draft change and less than 10° in terms of pitch angle modification in tests without debris. The incidence of large volumes of debris affected the resistance force, increasing R_T for the 5-module configuration ($\theta = 0°$), with various values for the same Fn. Meanwhile, the 7-module configuration ($\theta = 47.8°$) presented minor variations, where high volumes of debris led to higher resistance values for most of the runs compared to scenarios without debris. Debris showed a tendency of jamming at the downstream side when the line is inclined, even had been randomly distributed at the upstream region of the line.

The third part of the tests measured force and moments acting on a single log boom module. From the small variations in terms of motion observed at $Fn \leq 0.3$, experiments were done with a captive module at a limited range of Fn and analyzed in terms of non-dimensional coefficients. C_D, C_L, and C_M as a function of β were assumed as independent of Fn, given their slight variation. For all conditions (single module, 3-module, and with debris), the log boom model presented more significant drag behavior than a lift one for most of the β range. The log boom module geometry did not generate high values of moment, being at least fifteen times lower than drag for the same Fn and β.

The interference generated by the wake of adjacent modules was noticed, with reductions in C_D and C_L for $\beta > 40°$, which gives some support that an inclined line

of log booms could present lower values of tension at its ends. A comparison among results of the 1st round of experiments and the catenary formulation applied with the obtained equations from 1-module and 3-module configurations showed similarity of forces, which indicates that C_D and C_L curves could be helpful to estimate forces on lines for $Fn \leq 0.3$. The catenary formulation is conservative and may be considered a first iteration to calculate loads in a complex geometry as a line of log booms. An interesting numerical tool, originated from the work of IPT and using CFD techniques, is presented by Chreim and Dantas (2020).

Tests at the NDF's Water Channel without debris presented higher magnitudes than tests performed at IPT's Towing Tank because of the blockage effect. A correction method based on the velocity increase was applied and produced good results. That indicates that porous geometries like log booms with high blockage ratios ($BR \leq 30\%$) may be corrected by the same method.

Visual measurement of debris longitudinal (ℓ_L) and vertical (ℓ_V) lengths were performed for the $\beta = 0°$ with the variation of Fn. Debris started to accumulate on the model at $Fn > 0.203$, with more effects seen for $Fn = 0.273$ and $Fn = 0.306$.

The model's load behavior in the presence of debris was analyzed at $0 \leq \beta \leq 45°$ and increased the drag response while producing minor changes in the lifting behavior. Drag results seemed to be associated with debris compactness ratio ℓ_V/ℓ_L, which increased as a function of Fn and were characterized by the blockage on the grid caused by the wooden debris. The variability in results shows the phenomenon of debris randomness that may happen in more significant proportions in the actual size prototype.

In general, tests were innovative in the field of solutions designed to retain debris since generally fixed structures are the object of study. The adopted methodology, understanding the main aspects regarding a line of log booms firstly to measure the local particularities of a single module, has produced exciting results. The present study aims to contribute to the log boom problem in the actual size proportions. Some of the main conclusions should also be useful to be extended and applied on similar problems of containment of floating debris.

For future works, we may suggest a more detailed experimental study on the dynamic behavior of log booms considering its heave and pitch motion at high Fn values. Furthermore, it should be interesting to improve the numerical tool to predict the shape and loads on the line of log booms, based on experimental results that include the effects caused by the debris.

Bibliography

ABDELNOUR, R. Ice Booms in Rivers ; Lessons Learned and the Development of Reliable Solutions Ice Booms Main Characteristics The Wakefield Ice Boom. *11th Workshop on River Ice*, n. April, p. 1–10, 2001. Available from: <http://cripe.ca/docs/proceedings/11/Abdelnour-2001.pdf>. Cited on page 23.

ASSI, G. R. da S. *Estudo experimental do efeito de interferência no escoamento ao redor de cilindros alinhados.* Thesis (Master's Thesis), 2005. Available from: <https://doi.org/10.11606/d.3.2005.tde-11012006-154457>. Cited on page 72.

BIRK, L. *Fundamentals of ship hydrodynamics : fluid mechanics, ship resistance and propulsion*. Hoboken, NJ: John Wiley & Sons, Ltd, 2019. ISBN 9781118855515. Cited 3 times on pages 37, 40, and 41.

BLEVINS, R. D. *Applied Fluid Dynamics Handbook*. New York: Van Nostrand Reinhold Company, 1984. 570 p. ISBN 0-442-21296-8. Cited 2 times on pages 33 and 41.

BRADLEY, J. B.; RICHARDS, D. L.; BAHNER, C. D. *Debris Control Structures Evaluation and Countermeasures*, Washington, 2005. 179 p. Available from: <www.fhwa.dot.gov/engineering/hydraulics/pubs/04016/hec09.pdf>. Cited on page 30.

BRAMBINI, R. et al. Hydrodynamics and capture efficiency of plastic cleanup booms: Part i — experiments and dynamic analysis. In: *Volume 1: Offshore Technology*. American Society of Mechanical Engineers, 2017. Available from: <https://doi.org/10.1115/omae2017-61950>. Cited on page 23.

BRAUDRICK, C. A. et al. Dynamics of Wood Transport in Streams: A Flume Experiment. *Earth Surface Processes and Landforms*, v. 22, n. 7, p. 669–683, 1997. ISSN 01979337. Cited on page 29.

BUCKINGHAM, E. On physically similar systems illustrations of the use of dimensional equations. *Physical Review*, American Physical Society (APS), v. 4, n. 4, p. 345–376, out. 1914. Available from: <https://doi.org/10.1103/physrev.4.345>. Cited on page 37.

CASTRO, F. S.; DANTAS, J. L. D. Motion analysis of scale truncated log boom structures tested in a towing tank. In: *Proceedings of the 25th International Congress of Mechanical Engineering*. ABCM, 2019. Available from: <https://doi.org/10.26678/abcm.cobem2019.cob2019-1262>. Cited 3 times on pages 26, 27, and 63.

CASTRO, F. S.; KATSUNO, E. T.; DANTAS, J. L. L. Instrumentation methodology for a log containment grid model in towing tank tests. In: *Procceedings of the 30th Towing Tank Conference*. [S.l.]: SNAME, 2017. Cited on page 47.

CASTRO, F. S. et al. Structural Analysis for a Reduced Scale Model of a Hydropower Plant Debris Containment Grid. In: *Procceedings of the 24th ABCM International Congress of Mechanical Engineering*. Curitiba: ABCM, 2017. Available from: <http://abcm.org.br/anais-de-eventos/COB17/0578>. Cited on page 47.

CENAC, W. A. *Vertically Loaded Anchor: Drag Coefficient, Fall Velocity, and Penetration Depth Using Laboratory Measurements*. 127 p. Thesis (Master's thesis) — Texas A&M University, 2011. Available from: <http://oaktrust.library.tamu.edu/handle/1969.1/ETD-TAMU-2011-05-9310>. Cited 2 times on pages 34 and 35.

CHREIM, J. R.; DANTAS, J. L. D. Nonlinear truss-based finite element methods for catenary-like structures. In: *Truss and Frames - Recent Advances and New Perspectives*. IntechOpen, 2020. Available from: <https://doi.org/10.5772/intechopen.87034>. Cited on page 98.

CREAGER, W. P.; JUSTIN, J. D. *Hydroelectric Handbook*. Second. New York: John Wiley & Sons, 1950. 533–538 p. Cited on page 31.

CURRAN, J. C. Mobility of large woody debris (LWD) jams in a low gradient channel. *Geomorphology*, Elsevier B.V., v. 116, n. 3-4, p. 320–329, 2010. ISSN 0169555X. Available from: <http://dx.doi.org/10.1016/j.geomorph.2009.11.027>. Cited on page 29.

DANTAS, J. L. D. *Ensaios Hidrodinâmicos do Modelo Reduzido e Truncado do Log Boom da UHE Santo Antônio em Tanque de Provas*, São Paulo, 2017. 55 p. Instituto de Pesquisas Tecnológicas do Estado de São Paulo. In Portuguese. Cited on page 25.

DANTAS, J. L. D. *Ensaios Hidrodinâmicos do Modelo Reduzido e Truncado do Log Boom da UHE Santo Antônio em Tanque de Provas com Diferentes Configurações de Linhas de "Log Boom"*, São Paulo, 2018. 169 p. Instituto de Pesquisas Tecnológicas do Estado de São Paulo. In Portuguese. Cited 2 times on pages 58 and 60.

DAVIDSON, S. L.; MACKENZIE, L. G.; EATON, B. Large wood transport and jam formation in a series of flume experiments. *Water Resources Research*, v. 51, n. 12, p. 10065–10077, dec 2015. ISSN 00431397. Available from: <http://doi.wiley.com/10.1002/2015WR017446>. Cited on page 29.

ÅDNANES, H. *Forces on a Net Panel*. 97 p. Thesis (Master's Thesis) — Norwegian University of Science and Technology, 2011. Cited 2 times on pages 36 and 81.

DURGUN, O.; KAFALI, K. Blockage correction. *Ocean Engineering*, v. 18, n. 4, p. 269–282, 1991. ISSN 0029-8018. Available from: <https://www.sciencedirect.com/science/article/pii/002980189190014H>. Cited on page 87.

FALTINSEN, O. M. *Hydrodynamics of high-speed marine vehicles*. Cambridge New York: Cambridge University Press, 2005. ISBN 0-511-13506-8. Cited on page 40.

FERNANDES, A. C. et al. Torpedo Anchor Installation Hydrodynamics. *Journal of Offshore Mechanics and Arctic Engineering*, v. 128, n. November 2006, p. 286–293, 2006. Available from: <https://doi.org/10.1115/1.2355514>. Cited on page 34.

FERNANDES, A. C. et al. Towards the Understanding of Manifold Fluttering During Pendulous Installation: Flow Induced Rotation of Flat Plates in Uniform Flow. In: *29th International Conference on Ocean, Offshore and Arctic Engineering: Volume 1*. Shanghai, China: ASME, 2010. p. 603–609. Available from: <http://dx.doi.org/10.1115/OMAE2010-20950>. Cited 2 times on pages 34 and 40.

FERNANDES, A. C.; MINEIRO, F. P. S. Assessment of hydrodynamic properties of bodies with complex shapes. *Applied Ocean Research*, v. 29, n. 3, p. 155–166, 2007. Available from: <http://www.sciencedirect.com/science/article/pii/S0141118707000405>. Cited 2 times on pages 34 and 35.

FOLTYN, E. P.; TUTHILL, A. M. *Design of Ice Booms*, Hanover, 1996. 31 p. Cited 3 times on pages 31, 32, and 33.

GAD-EL-HAK, M. *Advances in Fluid Mechanics Measurements*. Heidelberg: Springer-Verlag Berlin, 1989. 606 p. ISBN 13:978-3-540-51136-6. Cited on page 33.

GANESAN, V. *Gas turbines*. New Delhi Singapore: Tata McGraw-Hill, 2010. ISBN 0-07-068192-9. Cited on page 37.

GIRLING, B. et al. *World Energy Resources 2016: Hydropower*, London, 2016. 51 p. Available from: <https://www.worldenergy.org/wp-content/uploads/2017/03/WEResources_Hydropower_2016.pdf>. Cited on page 23.

Google Maps. *Map of Santo Antônio hidropower plant*. 2018. [Online; accessed April 5th, 2019]. Available from: <https://www.google.com/maps/place/8%C2%B048'06.0%22S+63%C2%B057'03.0%22W/@-8.8023163,-63.9553207,5452m/data=!3m1!1e3!4m5!3m4!1s0x0:0x0!8m2!3d-8.8016667!4d-63.9508333>. Cited on page 25.

GUEDES, D. L. et al. Maneuverability Towing Tank Experiments with Manifold Models: Part II — PMM Oscillation Tests. In: *International Conference on Offshore Mechanics and Arctic Engineering, Volume 1: Offshore Technology*. Madrid, Spain: ASME, 2018. p. 1–10. Available from: <http://dx.doi.org/10.1115/OMAE2018-78123>. Cited on page 34.

HARTLIEB, A. Decisive parameters for backwater effects caused by floating debris jams. *Open Journal of Fluid Dynamics*, Scientific Research Publishing, Inc., v. 07, n. 04, p. 475–484, 2017. Available from: <https://doi.org/10.4236/ojfd.2017.74032>. Cited 2 times on pages 42 and 90.

HASANLOO, D.; PANG, H.; YU, G. On the estimation of the falling velocity and drag coefficient of torpedo anchor during acceleration. *Ocean Engineering*, Elsevier, v. 42, p. 135–146, 2012. ISSN 0029-8018. Available from: <http://dx.doi.org/10.1016/j.oceaneng.2011.12.022>. Cited on page 34.

HOERNER, S. *Fluid-dynamic drag : practical information on aerodynamic drag and hydrodynamic resistance*. Bakersfield: Hoerner Fluid Dynamics, 1992. ISBN 978-9991194448. Cited on page 41.

IRVINE, H. *Cable structures*. Cambridge, Mass: MIT Press, 1981. ISBN 0262090236. Cited on page 35.

ITTC. *ITTC - Recommended Procedures and Guidelines: Resistance Test*. [s.n.], 2011. Available from: <https://ittc.info/media/1217/75-02-02-01.pdf>. Cited on page 87.

KENNEDY, R. J.; LAZIER, S. S. *The Water Transportation of Pulpwood III: Strucutres*. Montreal: Pulp and Paper Research Institute of Canada, 1965. Cited 2 times on pages 33 and 90.

KHOSHNEVIS, A. B.; MAMOURI, A.; MIR, F. An investigation of reynolds number effect on the aerodynamics of bluff body with sharp edges. *ADMT Journal*, Islamic Azad University Majlesi Branch, v. 8, n. 3, p. –, 2015. ISSN 2252-0406. Available from: <http://admt.iaumajlesi.ac.ir/article_534934.html>. Cited on page 40.

KLEINE, F. A. d. S. et al. Maneuverability Towing Tank Experiments with Manifold Models: Part I — Static Tests. In: *International Conference on Offshore Mechanics and Arctic Engineering, Volume 1: Offshore Technology*. Madrid, Spain: ASME, 2018. p. 1–10. Available from: <http://dx.doi.org/10.1115/OMAE2018-77036>. Cited on page 34.

LADER, P. F.; ENERHAUG, B. Experimental Investigation of Forces and Geometry of a Net Cage in Uniform Flow. *IEEE Journal of Oceanic Engineering*, v. 30, n. 1, p. 79–84, 2005. Available from: <https://ieeexplore.ieee.org/document/1435578>. Cited on page 35.

LAROSE, G.; D'AUTEUIL, A. On the reynolds number sensitivity of the aerodynamics of bluff bodies with sharp edges. *Journal of Wind Engineering and Industrial Aerodynamics*, Elsevier BV, v. 94, n. 5, p. 365–376, maio 2006. Available from: <https://doi.org/10.1016/j.jweia.2006.01.011>. Cited on page 40.

LøLAND, G. *Current forces on and flow through fish farms*. Thesis (PhD thesis) — Norwegian Institute of Technology, Trondheim, 1991. Cited 3 times on pages 35, 36, and 81.

LØLAND, G. Current forces on, and water flow through and around, floating fish farms. *Aquaculture International*, v. 89, p. 72–89, 1993. Cited on page 35.

LO, J.-M. Laboratory investigation of single floating booms a and series of booms in the prevention of oil slick and jellyfish movement. *Ocean Engineering*, v. 23, n. 6, p. 519–531, 1996. Cited 2 times on pages 23 and 33.

MORSE, B. Dynamics of ice forces on booms. *Cold Regions Science and Technology*, v. 33, n. 1, p. 29–43, 2001. ISSN 0165232X. Cited on page 23.

MUNSON, B. R. et al. *Fundamentals of fluid mechanics*. Hoboken, NJ: J. Wiley & Sons, 2009. ISBN 978-0470-26284-9. Cited 2 times on pages 38 and 40.

NEWMAN, B. G. Shape of a towed boom of logs. *Proceedings of the Royal Society of London. Series A, Mathematical and Physical Sciences*, The Royal Society, v. 346, n. 1646, p. 329–348, 1975. ISSN 00804630. Available from: <http://www.jstor.org/stable/78852>. Cited on page 30.

PAGLIARA, S.; CARNACINA, I. Influence of large woody debris on sediment scour at bridge piers. *International Journal of Sediment Research*, International Research and Training Centre on Erosion and Sedimentation and the World Association for Sedimentation and Erosion Research, v. 26, n. 2, p. 121–136, 2011. ISSN 10016279. Cited on page 29.

PAPINI, D. *On Shape Control of cables under vertical loads*. 102 p. Thesis (Master's Thesis) — Lund University, 2010. Cited on page 43.

PERHAM, R. E. *Floating Debris Control; A literature Review*, Hanover, 1987. 67 p. Cited 3 times on pages 29, 31, and 33.

PESCE, C. P. *Mecânica de Cabos e Tubos Submersos Lançados em "Catenária": Uma Abordagem Analítica e Experimental*. 388 p. Thesis (Tese de Livre Docência) — University of São Paulo, 1997. In portuguese. Cited on page 35.

PITON, G.; RECKING, A. Design of Sediment Traps with Open Check Dams. II: Woody Debris. *Journal of Hydraulic Engineering*, v. 142, n. 2, p. 04015046, 2016. ISSN 0733-9429. Cited on page 29.

RAHIMI, E. et al. Effect of Debris on Piers Group Scour: An Experimental Study. *KSCE Journal of Civil Engineering*, v. 22, n. 4, p. 1496–1505, 2018. ISSN 19763808. Cited on page 29.

RATHAKRISHNAN, E. *Instrumentation, measurements, and experiments in fluids*. Boca Raton, FL: CRC Press, 2007. ISBN 978-0-8493-0763-8. Cited on page 40.

RUIZ-VILLANUEVA, V. et al. Two-dimensional modelling of large wood transport during flash floods. *Earth Surface Processes and Landforms*, v. 39, n. 4, p. 438–449, 2014. ISSN 10969837. Cited on page 29.

RUSYDA, M. I. Log jams at a bridge with a pier and a bridge without pier. *Procedia Engineering*, Elsevier B.V., v. 125, p. 277–283, 2015. ISSN 18777058. Cited on page 29.

Santo Antônio Energia. *Generation*. 2018. Available from: <http://www.santoantonioenergia.com.br/energia/energia1/>. Cited on page 23.

SCHEWE, G.; LARSEN, A. Reynolds number effects in the flow around a bluff bridge deck cross section. *Journal of Wind Engineering and Industrial Aerodynamics*, Elsevier BV, v. 74-76, p. 829–838, abr. 1998. Available from: <https://doi.org/10.1016/s0167-6105(98)00075-0>. Cited on page 40.

SCHMOCKER, L.; HAGER, W. H. Probability of Drift Blockage at Bridge Decks. *Journal of Hydraulic Engineering*, v. 137, n. 4, p. 470–479, 2011. ISSN 0733-9429. Cited on page 29.

SCHMOCKER, L.; WEITBRECHT, V. Driftwood: Risk Analysis and Engineering Measures. *Journal of Hydraulic Engineering*, v. 139, n. 7, p. 683–695, 2013. ISSN 0733-9429. Cited on page 30.

SHAUGHNESSY Jr, E. J.; KATZ, I. M.; SCHAFFER, J. P. *Introduction to Fluid Mechanics*. New York: Oxford University Press, 2005. 1018 p. ISBN 9780195154511. Cited on page 33.

SILVEIRA, L. M. Y. da; MARTINS, C. d. A. A Numerical Method to Solve the Static Problem of a Catenary Riser. In: *23rd International Conference on Offshore Mechanics and Arctic Engineering, Volume 1, Parts A and B*. ASME, 2004. p. 693–702. ISBN 0-7918-3743-2. Available from: <http://proceedings.asmedigitalcollection.asme.org/proceeding.aspx?articleid=1629288>. Cited on page 35.

SLAT, B. *How the Oceans can Clean Themselves - A Feasibility Study*, Delft, 2014. Available from: <https://www.theoceancleanup.com/>. Cited on page 23.

STOCKSTILL, R. L.; DALY, S. F.; HOPKINS, M. A. Modeling Floating Objects at River Structures. *Journal of Hydraulic Engineering*, v. 135, n. 5, p. 403–414, 2009. ISSN 0733-9429. Cited on page 29.

WAHL, T. L. *Investigation of Debris and Safety Boom Alternatives for Bureau of Reclamation Use*, Denver, 1992. 15 p. Cited on page 23.

WALCZAK, N.; WALCZAK, Z.; NIEć, J. Assessment of the resistance value of trash racks at a small hydropower plant operating at low temperature. *Energies*, v. 13, p. 1775, 04 2020. Cited on page 30.

ZOHURI, B. *Dimensional Analysis and Self-Similarity Methods for Engineers and Scientists*. Springer International Publishing, 2015. Available from: <https://doi.org/10.1007/978-3-319-13476-5>. Cited on page 41.